IQ Reflected Power Canceller for an FMCW radar

by

Anneke Stofberg

Thesis presented in partial fulfilment of the requirements for the degree of Master of Engineering in the Faculty of Electrical and Electronic Engineering at Stellenbosch University

Supervisors:

Prof. J.B. de Swardt
Prof. P.W. van der Walt

March 2014

Declaration

By submitting this thesis electronically, I declare that the entirety of the work contained therein is my own, original work, that I am the sole author thereof (save to the extent explicitly otherwise stated), that reproduction and publication thereof by Stellenbosch University will not infringe any third party rights and that I have not previously in its entirety or in part submitted it for obtaining any qualification.

Signature: .....
A. Stofberg

Date: 2013/13/12 .....

Abstract

Large close range environmental reflections or poor isolation between the transmit and receive paths of an FMCW radar can overload the receiver. The In phase and Quadrature phase (IQ) Reflected Power Canceller (RPC) provides a solution to the problem by cancelling any close range reflections. In this study a procedure to optimise the design of an RPC is developed and the performance limits of a practical RPC is investigated in depth.

There are four focus areas in the evaluation and design of the IQ Reflected Power Canceller. First, an analysis was performed on a theoretical IQ Reflected Power Canceller, which provided insight into how the system functioned and made it possible to identify practical application issues that would arise during the design.

The next focus area was the IQ Reflected Power Canceller's dynamic range. Equations, based on the power and noise characteristics of each component in the canceller, were derived. From these equations, a system, with an optimised dynamic range, could be developed.

Next, the IQ Reflected Power Canceller's feedback loop stability was investigated. The canceller is an active negative feedback control system but, in order to obtain the negative feedback, the feedback signal has to be phase shifted by 180 degrees to the phase of the input signal. An analysis of the canceller's RF phase contribution resulted in an equation that can be used to manage the nett RF phase in the feedback loop.

The evaluation model of the IQ Reflected Power Canceller produced favourable results. The tests performed on the system included measuring the level of cancellation that can be achieved, whether the dynamic range corresponds to the predicted values and the amount of RF phase error that can be introduced in the feedback path while maintaining a stable system.

The IQ Reflected Power Canceller was found to perform well in the evaluation. It provided a cancellation of more than 45 dB for close range reflections and the canceller remained stable across a wide range of RF centre frequencies (1 GHz). This means that the FMCW radar's frequency modulation bandwidth will not be limited because of the IQ Reflected Power Canceller. The evaluation clearly showed that the modulator in the feedback loop is the critical element that determines the dynamic range of the radar with an RPC.

Opsomming

Onvoldoende isolasie tussen die sender en ontvanger van 'n Frekwensie Gemoduleerde Kontinu Golf radar, sowel as groot weerkaatsings vanaf voorwerpe in die omgewing van die radar, veroorsaak dat die ontvanger versadig. Hierdie beperking veroorsaak dat die radar 'n verminderde dinamiese bereik het, en daarmee ook dat die radar se maksimum teiken-afstand verminder word. Die IQ Gereflekteerde Drywingskanselleerder kan as 'n oplossing gebruik word teen hierdie ongewenste refleksies. Hierdie navorsing poog om 'n kanselleerder te evalueer met die eind doel gestel daarop om 'n praktiese stelsel aanmekaar te sit.

Die kanselleerder word geëvalueer deur na vier fokus areas te kyk. Eerstens word 'n ideale model opgestel, wat 'n beter begrip van die kanselleerder bewerkstellig. Uit hierdie ideale model, is daar praktiese oorwegings wat die kanselleerder affekteer, geïdentifiseer.

Ten einde die dinamiese bereik van die radar ontvanger te verbeter, word 'n metode afgelei wat gebruik word om die kanselleerder se dinamiese bereik te optimeer. Hierdie metode neem die maksimum drywingsbeperkinge van die komponente in die kanselleerder in ag.

Die kanselleerder is 'n aktiewe terugvoer beheerstelsel, en aangesien 'n sommeerder in die terugvoer lus gebruik word, moet die fase deur die lus met 180 grade geskuif word om sodoende 'n kansellerende sein by die ontvangde sein te tel. Die RF fase foute in die kanselleerder word geanaliseer deur 'n nie-ideale model van die kanselleerder op te stel. Hierdie nie-ideale model maak dit moontlik om die effek van 'n RF fase fout op die kanselleerder se stabiliteit te ondersoek.

'n Praktiese kanselleerder is ontwerp uit die inligting wat versamel is gedurende die evaluasie, en 'n werkende stelsel is aanmekaar gesit. Met hierdie praktiese kanselleerder is die hoeveelheid drywing-onderdrukking wat bereik kan word, gemeet. Die dinamiese bereik van die kanselleerder is ook bepaal en vergelyk met die teoreties berekende waardes. Die aannames oor die effek van die RF fase fout in die kanselleerder, is bevestig deur metings te neem.

Goeie resultate is met die kanselleerder behaal. 'n Kansellasie van meer as 45 dB is gemeet vir naby-geleë refleksies. Die kanselleerder het ook stabiel gebly oor 'n wye band van senter-frekwensies (1 GHz). Dus sal die Frekwensie Gemoduleerde Kontinu Golf radar se modulasie bandwydte nie beperk word as gevolg van die kanselleerder nie. Uit die evaluasie is daar gevind dat die modulator die kritieke element in the kanselleerder se terugvoer lus is, dus bepaal die modulator die dinamiese bereik van die radar met 'n kanselleerder.

Acknowledgements

I would like to thank the following people for their support throughout the project.

Thank you to my supervisor, Prof. J.B. de Swardt, for your guidance and advice throughout the project.

Thank you to my co-supervisor, Prof. P.W. van der Walt, for your valuable insights. It was an honour to learn from you.

Thank you to Reutech Radar Systems for providing me with the financial support to carry out this project.

Thank you to my family for the support and encouragement throughout the project.

Contents

Nomenclature

Abbreviations

dB	Decibel
DUT	Device Under Test
ENR	Excess Noise Ratio
FOM	Figure of Merit
I	In phase
IF	Intermediate Frequency
MATLAB	Matrix Laboratory (Mathworks, Inc.)
LO	Local Oscillator
Q	Quadrature
RF	Radio Frequency
RMS	Root Mean Square
RPC	Reflected Power Canceller
Rx	Received signal
MDS	Minimum Detectable Signal
Tx	Transmitted signal

Constants

c =	$3\text{x}10^{8}$ m/s
k =	$1.380\text{x}10^{-23}$ J/K

Chapter 1

Introduction

1.1 Motivation and thesis topic

Frequency Modulated Continuous Wave (FMCW) radars are used in a large range of applications today, including military, mining and weather radars [1]. However, there are some limitations facing FMCW radar such as large reflections that desensitise the receiver and make it impossible to detect small targets [2]. These reflections can be caused either by large objects in the transmitting path or by insufficient isolation between the transmitter and receiver antennas, since the leakage from the transmitter resembles a close range reflection to the receiver. These limitations affect the performance of the radar. During the 1960's, a solution was presented which could reduce these unwanted reflected signals: the IQ Reflected Power Canceller (RPC) [1]. The aim of the RPC is to cancel these unwanted or clutter reflections and improve the sensitivity of the receiver.

The thesis topic includes the evaluation and design of an RPC.

1.2 Background

In order to fully understand the function of the RPC, some background information regarding FMCW radar is required. The aim of this section is to describe FMCW radar, focusing on a visual representation of how it works.

1.2.1 FMCW radar

A very basic block diagram of an FMCW radar is given in Figure 1.1.

Continuous Wave (CW) radar is widely used as a method for determining the velocity of targets [2]. As the name suggests, a CW radar transmits a sine wave of constant frequency and it uses the Doppler frequency shift to determine the velocity of a target [2]. However, it is not possible to detect the range of a target with CW radar, since the time lag between transmitted and received signals can not be determined. This shortcoming is due to the narrow bandwidth of the transmitted waveform [2], for this reason FMCW radar is used.

FMCW radar modulates the constant sine wave frequency of CW radar with a periodic signal, giving the transmitted signal a larger bandwidth [2]. In the case of

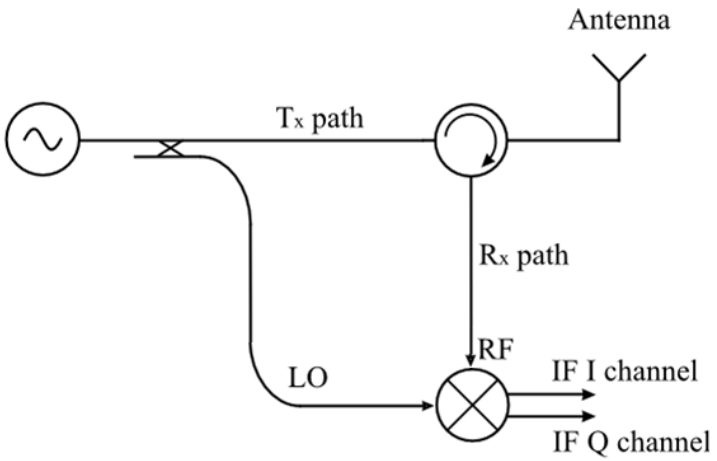

Figure 1.1: A Basic block diagram showing an FMCW Radar using a single antenna configuration with a circulator.

the time domain, a time difference is observed between the transmitted and received signals [2]. There are several types of waveform that can be used to modulate the carrier for FMCW radar, for example a sawtooth, triangular or sinusoidal waveform [2]. Any of the listed types of modulation can be used; however, the sawtooth waveform was chosen for this study. From Figure 1.1 it is seen that the basic FMCW radar consists of a sinusoidal generator, frequency modulated by a sawtooth waveform, a circulator, an antenna and a mixer. The mixer is driven with the received Radio Frequency (RF)/input signal and the Local Oscillator (LO) signal, which consists of a signal that is coupled out from the transmitted signal's path.

Figure 1.2 shows the transmitted (Tx) and received (Rx) signals for two targets of an FMCW radar. The round trip delay is indicated on the figure as well as in equation 1.2.1 (where R is range to target and c is the velocity of propagation), which is used to calculate the range to the target based on the time delay between the transmitted and received signals. However this time delay between the transmitted and received signals can be detected as a frequency, which is discussed further.

$$delay = \frac{2R}{c} \tag{1.2.1}$$

From Figure 1.2, the transmitted and received signals are indicated on a frequency vs. time axis, which means that the frequency of these signals increases with time for a certain period $1/f_m$. From the information provided on Figure 1.2 the range to the target can be calculated. If Figure 1.1 is considered again, it can be seen that when the transmitted and received signals are mixed (down converted), they produce an Intermediate Frequency (IF) output which is also the output of the radar.

Down conversion follows the process illustrated in Figure 1.3. The input signals consist of a high frequency LO and another high frequency RF signal. The mixer's frequency at the output is down converted to baseband as shown in the spectrum diagram in Figure 1.3 [3]. The desired Intermediate Frequency (IF)/baseband output

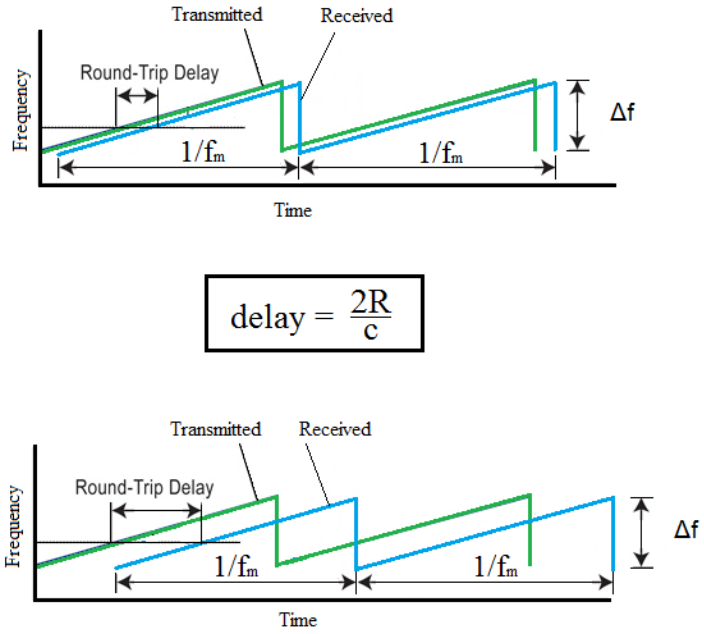

Figure 1.2: Transmitted and Received signals of an FMCW radar for two targets. The sawtooth is used as modulating waveform and the results are indicated on a frequency vs. time axis.

is the difference frequency which is easily selected by low pass filtering. The down conversion is demonstrated by equation 1.2.2.

$$f_{IF} = f_{LO} - f_{RF} \tag{1.2.2}$$

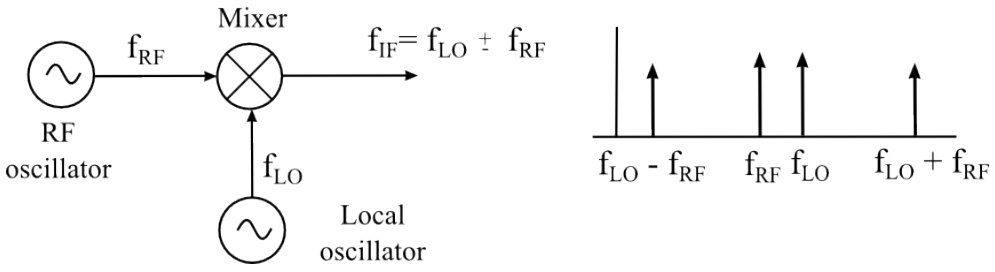

Figure 1.3: The symbol and functional diagram of a mixer that illustrates frequency down conversion.

The mixer of the FMCW radar in Figure 1.1 is used to down convert the transmitted and received signals, thus equation 1.2.2 is used to determine the IF frequency. Consider Figure 1.2, where there are two examples of a transmitted and a received signal. These are both examples of a stationary target, the time delay between the transmitted and the received signal is constant on both accounts, and is indicated

in Figure 1.4. Once the frequency in Figure 1.4 has been identified, the range to the target can be calculated using the equation given in 1.2.3. The IF frequency in Figure 1.4 is often referred to as the beat frequency [2].

$$f_b = \frac{2Rf_m\Delta f}{c} \tag{1.2.3}$$

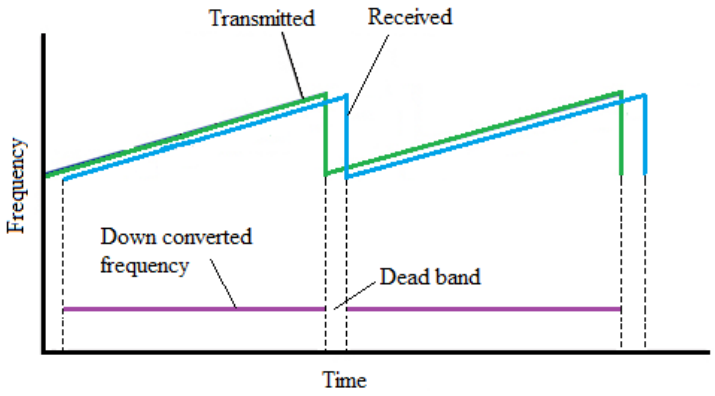

Figure 1.4: Down converted frequency output of the FMCW radar's mixer. By determining this frequency, the range to the target can be calculated.

From equation 1.2.3 it is seen that the range to the target is linearly proportional to the beat frequency: a low beat frequency is indicative of a close range target, while the higher the beat frequency becomes the further the range of the detected target is.

1.3 Objectives of this study

The objective of this study is to research and evaluate an RPC. This objective is attained by obtaining a model for an ideal RPC and later expanding on that model to evaluate the attributes of a practical RPC.

1.4 Overview of this work

In order to evaluate an RPC, it had first to be described as an ideal system. Thus Chapter 2 describes a mathematical model for an ideal RPC followed by a literature review which was based on the knowledge gained from the ideal RPC derivation. The ideal model and literature review was finally supplemented with an LTSpice simulation. Chapter 3 describes the practical considerations that needed to be taken into account when designing an RPC. Next, Chapter 4 elaborates on one of the practical considerations from Chapter 3: Designing an optimised dynamic range. Chapter 5 expands on another practical consideration introduced in Chapter 3: the RF phase error calculation. Next Chapter 6 contains the final design of a practical RPC, including measurements of the chosen components and the final cancellation

bandwidth design. Finally, Chapter 7 was used to describe the test set up and corresponding measurements that characterised the RPC.

Chapter 2

Ideal IQ Reflected Power Cancellers

The RPC is an active control system used to cancel unwanted reflections in an FMCW radar. An ideal RPC was described using a mathematical model. The control system was included in this model and the control applied to the RPC was explained by means of a transfer function (TF) and an applied MATLAB simulation. After the ideal RPC was developed, a literature review was used to highlight the most important concepts with reference to an RPC that had been developed thus far. Next, an LTSpice simulation introduced the practical components that are necessary to produce a fully functional RPC. It also gave an indication of whether the RPC was a practically applicable solution.

2.1 Mathematical model

The conditions for this mathematical derivation are the following:

- Assume the bandwidth of the FMCW radar is narrow. The centre frequency ω_0 can be used as the transmitting signal.
- The target is stationary. Let the target information be represented by $\phi(t)$, which is a phase variable that slowly varies with time.
- The system exists under ideal conditions. There is no time delay contribution by sections of transmission line in the RPC.

The down converted baseband signal is represented by the difference in frequency between the RF and the LO, which can either be zero if $\omega_{RF} = \omega_{LO}$ or ω_r (i.e. $\phi(t) = \omega_r t$) if the RF signal's frequency equals $\omega_r + \omega_0$ where the LO frequency is ω_0.

2.1.1 Signal representation

An RF signal with centre frequency ω_0 and phase shift $\phi(t)$ is described by equation 2.1.1, which can be rewritten into its exponential form.

$$\begin{aligned} x(t) &= A\cos(\omega_0 t + \phi(t)) \\ &= \frac{1}{2}(e^{j\omega_0 t + j\phi(t)} + e^{-(j\omega_0 t + j\phi(t))}) \end{aligned} \tag{2.1.1}$$

Consider a mixer with a real RF input $x(t)$ which is driven by an LO signal $l(t) = \cos(\omega_0 t)$ in Figure 2.1.

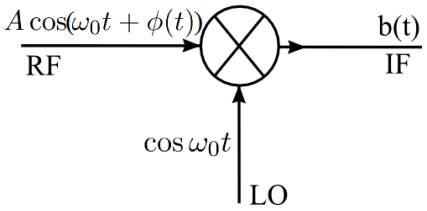

Figure 2.1: Ideal mixer with a real RF input signal.

The IF output of the mixer is represented by b(t) in equation 2.1.2. From this equation the sum and difference frequencies of the mixer's output can be seen. For the down conversion required in an RPC, only the difference frequency is used.

$$\begin{aligned} b(t) &= A\cos(\omega_0 t + \phi(t))\cos(\omega_0 t) \\ &= \frac{A}{2}(\cos(2\omega_0 t + \phi(t)) + \cos(\phi(t))) \end{aligned} \tag{2.1.2}$$

If b(t) is rewritten in its exponential form as in equation 2.1.3, the difference frequency occurs once again in its complex conjugate pairs, as was found for the RF input signal in equation 2.1.1.

$$\begin{aligned} b(t) &= A\cos(\omega_0 t + \phi(t))\cos(\omega_0 t) \\ &= \frac{A}{4}(e^{j(\omega_0 t + \phi(t))} + e^{-j(\omega_0 t + \phi(t))})(e^{j\omega_0 t} + e^{-j\omega_0 t}) \\ &= \frac{A}{4}(e^{j(2\omega_0 t + \phi(t))} + e^{j\phi(t)} + e^{-j\phi(t)} + e^{-j(2\omega_0 t + \phi(t))}) \end{aligned} \tag{2.1.3}$$

The complex conjugate pairs in equations 2.1.1 and 2.1.3 represent a real signal. If the phasor representation of equation 2.1.1 is used as the input to the RPC, it is represented by equation 2.1.4 which is also expanded using the Euler formula.

$$\begin{aligned} v(t) &= Ae^{j(\omega_0 t + \phi(t))} \\ &= A[\cos(\omega_0 t + \phi(t)) + j\sin(\omega_0 t + \phi(t))] \end{aligned} \tag{2.1.4}$$

The original signal $x(t)$ can be found again if the $\Re[v(t)]$ is taken. From equation 2.1.3 it can be seen that only the $e^{j(\omega_0 t + \phi(t))}$ and $e^{-j\omega_0 t}$ terms are required to obtain the positive half of the baseband's (difference frequency) output conjugate pair through multiplication.

2.1.2 Demodulator and modulator

Consider $v(t)$ in equation 2.1.4, from its Euler form it is seen that $v(t)$ is represented by both a complex real and an imaginary component. These complex values represent a phasor which can be drawn on a real and imaginary axis as in Figure 2.2. The phase of the centre frequency $\omega_0 t$ changes quickly over time but the term $\phi(t)$ represents the baseband frequency and changes much more slowly over time. These real and imaginary components contain the phase information of the RF input signal and in order retain this phase information, both the real and imaginary components of the input have to be measured.

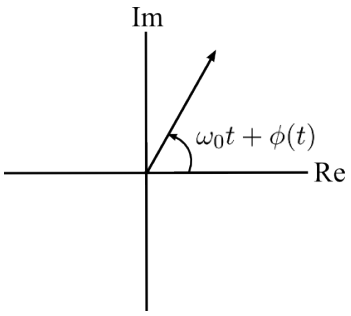

Figure 2.2: Phasor diagram of RF input signal.

A mixer as shown in Figure 2.1 can not be used since its output does not retain the phase information of the downconverted signal. A demodulator can be used instead of a mixer, which will provide the output in its real (I) and imaginary (Q) components as shown in Figure 2.3(a). Figure 2.3(b) shows the demodulator with its inputs as phasors. The output frequency of Figure 2.3(b) is the difference frequency of the RF and the LO.

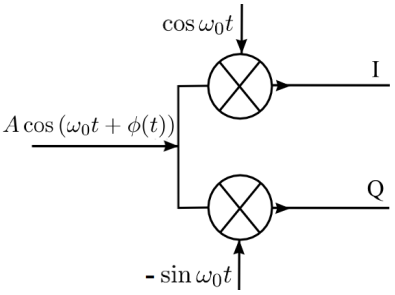

(a) Demodulation for a real RF input signal.

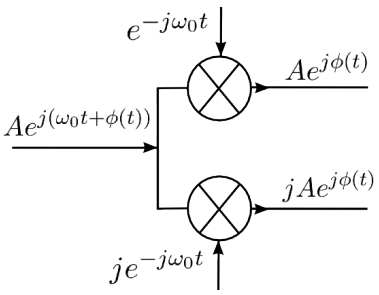

(b) Demodulation using phasors.

Figure 2.3: Demodulation for RF input signal.

The baseband signal output in Figure 2.3(b) contains the distance and velocity information of the target in the term $\phi(t)$. This is verified by expanding the RF input signal from equation 2.1.1 using the compound angle formulas:

$$\begin{aligned} A\cos(\omega_0 t + \phi(t)) &= A[2\cos\omega_0 t \ \cos\phi(t) - \cos(\omega_0 t - \phi(t))] \\ &= A[2\cos\omega_0 t \ \cos\phi(t) - (2\sin\omega_0 t \ \sin\phi(t) \\ &\quad + \cos(\omega_0 t + \phi(t)))] \\ &= A[\cos\omega_0 t \ \cos\phi(t) - \sin\omega_0 t \ \sin\phi(t)] \end{aligned} \tag{2.1.5}$$

From equation 2.1.5 the I and Q baseband information can be seen as a part of the input signal. The I channel output of Figure 2.3(b) is related to the I output in Figure 2.3(a) by using only the real component of the phasor output as shown in equation 2.1.6.

$$\begin{aligned} \Re[Ae^{j\phi(t)}] &= \Re[A(\cos\phi(t) + j\sin\phi(t))] \\ &= A\cos\phi(t) \end{aligned} \tag{2.1.6}$$

This process can be repeated for the Q channel of Figure 2.3(b) and Figure 2.3(a) as in equation 2.1.7.

$$\begin{aligned} \Re[jAe^{j\phi(t)}] &= \Re[A(j\cos\phi(t) - \sin\phi(t))] \\ &= -A\sin\phi(t) \end{aligned} \tag{2.1.7}$$

Thus only the difference frequencies of the RF and LO remain and are expressed as a quadrature pair.

The RPC is used to cancel out close range reflections by subtracting a cancelling signal from the input. In order to obtain a cancelling signal the baseband information has to be up converted again to the RF range. This is achieved by a modulator, shown in Figure 2.4, where the output is given on the figure.

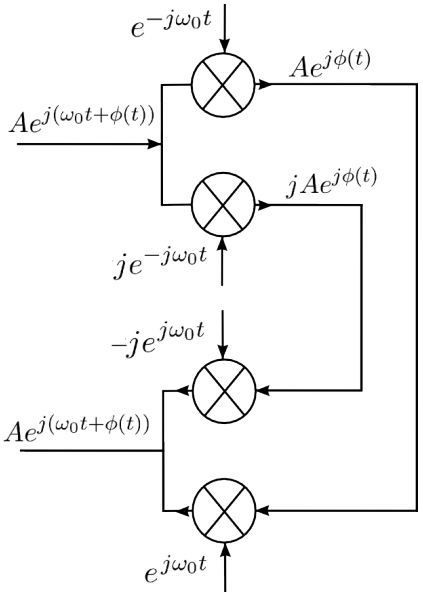

Figure 2.4: Down conversion and up conversion of RF input signal using a demodulator and modulator.

In order to produce a cancelling signal some form of control is required to be applied to the baseband signal from Figure 2.4. Also, this cancelling signal has to be subtracted from input. The next subsection aims to describe the feedback system that is used to create an RPC.

2.1.3 Ideal RPC

Consider Figure 2.5, where feedback has been added to the system in Figure 2.4. This is a simple first order integrator feedback control system. From the figure it can be seen that the RPC can be divided into two separate systems, where one follows the I signals and the other follows the Q signals. This is shown in Figure 2.6. Since the I and Q paths are identical, the control system's derivation is done only for the I channel.

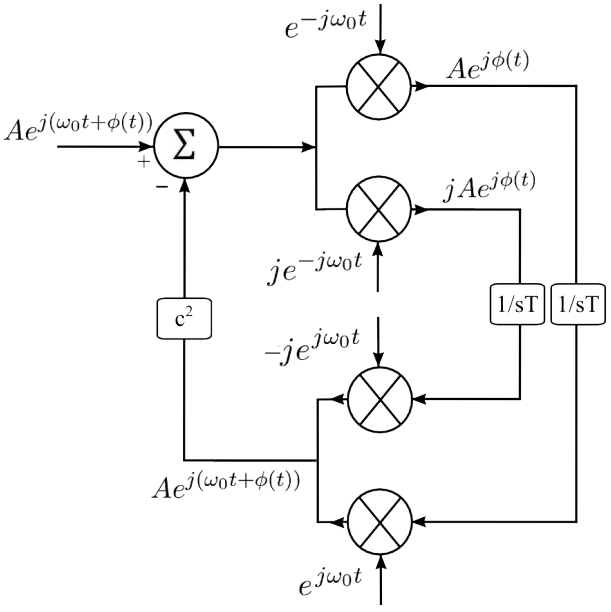

Figure 2.5: RF phasor representation of a first order integrator control system.

The equivalent baseband input signals are indicated on Figure 2.6, the demodulator and modulator are represented by their corresponding gains. The subtraction between the RF input and the modulator output is achieved with the help of an RF coupler which is represented by its equivalent loss (coupling factor) c^2 in Figure 2.6.

The closed loop response of this system is given by

$$\begin{aligned}\frac{Y(s)}{X(s)} &= \frac{G_D}{1+\frac{G_D G_M c^2}{sT}} \\ &= \frac{G_D sT}{sT + G_M G_D c^2}\end{aligned} \tag{2.1.8}$$

where G_D refers to the demodulator's conversion gain and G_M is the modulator's conversion gain. If the closed loop response in Figure 2.6 is considered, for a signal input with $s = j\omega_r$ where $\phi(t) = \omega_r t$, it can be rewritten as in equation 2.1.9.

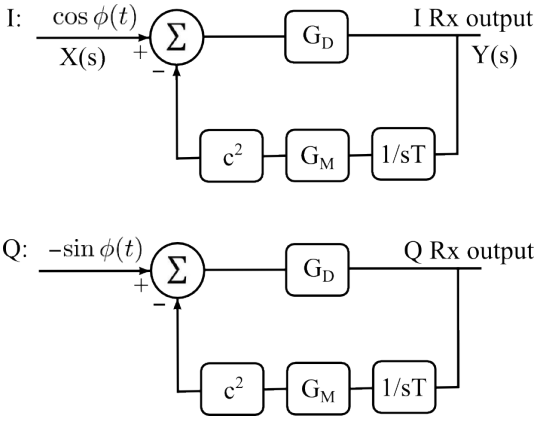

Figure 2.6: Baseband model of control system.

$$\frac{Y(j\omega_r)}{X(j\omega_r)} = \frac{G_D j\omega_r T}{j\omega_r T + G_M G_D c^2} \tag{2.1.9}$$

If the frequency of the input signal (ω_r) is very small $\omega_r << G_M G_D c^2$, the output magnitude of equation 2.1.9 $\frac{Y(j\omega_r)}{X(j\omega_r)} \approx \frac{j\omega_r T}{G_M c^2}$ which becomes zero for a DC input and increases in magnitude for each higher frequency value. If the input frequency $\omega_r >> G_M G_D c^2$, $\frac{Y(j\omega_r)}{X(j\omega_r)} \approx G_D$ which means that for high frequency values the output's magnitude remains constant. This is represented graphically by the closed loop response shown in Figure 2.7.

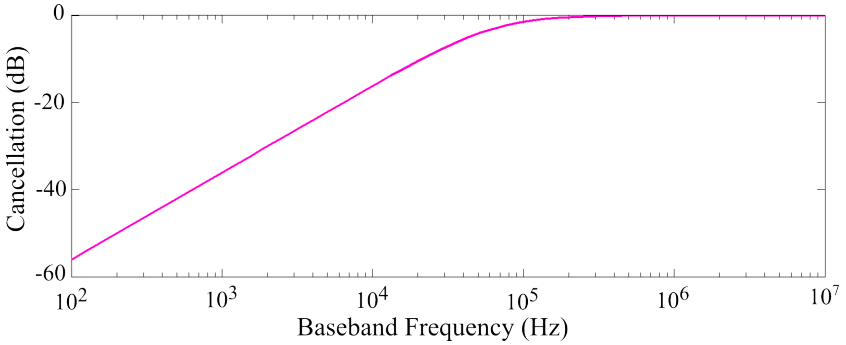

Figure 2.7: First order integrator control system's closed loop response.

By using both the I and the Q channels you are enabled to determine the phase information of the RF input signal. The control is applied to both the I and the Q baseband signals and thus it allows the control system to feed back a cancelling signal with reference to the input signal's phase.

Figure 2.8 shows the two baseband models for the I and Q channels of the RPC, but in this figure cross coupling is added between the two channels. This cross coupling occurs when there is additional RF phase error through the control loop. If the RF phase error exceeds a certain value, this cross coupling will cause the RPC to

become unstable. Also if the phase error (ϕ_e) is within the stable window, but not at its optimum value (zero), the cancellation of the loop is affected by up to 3 dB.

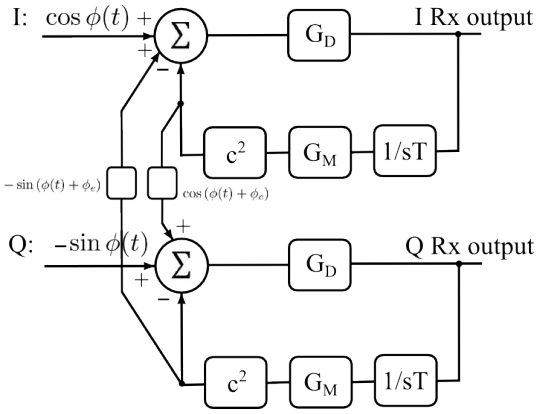

Figure 2.8: Cross coupling between I and Q baseband control systems.

2.2 Literature review

The RPC was described as an ideal system in section 2.1 and this section summarises the available literature on the subject. This summary first views the similarities and differences between the available RPCs. Next, the different implementations are analysed. Finally the literature summary provides some insight into the difficulties of implementing an RPC.

2.2.1 Problem statement

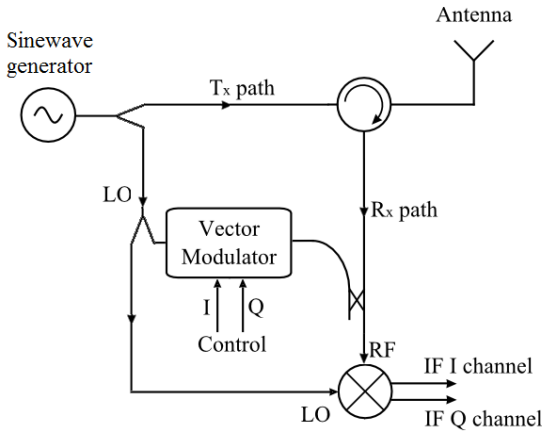

Figure 2.9: A basic block diagram showing the IQ Reflected Power Canceller implemented using a vector modulator.

Figure 2.9 shows a basic block diagram of an FMCW radar configuration with an RPC, using a vector modulator in the feedback path [1]. From this figure, it can also be seen that a circulator is used to make it possible to transmit and receive using a single antenna. A problem with this single antenna configuration is the low isolation of the circulator. The transmitted signal is leaked through the circulator into the receiver's path and, as a result, desensitises the radar's receiver [1], [4], [5]. Another reason for using the RPC is to improve the receiver's dynamic range [6], [7], [8]. The RPC cancels out close range reflections, improving the dynamic range by making it possible to transmit more power without large close range reflections desensitising the receiver.

2.2.2 Comparing Reflected Power Cancellers

The main advantage that the RPC has over other cancellation schemes for FMCW radar is that this RPC is implemented as an active control system [1]. The RPC's in the available literature follow the same basic scheme as the RPC that was described by a mathematical model in the previous section 2.1.

The baseband integrator in the control system as described in section 2.1 can be implemented using either digital or analogue techniques. A digital technique is shown in Figure 2.10(a), where an integrator is applied using an FPGA (Field Programmable Gate Array) and a digital vector modulator is used to up convert the baseband control signal to a cancelling signal in the RF range. This digital vector modulator provides a precise control over the error signal that is fed back into the receiver path [8]. More examples of systems implemented using a digital scheme can be found in [6], [7], [9], [8]. However, using a digital implementation for an RPC sets several restrictions on the components that are used. For example, a high accuracy quantisation is needed for the regulating component and the delay of the digital processing should also be as small as possible [4].

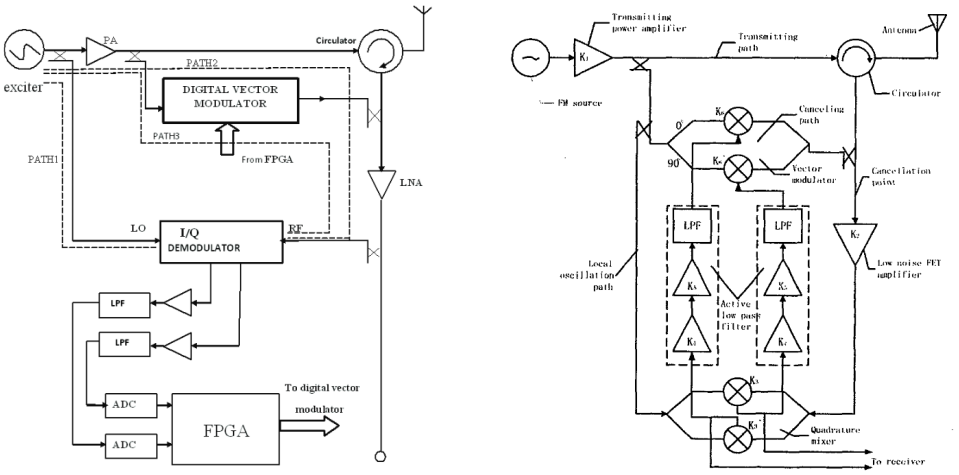

(a) RPC implemented using a digital system.

(b) RPC implemented using an analogue system.

Figure 2.10: Two examples of different RPC implementations.

The system in Figure 2.10(b) uses an analogue integrator to produce a control signal for the RPC. According to Qi [4], an analogue system can achieve a higher cancellation ratio for a lower implementation cost. More examples of systems implemented using an analogue design can be found in [1], [10], [4], [5]. There have been favourable results from both the digital and the analogue implementations [10], [4], [5]. [6], [7], [9] and [8].

2.2.3 Practical considerations

If Figure 2.9 is considered again, the main components of an RPC are listed in Table 2.1.

Table 2.1: A list of the components of an IQ RPC.

Components:
Vector modulator
Coupler
Demodulator
Control

The vector modulator was a popular choice to up convert the I and Q control signals from baseband to the Rx frequencies and was used by Beasly, Stove and Reits [1], Jiming, Xinjian and Zhijiu [4], Lin and Wang [6] to name only a few. However, according to Grazzini, Pieraccini, Parrini and Atzeni [7], the IQ modulator is a better choice since its dynamic range is better than that of the vector modulator. Consider Figure 2.11(a) which shows a block diagram of a vector modulator. The I and Q signals are used to control the up conversion of the RF_{in} signal. The power of the RF_{in} signal is proportional to the power at the output of the vector modulator RF_{out} and the I and Q inputs are merely used to control the amount of gain and phase that is changed towards the output. Figure 2.11(b) shows a block diagram of an IQ modulator. It is similar to that of a vector modulator, but the LO input to the IQ modulator has a limited input power range. The LO signal of the IQ modulator is also changed into a square wave before it is used. The magnitude of the output power is dependent on the I and Q signals only.

From the literature given in Beasly, Stove and Reits [1], Jiming, Xinjian and Zhijiu [4] Lin and Wang, [6] and Grazzini, Pieraccini, Parrini and Atzeni [7] it is found that the choice of modulator for the RPC is very important, since it directly determines the largest signal that can be cancelled. In Pursula, Kiviranta and Seppa [9], PIN diodes are presented as a possible up converting method, since their power handling capacity exceeds +20 dBm and their noise floor is limited only by the thermal noise floor. However, PIN diodes have a very slow reaction time to current control and cannot be used to down convert directly [9]. An IQ modulator is used throughout the rest of the report.

From Table 2.1, the next component in the RPC list is the coupler in the Rx path, which is used to sum the modulator's output with the RF input. In Stove [10], a 6 dB coupler is used in the preliminary tests, but later it is indicated that a different

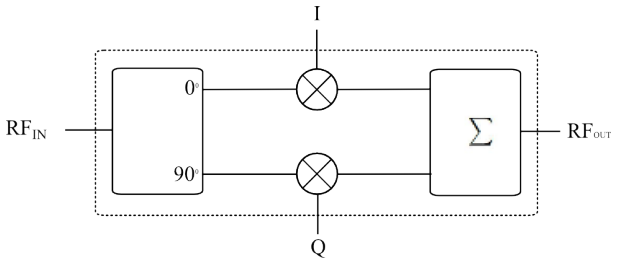

(a) Vector modulator block diagram.

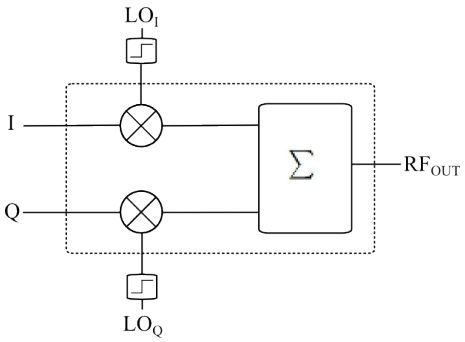

(b) IQ modulator block diagram.

Figure 2.11: Comparing vector modulators and IQ modulators.

coupler is used in the final system due to the limitation the coupler places on the power capabilities of the radar's receiver. Care should be taken when choosing the coupling value, since it will affect the RF input power of the radar by reducing the maximum signal power that can be cancelled. A method is needed of predicting the required coupling factor value to achieve a certain level of power input.

In Pursula, Kiviranta, and Seppa [9] a transfer function is derived for the closed loop system taking into account all the compensation terms for phase shift due to delay and parasitics in the signal path. If this is compared to the ideal derivation of an RPC in section 2.1, it is seen that the phase shift caused by transmission line and non-ideal modulators and demodulators has to be compensated for. This requires an analysis of the RPC which includes the transmission lines etc. Also, Pursula, Kiviranta and Seppa [9] determines an equation to calculate the sensitivity of the receiver by using the input referred noise power spectral density. However, no attempt is made to maximise these terms in order to obtain an optimum system. The importance of a wide dynamic range is mentioned in several articles [10], [6], [7], [9] and [8].

Finally, the phasor representation of the RPC control system is repeated in Figure 2.12. In this figure the assumption is made that the modulator's output is subtracted from the input, thus the phase difference of the two signals has to be zero. However in the system described in this section it is seen that a coupler is used to sum the modulator's output with that of the RF input. This means that the negative feedback has to be created by a 180 degree RF phase shift through the control loop. This 180 degree requirement is documented by several resources [10], [4], [5]. [6], [7], [9] and [8]. According to Stove [10] this 180 degree RF phase shift is allowed to vary

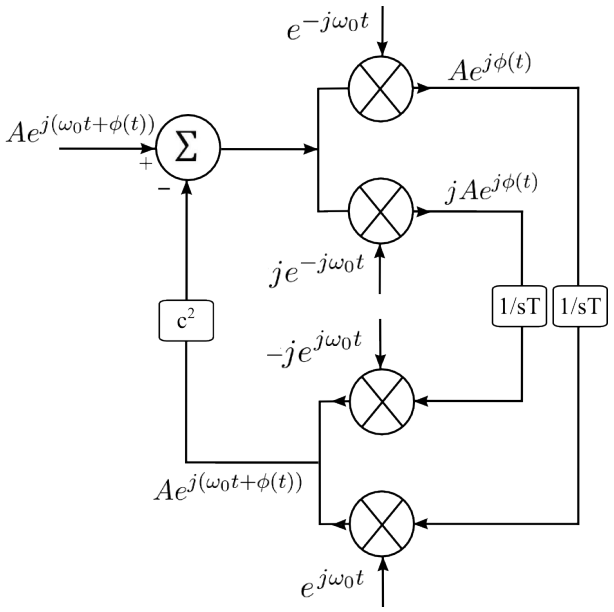

Figure 2.12: RF phasor representation of a first order integrator control system.

by about 90 degrees (absolute). This was noted in section 2.1 as the cross coupling between the I and Q baseband channels. A method of predicting the RF phase is required in order to remain within linear cross coupling region.

2.3 Spice analysis

The RPC discussed in the previous two sections is simulated using LTSpice. The LTSpice simulation was based on the assumption that the RPC had to be applied to an FMCW radar, thus the specifications listed in Table 2.2 was used as the simulated radar's values.

Table 2.2: Specifications of the FMCW radar that is used to simulate the IQ RPC.

Symbol	Frequency
f_0	2.45 GHz
Δf	100 MHz
f_m	130 Hz
f_b	100 Hz : 1 MHz

Figure 2.13 gives an overview of the LTSpice RPC block diagram. The FMCW radar transmitter is represented by a source and an antenna. The radar's receiver consists of a second antenna and the RPC. From section 2.1, the up conversion and down conversion is applied using as a modulator and demodulator since the RPC requires its baseband signal in quadrature. Once again a sawtooth wave is used as the modulating waveform. In order to understand the simulation each of the

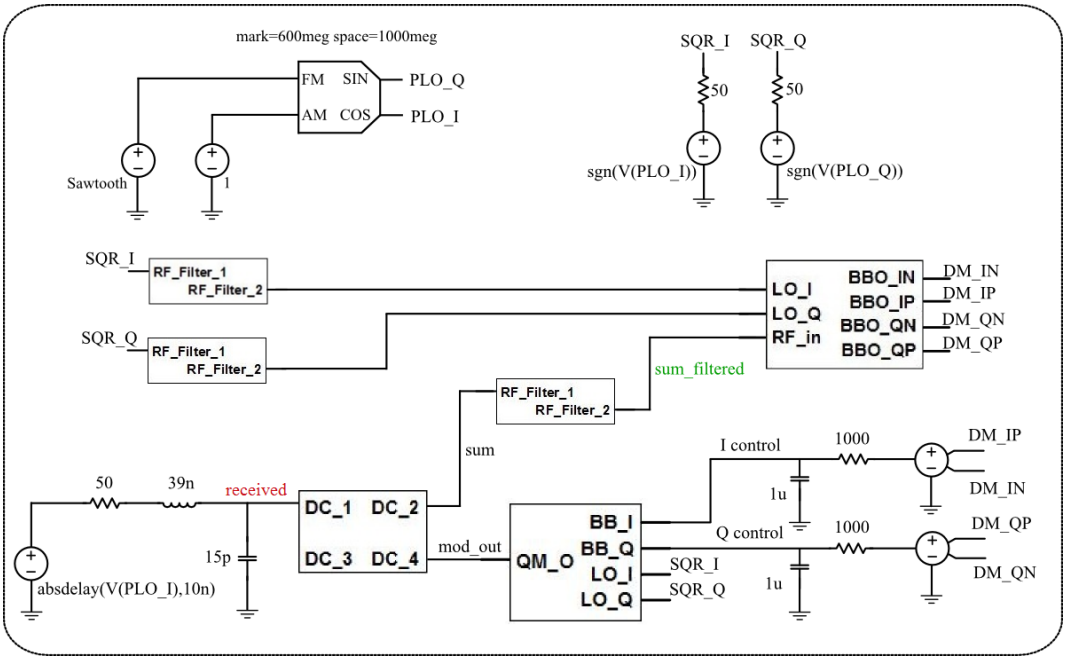

Figure 2.13: Block diagram illustrating the LTSpice transmitter and receiver of the FMCW radar using two antennas. The IQ Reflected Power Canceller is added to the receiver of the system.

components are explained separately. Finally, the combined LTSpice simulation is given with an explanation of the results.

2.3.1 Tx and Rx signals

Figure 2.14 shows the first of three LTSpice sections that are used to simulate the transmitted and received signals.

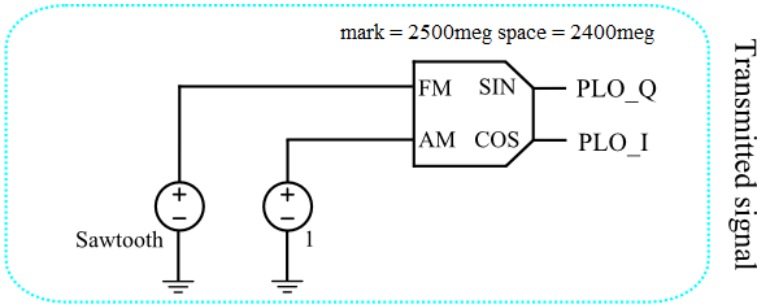

Figure 2.14: The LTSpice schematic diagram that is used to generate the FMCW chirp signal.

The transmitted signal in Figure 2.14 is generated with the help of a modulator block in LTSpice. In the LTSpice library it is described as a behavioural VCO (Voltage Controlled Oscillator) and modulator. The output is modulated by AM

and FM input voltages. This version supplies its outputs in quadrature (I and Q). The FM input is a voltage sawtooth waveform with a period of 130 Hz (f_m)which is indicated on Figure 2.15, while the AM input is simply unity gain. The output is a frequency chirp between 2400 MHz and 2500 MHz in quadrature which is also shown on Figure 2.15.

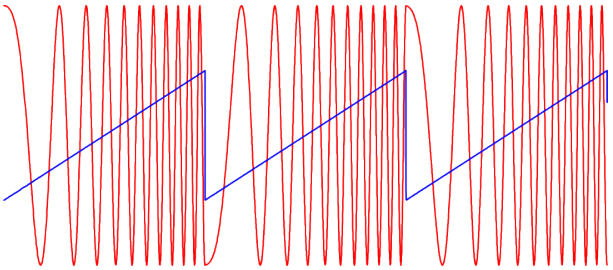

Figure 2.15: The transmitted FMCW chirp signal with its modulating waveform.

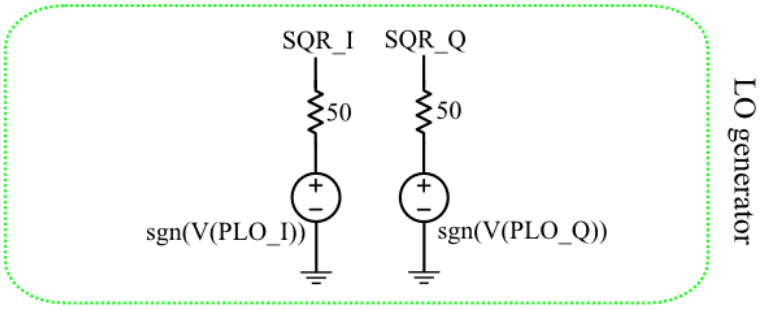

Figure 2.16: The LTSpice schematic diagram that is used to produce the quadrature LO signals with harmonics.

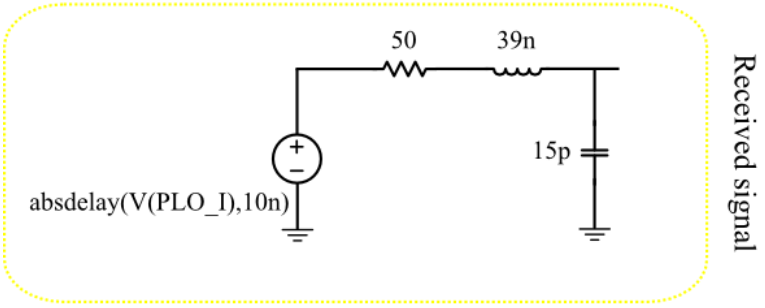

Figure 2.17: The LTSpice schematic diagram that is used to simulate the received signal of the FMCW radar.

Next, the transmitted signals are made into a square wave chirp by LO generator in Figure 2.16. This is done to simulate harmonics that would be present in a practical system. Finally, the received signal is generated in Figure 2.17 by applying a time delay to the transmitted signal after which a filter is used to reduce its amplitude. This strengthens the concept that the only difference between the transmitted and received signals of an FMCW radar is the time difference (and amplitude) which is indicative of the target's range.

2.3.2 Modulator and Demodulator

Figure 2.18 shows the LTSpice block diagram that is used as the IQ modulator, as well as the circuitry that is used to simulate the IQ modulator. The input to the IQ modulator is two baseband signals in quadrature (I and Q) together with its LO signal, also in quadrature. The output is the sum of the up converted I and Q baseband signals.

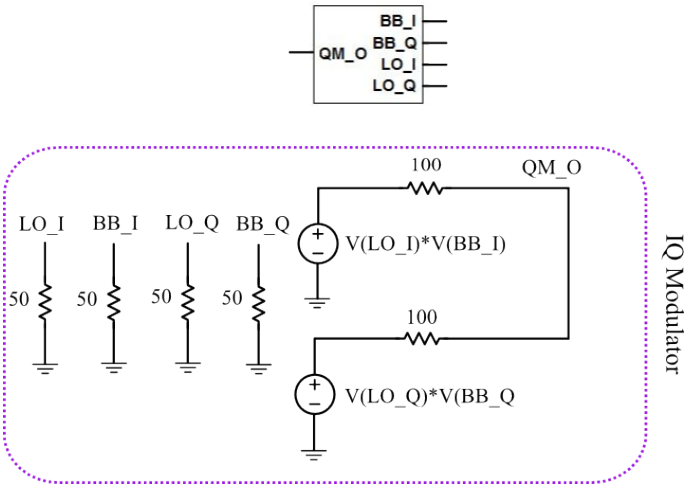

Figure 2.18: The LTSpice schematic representation of the IQ modulator.

Figure 2.19 gives the LTSpice block diagram of the IQ demodulator. The circuitry used to simulate the IQ demodulation is also shown. The inputs to the IQ demodulator are the quadrature LO signals as well as the single-ended RF input. The output of the IQ demodulator is the differential I and Q baseband signals ($IF_{I,Q}$).

2.3.3 RF filter

Figure 2.20 shows the LTSpice block diagram as well as the RF filter's circuit diagram. The filter is simply a low pass filter with S11 = −20 dB.

Figure 2.21 shows the magnitude response of S11 and S21 of the RF filter. The -3 dB cut off frequency is at 1300 MHz.

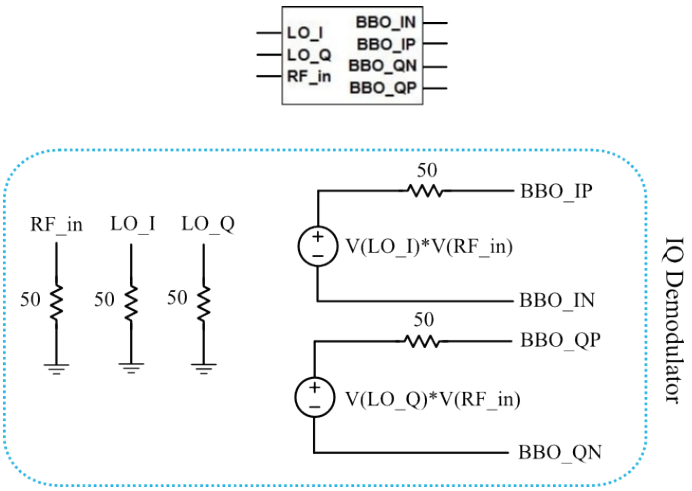

Figure 2.19: The LTSpice schematic representation of the IQ demodulator.

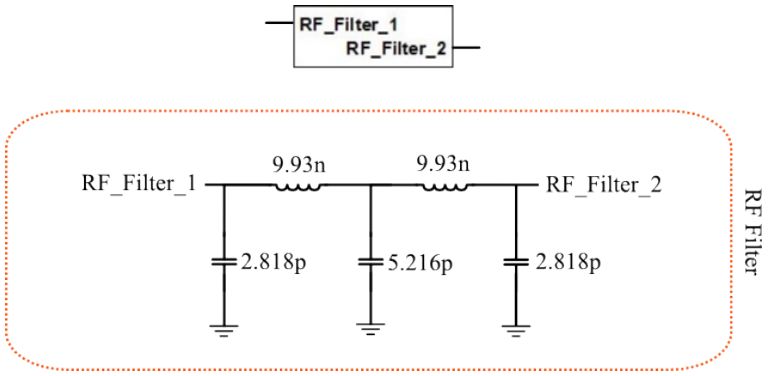

Figure 2.20: The LTSpice representation of the RF filter used in the simulation.

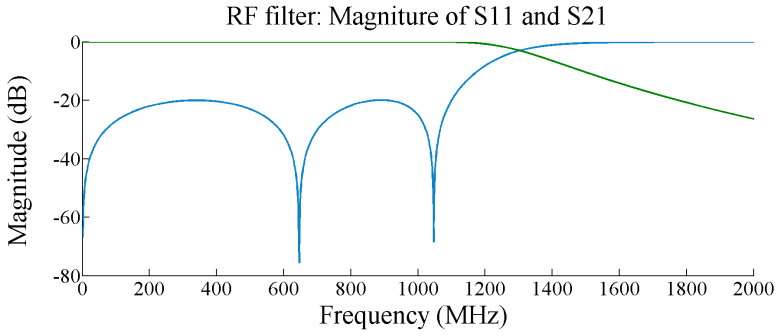

Figure 2.21: S11 and S21 of the RF filter in Figure 2.20.

2.3.4 Coupler

The coupler has a coupling factor of 10 dB. A very small amount of the power from the input port is lost towards the through port which can be calculated by $(1 - c^2)$ where c^2 is the coupling factor in linear units. The IQ modulator output power is

reduced by 10 dB and added to the through path of the coupler. Thus the input to the coupler (the input of the FMCW radar) is summed with the output of the IQ modulator (which has been reduced by 10 dB).

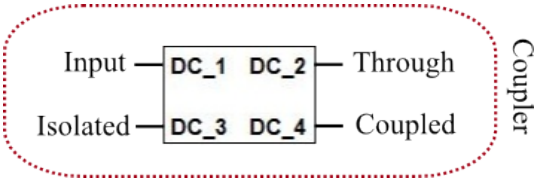

Figure 2.22: LTSpice block diagram representation of the 10 dB coupler used in the IQ Reflected Power Canceller simulation.

2.3.5 Integrator

The integrators are simulated as a low pass filter with high gain. This is a non-ideal integrator since it has a fixed amount of gain at DC, while a real integrator would have infinite gain at DC [11]. The non-ideal integrators are shown in Figure 2.23. The input to the integrators are the outputs from the IQ demodulator. The gain necessary to simulate the integrators is applied at the summation of the differential inputs.

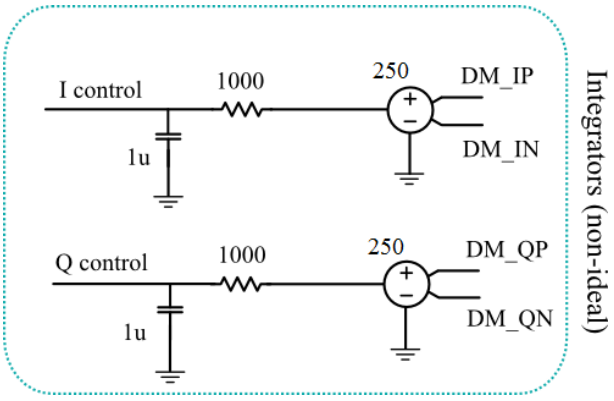

Figure 2.23: The LTSpice representation of the non-ideal integrators used in the IQ RPC simulation.

2.3.6 IQ Reflected Power Canceller

Figure 2.24 repeats the LTSpice diagram used to simulate an RPC. This simulation utilises components that would be present in a practical system and has been described in the previous sections.

The LTSpice simulation's closed loop response as discussed in section 2.1 is shown in Figure 2.25 where the cancellation bandwidth is also indicated. The cut off frequency is about 10 kHz and therefore a target that has a baseband frequency above 10 kHz will not be cancelled. Two results are given in this section, one for a close

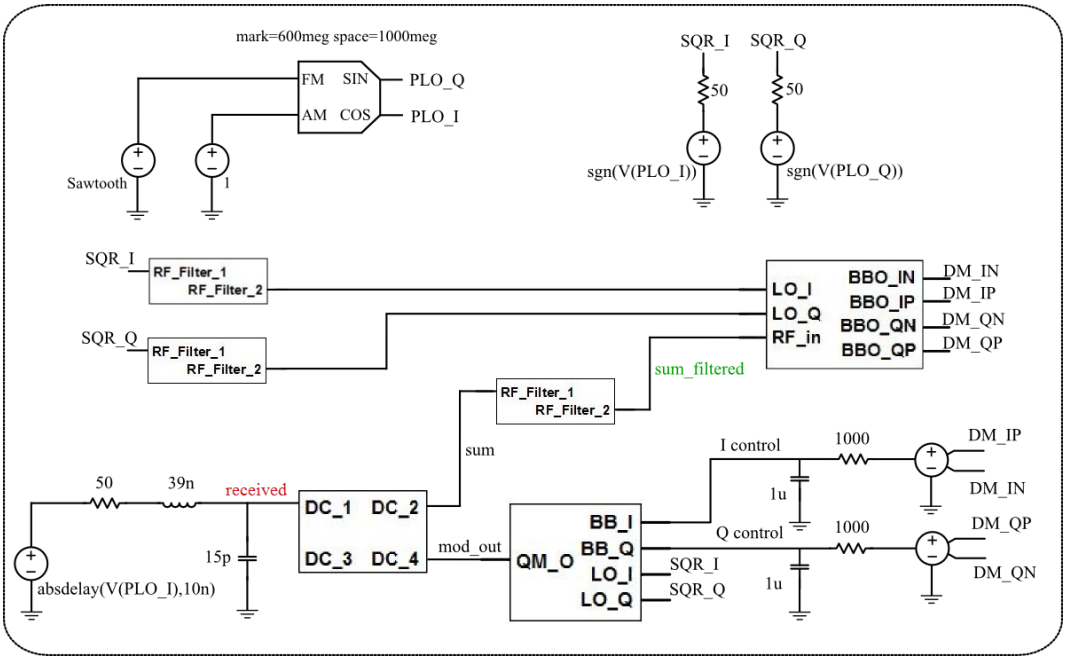

Figure 2.24: LTSpice diagram of IQ Reflected Power Canceller containing all the components of a practical system.

range reflection where it is expected that the signal will be cancelled and the other result is presented for a signal that does not fall within the cancellation bandwidth. Equation 2.3.1 is used to calculate the range to the target for a specific time delay while equation 2.3.2 is used to calculate whether this range is within the cancellation bandwidth.

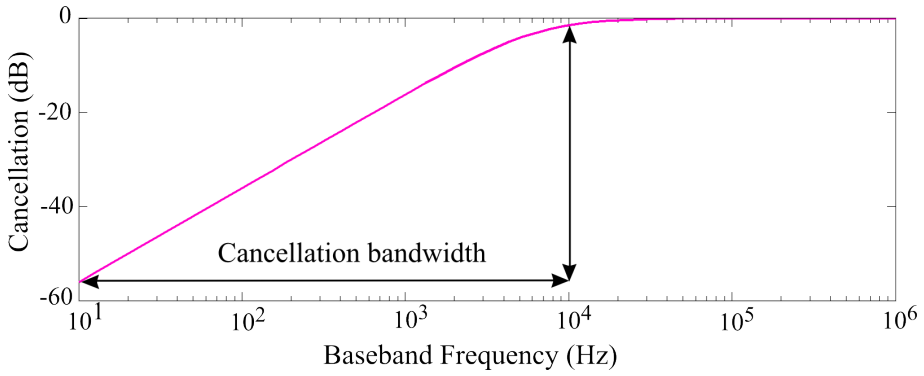

Figure 2.25: Cancellation bandwidth of LTSpice simulation with an open loop gain K_I of 40000.

$$t_{delay} = \frac{2R}{c} \tag{2.3.1}$$

$$f_b = \frac{2Rf_m\Delta f}{c} \tag{2.3.2}$$

For the plot given in Figure 2.26 a 10 ns delay is applied to the received signal. The returned signal falls within the cancellation bandwidth since the IF frequency is calculated as 1.3 kHz. It can clearly be seen in Figure 2.26 that the $V(sumfiltered)$ signal has been reduced by a large amount.

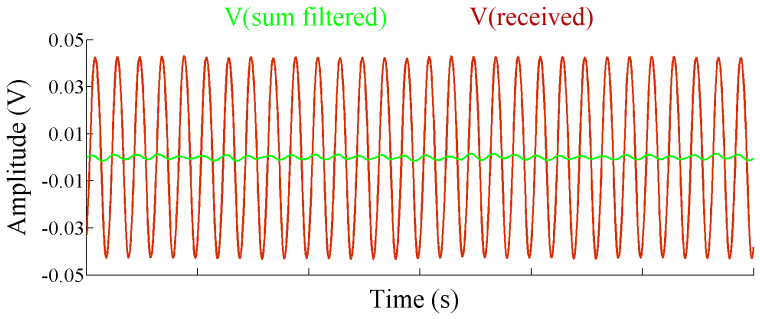

Figure 2.26: The signal at the output of the coupler is reduced with reference to the amplitude of the received signal.

Figure 2.27 shows the result of when a delay of 5000 ns was placed on the received signal. The delay is long enough for the received signal to not fall within the cancellation bandwidth with an IF frequency of 65 kHz. From Figure 2.27 it is clear that the amplitude of $V(sumfiltered)$ is unchanged and still follows that of $V(received)$.

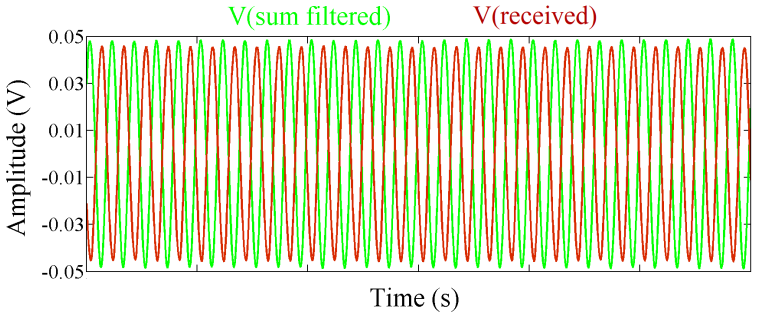

Figure 2.27: The signal at the output of the coupler is unchanged with reference to the received signal. This is due to the "target's" range that does not fall within the cancellation bandwidth.

From the above results, it is found that the RPC performs as predicted.

2.4 Conclusion

This chapter has introduced a theoretical RPC, with the help of an ideal mathematical model, which was analysed and simulated with the help of both MATLAB and LTSpice. In the MATLAB simulation, the control system was described and the cancellation bandwidth of an RPC was first introduced. Next the LTSpice simulation

was broken into its separate components, where each component was described with reference to its use in the simulation. The cancellation bandwidth was calculated for the LTSpice simulation using the given equations. This allowed for the magnitude vs. frequency graph in Figure 2.25 to be compared with the LTSpice RPC's output in Figures 2.26 and 2.27. By using simulated components, the concept of the RPC was found to be plausible. The aim of the next chapter is to translate this theoretical knowledge into a practical system.

Chapter 3

Practical considerations

An ideal model of an RPC was derived and simulated in Chapter 2. A literature review was also carried out and some practical considerations were identified which could influence the design of an RPC. This chapter aims to describe these practical considerations:

- Investigating practical modulators and demodulators.
- Considering the RF phase influence of the RPC's components, specifically the modulator and demodulator.
- The dynamic range of the RPC with an introductory explanation of the terms that influence the dynamic range.

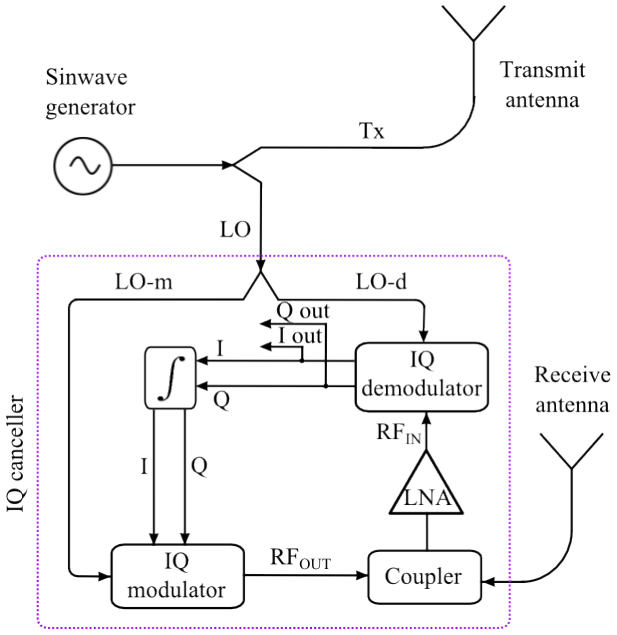

Figure 3.1: Block diagram of a theoretical IQ Reflected Power Canceller implemented for an FMCW Radar using the two antenna configuration.

The block diagram of the theoretical RPC is given in Figure 3.1 to serve as a reference against which the practical system can be compared. An RPC using an modulator and demodulator is discussed first. Secondly, adding an RPC to a radar receiver will impact the receiver's maximum power handling capabilities, as well as its noise characteristics. It is important that the RPC adds the minimum amount of interference within the current system's dynamic range.

3.1 Modulator/Demodulator attributes

In the RPC derivation in Chapter 2, the modulator and demodulator were used as ideal components, and they did not contribute any extra RF phase to the total phase through the loop. The modulator and demodulator are discussed in this section as practical components. This is achieved by using several modulators and demodulators as examples and comparing their applied attributes. A practical modulator model is used to identify the relevant parts of the modulator which would influence the RPC.

3.1.1 Practical IQ modulators

Consider the modulator model used in Chapter 2 again (Figure 3.2). It was assumed that the LO's I and Q inputs were ideally generated signals: no phase delays due to transmission lines or phase offsets due to its LO's quadrature generation. The product options in the next subsection investigate the non-ideal behaviour of the modulators and demodulators. The method for splitting the LO signal into its quadrature components merits further investigation.

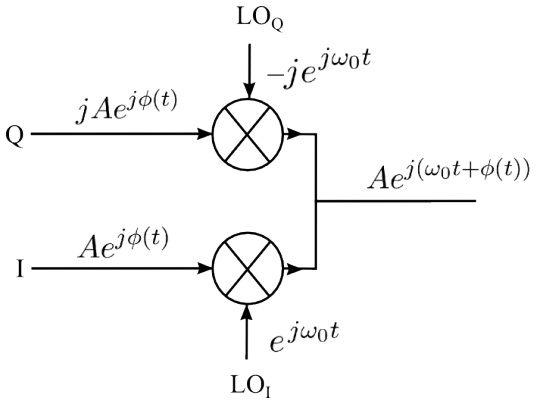

Figure 3.2: Up conversion of I and Q baseband input signals using an ideal modulator.

3.1.2 Product options

This section provides a list of modulators and demodulators that can be used for the RPC. The criteria that are listed to compare the different components are the $P1dB$ output power, noise floor and the method used for LO quadrature generation. $P1dB$ refers to the output power of a component where the output power is 1 dB

below the straight line expected value. The $P1dB$ and noise floor are considered further in the dynamic range introduction in section 3.2. The modulators are listed in Table 3.1 and the demodulators are given in Table 3.2.

Table 3.1: Comparing IQ modulators, with f_{LO} = 2600 MHz, P_{LOM} = 0 dBm

Part number	P1dB (dBm)	Noise floor (dBm/Hz)	LO quadrature generation
ADL5375	9.6	-159	Polyphase splitter
LTC5588-1	11.4	-160.5	Polyphase splitter
HMC697LP4	8	-165	Polyphase splitter
TRF370317	13	-163	Polyphase splitter
ADL5385	8	-160	Digital

Table 3.2: Comparing IQ demodulators, with f_{LO} = 260 0MHz, P_{LOD}= 0 dBm

Part number	P1dB (dBm)	Noise figure (dBm/Hz)	LO quadrature generation
ADL5380	11	12.3	Polyphase splitter
LTC5585	15.5	13.6	Polyphase splitter
ADL5387	12.8	16.5	Digital

The manufacturers whose product options were researched are: Analog Devices, Linear Technologies, Hittite and Texas Instruments. Manufacturers use different methods to produce their modulators and demodulators. The main differences occur in the generation of the quadrature LO signals, where two LO phase splitter methods were observed [12]. The method of interest is the polyphase splitter. There are several topologies in which the polyphase splitter can be applied, but only the topology shown in Figure 3.3 is considered [13].

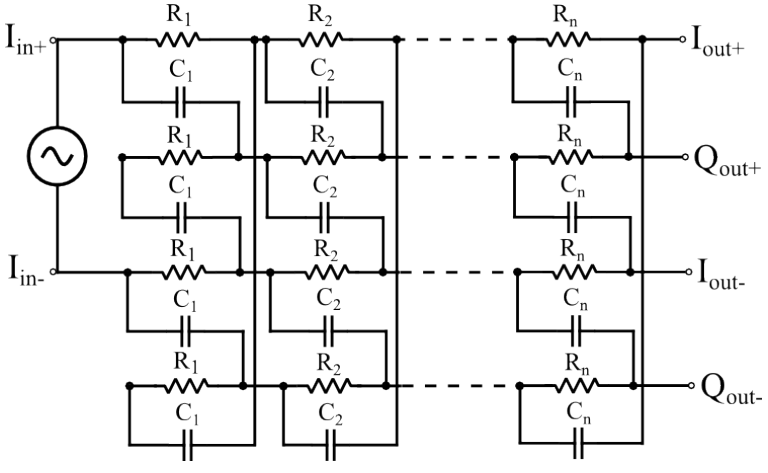

Figure 3.3: Polyphase filter topology.

For this topology, the polyphase splitter accepts a real differential input. Depending on the order of the filter and the centre frequency of each stage of the polyphase splitter, the polyphase splitter's output within the chosen bandwidth will have an equal amplitude and a 90 degree phase shift. This is demonstrated with a derivation of a first order polyphase splitter's transfer function.

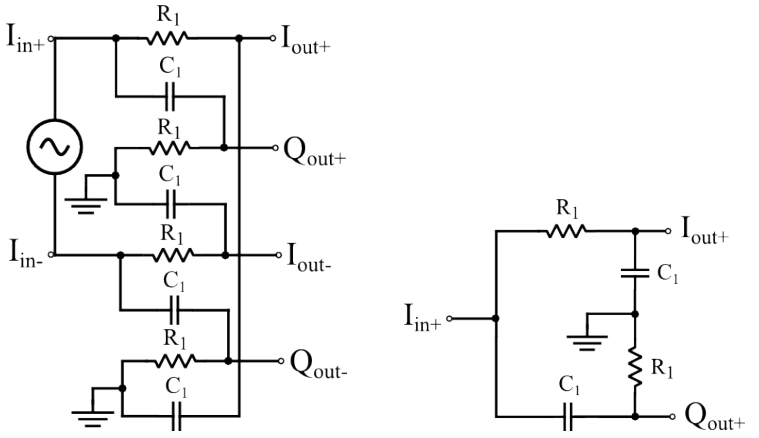

(a) First order polyphase filter.

(b) Simplified first order polyphase filter model.

Figure 3.4: Polyphase filter.

Consider a first order polyphase filter as in Figure 3.4(a). This model can be reduced to the model given in Figure 3.4(b). The transfer function from I_{in}^{+} to I_{out}^{+} and Q_{out}^{+} is given in equation 3.1.1 which is a low pass filter for $\frac{I_{out}^{+}(j\omega)}{I_{in}^{+}(j\omega)}$ and a high pass filter for $\frac{Q_{out}^{+}(j\omega)}{I_{in}^{+}(j\omega)}$ [14].

$$\begin{aligned} \frac{I_{out}^{+}(j\omega)}{I_{in}^{+}(j\omega)} &= \frac{1}{j\omega R_1 C_1 + 1} \\ \frac{Q_{out}^{+}(j\omega)}{I_{in}^{+}(j\omega)} &= \frac{j\omega R_1 C_1}{j\omega R_1 C_1 + 1} \end{aligned} \tag{3.1.1}$$

The magnitude and phase response of the two transfer functions is given in Figure 3.5. From this figure it is seen that the I_{out}^{+} and Q_{out}^{+} outputs have an equal magnitude and 90 degree relative phase shift for one frequency point. If more stages are added in cascade, the bandwidth across which the polyphase splitter has an equal amplitude and 90 degree phase difference output broadens.

The magnitude and phase output of a third order polyphase splitter is shown in Figure 3.6. The 90 degree phase shift between the I and Q output is indicated on Figure 3.6.

The order of the polyphase splitter used to produce the LO signal will have an effect on the total phase contribution of the modulator and demodulator in the RPC. The phase delay and the order of the polyphase splitters will have an effect on the required 180 degree phase shift of the RPC. This, in turn, will affect the bandwidth across which the canceller will work.

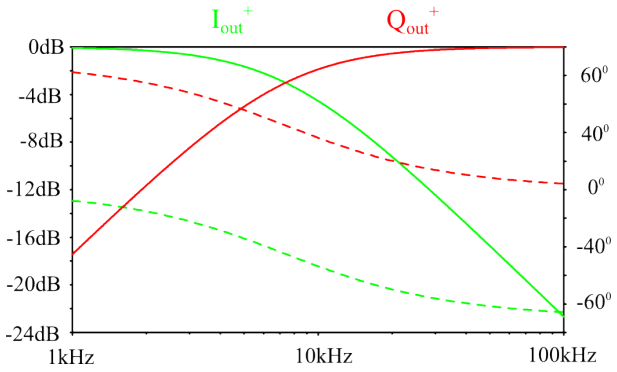

Figure 3.5: Magnitude and phase response of first order polyphase filter outputs.

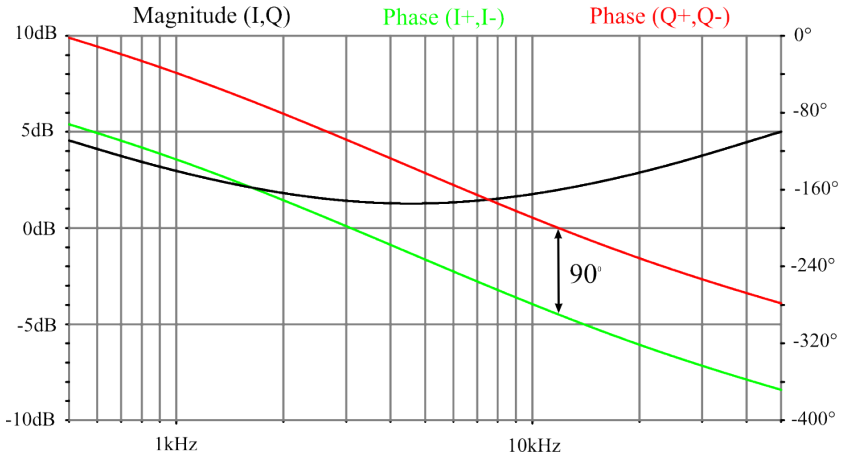

Figure 3.6: Polyphase filter output where the magnitudes of the two outputs is equal and the phase differs by 90 degrees between 1 kHz and 20 kHz.

3.1.3 LO generation and polyphase splitters

A practical consideration for the RPC is whether it will limit the modulating bandwidth of the FMCW radar. In Chapter 2 it was established that the phase through the RPC control loop has to be shifted by 180 degrees, with a ±45 degree RF phase shift tolerance. This constraint is accomplished easily if the modulator and demodulator's LO polyphase network have the same phase slope. If the phase slopes of the modulator and demodulator are very different, the phase through the RPC's control loop will change at a different rate as the frequency of the transmitted and received signal changes.

A third and a fifth order polyphase splitter are simulated in LTSpice. The two polyphase splitters' phase response in Figure 3.7 shows the difference in their phase slopes. If the phase response in Figure 3.7 is considered, the time delay caused by the polyphase splitters can be calculated as in equation 3.1.2 [3].

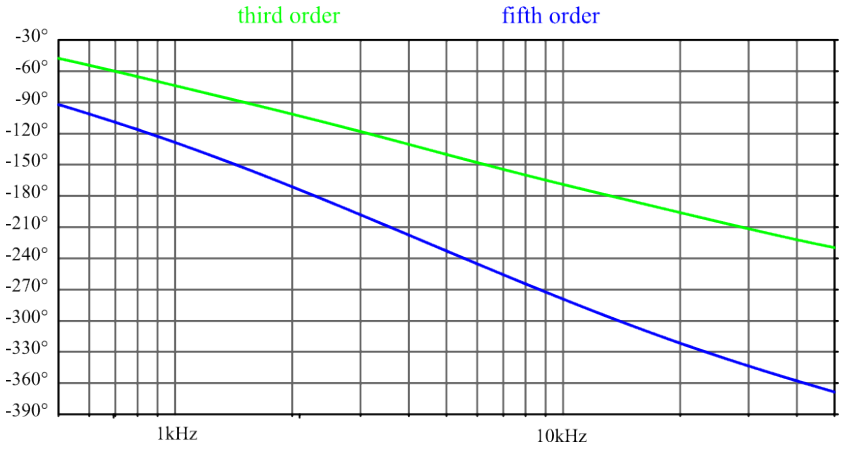

Figure 3.7: The figure shows the phase response of two polyphase splitters. The first of which is a third order splitter and second a fifth order. The phase responses clearly indicate the different gradients of the phase for the two polyphase splitters.

$$\begin{aligned} e^{-sT} &= e^{-j2\pi\Delta fT} \\ \Delta\theta &= 2\pi\Delta fT\frac{180}{\pi} \\ T &= \frac{\Delta\theta}{360\Delta f} \end{aligned} \tag{3.1.2}$$

where T refers to a time delay, Δf is the change in frequency over which the change in phase θ is taken. The responses of the two polyphase filters do not follow the same gradient and from equation 3.1.2 it is seen that two different order filters will affect the total RF phase of the loop differently for varying frequency values. If the modulator and demodulator use polyphase splitters of a different order, this would add a limitation to the bandwidth of the RPC and thus the bandwidth that the FMCW radar can transmit.

3.1.4 Product choice

In the case of the modulator, from the specifications shown in Table 3.1, the ADL5375 and the TRF370317 show the most promise. From Table 3.1 it was found that both these modulators use polyphase splitters to produce their LO signals [12; 15].

Of the appropriate demodulators listed in Table 3.2, only the ADL5380 makes use of a polyphase splitter to produce its quadrature LO signals. In order to maintain control over the RF phase in the RPC, the ADL5375 and ADL5380 are chosen. In the datasheet of the demodulator (ADL5380), it is not specified whether the noise figure is given as a double sideband or a single sideband value. The double sideband noise figure will have a 3 dB higher noise figure than that of the single sideband noise figure [16]. An assumption is thus made that the noise figure given in the datasheet of the ADL5380 is for a single sideband measurement.

3.1.5 RF phase error

Even though the modulator and demodulator were chosen to minimise the risk of different order polyphase splitters causing a reduced modulation bandwidth, the RF components in the RPC (including the modulator and demodulator) still contribute phase delays not taken into account in the ideal RPC derivation. The phase delay caused by these polyphase splitters will still have to be taken into account when the practical model is derived.

The loop phase calculations are developed in detail in Chapter 5, where the phase contribution of all the components is taken into account.

3.2 Dynamic range

Ideal radar receivers are required to amplify the received signals without adding noise or any form of distortion, as well as to reject interfering signals so that the required information can be optimally detected [17]. Another requirement of a radar receiver that is more relevant to this discussion is that it has to provide a large dynamic range to accommodate large clutter signals [17]. Important concepts related to the dynamic range of the receiver include noise, noise figure, Minimum Detectable Signal (MDS) and the maximum receivable signal (large clutter signals).

The dynamic range of a radar receiver containing an RPC is described on a systems level in this section. All of the important definitions surrounding the concept of dynamic range is introduced. The first subsection is dedicated to describing dynamic range with a component example, this is followed by an explanation of noise and noise figure as it is encountered for different components.

Chapter 4 contains a detailed analysis of the impact of adding an RPC to a receiver on the dynamic range of that receiver. The aim of this section is to introduce the concept of dynamic range, noise and the effect of an RPC on a practical system.

3.2.1 What is dynamic range

The dynamic range of a system can be characterised by a set of receiver measurements: noise figure, second-order intercept, third-order intercept, 1-dB compression, phase noise, internal spurs and bandwidth. These measurements will indicate the system's ability to handle a wide range of signal strengths, from the weakest to the strongest [18]. The receiver measurements that are mentioned here are all very important; however, for this analysis, focus falls on two measurements in particular: Noise floor and 1-dB Compression. For the RPC to have a maximised dynamic range, all of its components should work within their linear output power regions.

3.2.2 1-dB Compression

In order to define the RPC's dynamic range with respect to the components in the system, it is necessary first to consider what the parameters of each component are. The 1 dB Compression point is described with the help of an example and Figure 3.8.

Consider a realistic microwave amplifier with 10 dB gain. Due to noise generated by the amplifier itself, there will always be a certain amount of noise power generated

by the circuit, even when there is no input power [3]. Figure 3.8 illustrates the dynamic range of a realistic amplifier as discussed in [3].

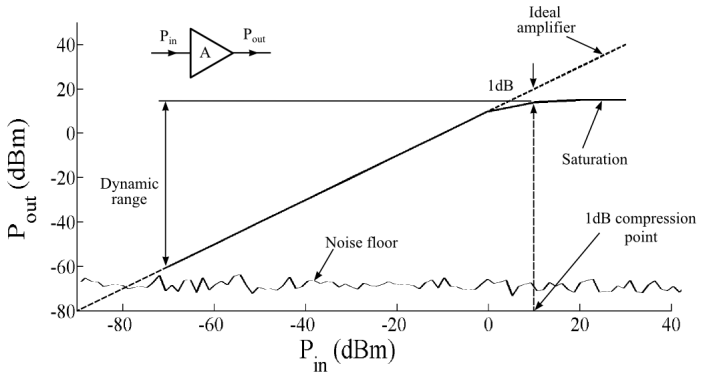

Figure 3.8: The dynamic range of an amplifier is indicated with reference to its noise floor and 1 dB compression point.

The noise floor indicates the lowest signal that can be detected. The 1 dB compression point is also shown on this figure. This point is the point at which the amplifier starts to saturate and it is defined as the point where the output power is 1 dB below the linear predicted output value [3]. Together, these values indicate the dynamic range of the component. This explanation is also valid for an entire system which consists of a range of components each with its own power and noise characteristics.

By keeping the above definition in mind, Chapter 4 derives the dynamic range of the RPC by taking into account the limitations of each component in the system. Most of the components in the RPC have a similar Pout to Pin graph as that shown in Figure 3.8. In the combination of components used for the RPC, there is only one that will reach its 1 dB compression point first. The component that reaches its 1 dB compression point first is referred to as the critical component. The aim of the design is to maintain a large dynamic range by considering the limitations of each component and maximising the result.

3.2.3 Noise and noise figure

This subsection aims to give a very brief overview of how to calculate noise and noise figure for different types of component and how these quantities can be used together. The typical components that are used to assemble an RPC are shown in Figure 3.9. First, the noise floor of the modulator is analysed, followed by the noise figure of the demodulator and LNAs. Lastly, the noise contribution of the fully differential operational amplifier is investigated.

The modulators present their noise contribution as the noise floor at its output. This value is a noise power, characterised by equation 3.2.1, where k is Boltzmann's constant (1.38 x $10^{-23} J/K$), T_e is the effective noise temperature in Kelvin of the circuit and B is the bandwidth in hertz [19].

$$N = kT_eB \tag{3.2.1}$$

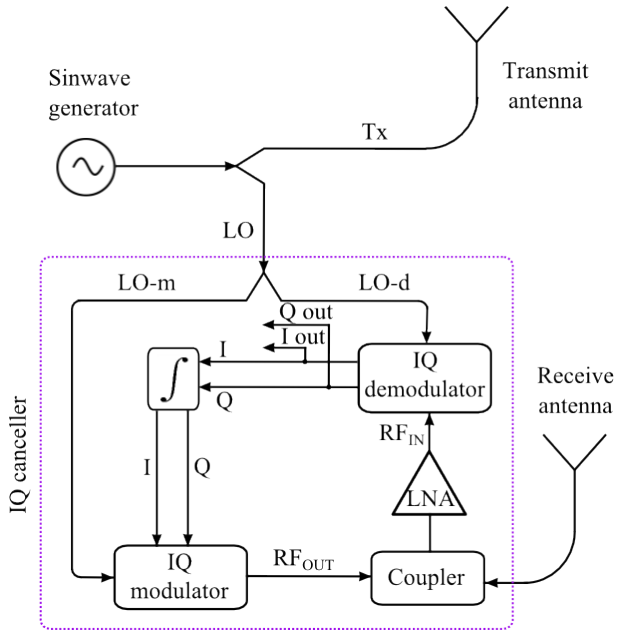

Figure 3.9: Block diagram showing the components in an IQ Reflected Power Canceller.

The units used when referring to the noise floor are dBm/Hz which would be 10 $log(N) - 10$ $logB$ where N is calculated as in equation 3.2.1. Uncorrelated noise power has the characteristic of being an additive quantity [3]. For a two stage cascaded system as given in Figure 3.10, the total noise N_0 is the sum of each component's noise multiplied by its gain, as shown in equation 3.2.2. As the noise moves through the system from N_i to N_1, the input noise is multiplied by the gain G_1 and the noise generated in system 1 is also multiplied by the gain G_1. This process is repeated for each cascaded system down the line [3].

$$\begin{aligned} N_o &= G_2 N_1 + G_2 k T_{e2} B \\ &= G_2(G_1 k T_0 B + G_1 k T_{e1} B) + G_2 k T_{e2} B \end{aligned} \tag{3.2.2}$$

Where kT_0B equals the input noise power.

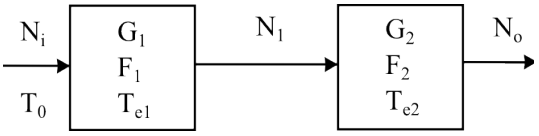

Figure 3.10: Two cascaded networks illustrating the additive property of noise power.

The demodulator and LNA present their noise contributions in the form of the noise figure (NF). The noise figure of a network, as defined by [20], is a ratio of the signal-to-noise ratio at the input to the signal-to-noise ratio at the output of a system or component. A perfect amplifier would amplify only the signal and the noise at its input, but a real amplifier would add some of its own internal noise. A low noise figure means that the component has added a very small amount of noise [21]. The

definition of noise figure is given in equation 3.2.3 [22]. Noise figure is defined for a system working under matched conditions. The noise source is modelled as a resistor at room temperature ($T_0 = 290$ K) [3].

$$NF = \frac{(S/N)_{in}}{(S/N)_{out}} \tag{3.2.3}$$

where $(S/N)_{in}$ is the input signal to noise power ratio and $(S/N)_{out}$ is the output signal to noise power ratio. Figure 3.11 gives a two port representation of a noisy system driven by a signal source with matched input resistance ($R = 50\ \Omega$ at $T = 290\ K$).

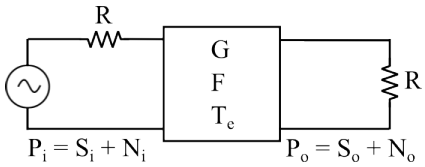

Figure 3.11: Model of a noisy two port system.

The noisy system has a gain G, a bandwidth B and an equivalent noise temperature T_e. The input signal power is represented by S_i and the output signal power $S_o = G\ S_i$. The noise power of the source is given by

$$N_i = kT_0B$$

Using the cascaded system from Figure 3.10, the output noise power is calculated as

$$\begin{aligned} N_o &= N_iG + kT_eGB \\ &= kGB(T_0 + T_e) \end{aligned}$$

Now the signal and noise powers can be applied to equation 3.2.3 and the noise figure of the noisy system in Figure 3.11 can be calculated as in equation 3.2.4.

$$\begin{aligned} NF &= \frac{S_i}{kT_0B}\frac{kGB(T_0 + T_e)}{GS_i} \\ &= \frac{T_0 + T_e}{T_0} \\ &= 1 + \frac{T_e}{T_o} \end{aligned} \tag{3.2.4}$$

If the two stage cascaded system in Figure 3.10 is considered again, the equivalent noise figure contribution of the cascaded system can be calculated using equation 3.2.5. With the input noise power $N_i = kT_0B$, and the output noise power equals equation 3.2.2 $N_o = G_2(G_1kT_0B + G_1kT_{e1}B) + G_2kT_{e2}B$ and the output signal power $S_o = G_1G_2S_i$.

$$
\begin{aligned}
NF_{cas} &= \frac{(S/N)_{in}}{(S/N)_{out}} \\
&= \frac{S_i}{kT_0B}\frac{G_2(G_1kT_0B + G_1kT_{e1}B) + G_2kT_{e2}B}{G_1G_2S_i} \\
&= \frac{G_1T_0 + G_1T_{e1} + T_{e2}}{T_0G_1} \\
&= 1 + \frac{T_{e1}}{T_0} + \frac{T_{e2}}{T_0G_1} \\
&= NF_1 + \frac{NF_2 - 1}{G_1}
\end{aligned}
\tag{3.2.5}
$$

Equation 3.2.5 can be expanded for a cascaded network that consists of more stages. However, each cascaded stage that is added to Figure 3.10 will have a weaker influence on the total noise figure, since each added stage's noise figure is divided by the preceding stages' compounded gain [3].

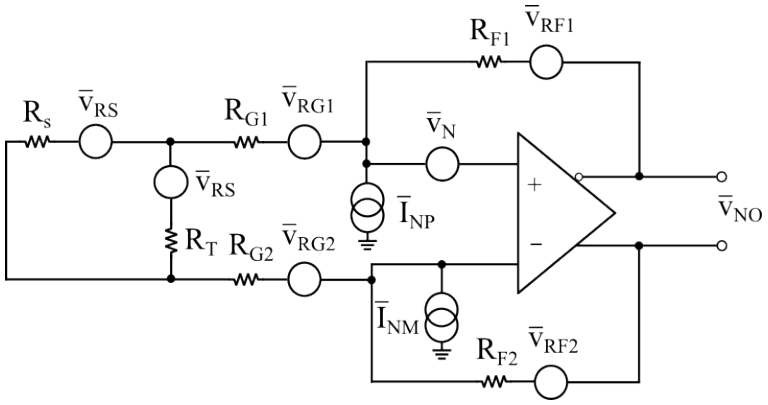

Figure 3.12: Fully differential operational amplifier model for calculating total noise figure.

Finally, the fully differential operational amplifier presents its noise in the form of an input referred voltage noise v_N with units $nV/\sqrt{Hz}$ and input current with units $pA/\sqrt{Hz}$ [23]. The noise voltage is modelled as a voltage source at the non inverting input of the operational amplifier, while the current noise is modelled as a current source from the non inverting and the inverting input to ground [24]. As discussed previously, noise is more generally presented in the form of noise figure [23]. However, it is not a trivial matter to obtain the noise figure of an operational amplifier since the noise figure is dependant on the source impedance levels, the feedback network and the device characteristics [23]. Figure 3.12 shows a fully differential amplifier noise model [24]. The output referred noise voltage density v_{NO} is indicated on the figure. Each resistor's noise contribution is indicated as an equivalent noise voltage source [24].

With operational amplifiers it is easier to work with voltage and current noise spectral density, rather than the power spectral density, since unmatched conditions are easier to manage using the voltage noise spectral density [23]. Uncorrelated voltage noise spectral densities add using the root sum squares. This is the only

noise considered in the following derivation because correlated noise sources usually contribute less than 10 - 15 percent of the total noise [25].

The definition of noise figure in terms of voltage noise spectral density is given by equation 3.2.6 [23]:

$$NF = \frac{v_{NO}^2}{v_{SO}^2} \tag{3.2.6}$$

First an equation for the output voltage noise spectral density (v_{NO}^2) is derived, followed by a derivation of the output voltage noise spectral density due to the source only (v_{SO}^2). In order to derive the output noise voltage the model in Figure 3.12 has to be simplified. The source impedance can be transformed into its thevenin equivalent

$$R_{TH} = \frac{R_S \ R_T}{R_S + R_T}$$

where the new noise model is given in Figure 3.13. The equivalent input impedance seen by the inverting and non inverting inputs of the operational amplifier is given by

$$R_{Geq} = R_G + \frac{R_{TH}}{2}$$

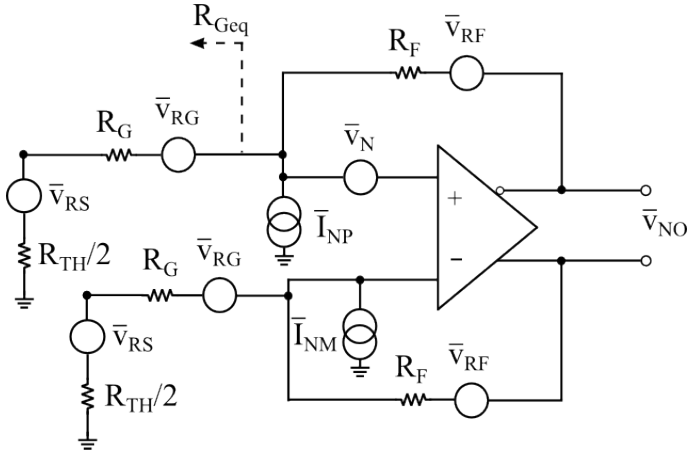

Figure 3.13: Fully differential operational amplifier model for calculating total noise figure.

The uncorrelated output referred noise voltage can be broken into two parts: the thermal noise of the resistive components in the feedback network (v_{FB}) and the noise added by the operational amplifier (v_{opamp}).

$$v_{NO} = \sqrt{v_{FB}^2 + v_{opamp}^2} \tag{3.2.7}$$

The noise contribution of a resistor is calculated using the Rayleigh-Jeans approximation $v_n = \sqrt{4kTBR}$. This equation is valid while hf « kT, where h is Planck's constant, k is Boltzmans's constant and K is the temperature in Kelvin.

The noise due to the feedback network can be calculated as in equation 3.2.8. Note that the output referred voltage is being calculated, thus all noise created before the feedback circuit is multiplied by the equivalent noise gain:

$$G_{FB} = \frac{R_F}{R_{Geq}}$$

$$\begin{aligned} v_{FB}^2 &= 2(\sqrt{4kTR_F})^2 + 2(\sqrt{4kTR_G})^2 G_{FB}^2 + 2(\sqrt{4kTR_{TH}/2})^2 G_{FB}^2 \\ &= 4kT2R_F + 4kT2R_G(\frac{R_F}{R_{Geq}})^2 + 4kTR_{TH}(\frac{R_F}{R_{Geq}})^2 \end{aligned} \tag{3.2.8}$$

Next, the total output referred noise voltage generated by the operational amplifier only is calculated in equation 3.2.9. This calculation is only for uncorrelated noise, thus the current noise I_{NM} and I_{NP} only contributes noise voltage due to the feedback resistors R_F.

$$v_{opamp}^2 = v_N^2(1 + \frac{R_F}{R_{Geq}})^2 + I_{NP}^2 R_F^2 + I_{NM}^2 R_F^2 \tag{3.2.9}$$

The derivation for the output spectral noise voltage density due to the source only is found as follows:

$$\begin{aligned} v_{SO}^2 &= \sqrt{4kTR_s}^2(\frac{R_F}{R_{Geq}})^2(\frac{R_T}{R_S + R_T})^2 \\ &= 4kTR_s G_{FB}^2(\frac{R_T}{R_S + R_T})^2 \end{aligned} \tag{3.2.10}$$

where $\sqrt{4kTR_s}$ is the noise voltage due to the source resistor only, G_{eq} translates the input referred noise voltage into an output referred value and $\frac{R_T}{R_S+R_T}$ is used for voltage dividing the noise gain G_{eq}.

It is useful to describe the differential amplifier's noise in terms of its noise figure in order to compare its noise contribution with that of the other components. The equation for this calculation is given in 3.2.11 where v_{NO} is calculated using equation 3.2.7 and v_{SO} is calculated using equation 3.2.10 [24].

$$NF_{diffamp} = \frac{v_{NO}^2}{4kTR_S G_{FB}^2(\frac{R_T}{R_S+R_T})^2} \tag{3.2.11}$$

Note that the noise figure is calculated as a linear quantity in this section. The dB quantity of the noise figure can be calculated by using $F = 10logNF$ [3]. When the dB quantity is used, this will be explicitly stated.

3.3 Conclusion

In conclusion, some practical considerations with the implementation of an RPC have been identified. Through the course of this chapter, a modulator and demodulator could be chosen for the RPC by comparing the attributes of the available products. The modulator and demodulator contributes to the RF phase through the RPC's control loop. The concept of non-ideal behaviour in the RPC's RF phase

due to delays in transmission lines was introduced. The RPC's influence on the dynamic range of the radar has been described in terms of maximum power handling capabilities and noise contributions.

Chapter 4

Dynamic range: Power calculations

Chapter 3 introduced practical considerations which affect the RPC. One of these practical considerations included the effect the RPC will have on the dynamic range of the radar's receiver. The aim of this chapter is to derive a set of equations to produce an RPC with an optimised dynamic range, in order to reduce noise contributions and improve the maximum receivable power to the receiver. These equations are derived by considering the maximum power handling capabilities of each component in the RPC system as well as each component's contribution to the total noise.

The dynamic range equations are developed, starting first at a system without an RPC, followed by the set of equations for a system with an RPC and finally the results of these calculations are interpreted and presented in the form of graphs and tables. The results provide a means of determining an optimised system by choosing different combinations of components and comparing their combined results. It has already been concluded in section 3.1.4 that the ADL5375 and the ADL5380 are to be used as the modulator and demodulator, respectively. The values obtained from their respective datasheets are the only set values in the calculations. Unless otherwise specified, all of the symbols used in the derivations throughout this chapter refers to their linear quantities. It is important that all the components work in their undistorted power region [26]. This is a very important power consideration of the RPC: if one of the components in the system starts to produce unwanted harmonics, the feedback system causes the output of the RPC to distort.

4.1 Initial system

This section introduces the receiver without an RPC or an initial system. Equations are derived to characterise the initial system's maximum receivable power, as well as the initial system's noise floor. The calculations are done with some initial assumptions.

- The received signal is noiseless.

- The initial minimum detectable signal is the thermal noise floor (-174 dBm/Hz) combined with the LNA and demodulator (Figure 4.1)
- There is no limit to the amount of transmittable power, the only limits arise as a result of the RPC
- The demodulator (ADL5380) is used in the initial system, as well as the system with the RPC
- All the values are converted to their equivalent values at the receiving antenna's base

For the system in Figure 4.1, the only limit to the initial input power is the combination of the 1 dB compression point of the demodulator (ADL5380) and the amount of gain in the LNA. The 1 dB compression point of the LNA has to be chosen at a higher value than that of the demodulator, otherwise the LNA will be the limit to the maximum power that can be accommodated. Since the dynamic range of the system is already limited by the choice of demodulator, the aim is for the rest of the components to remain linear within the available band. The constraint this places on the power inputs and outputs of the rest of the components are discussed further in section 4.4.1.

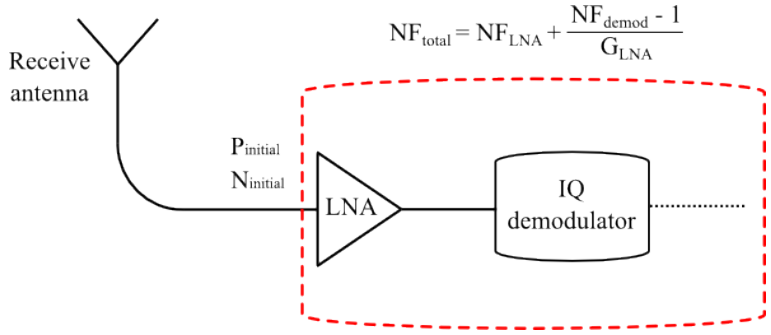

Figure 4.1: Initial system of a radar receiver (without an RPC).

The maximum initial input power is represented symbolically in equation 4.1.1 where $P_{initial}$ is the maximum input power of the receiver, $P_{demod1dB}$ is the demodulator's 1 dB input compression point and G_{LNA} is the gain of the LNA.

$$P_{initial} = \frac{P_{demod1dB}}{G_{LNA}} \tag{4.1.1}$$

The initial noise floor of the system in Figure 4.1 is determined by first calculating the cascaded noise figure (NF) of the LNA and the demodulator. The calculation of the cascaded noise figure is given on Figure 4.1. The initial noise floor is represented by equation 4.1.2,

$$N_{initial} = N_{noiseFloor} NF_{total} \tag{4.1.2}$$

where $N_{initial}$ is the initial noise floor of the receiver, $N_{noisefloor}$ is the thermal noise floor, and NF_{total} is the noise figure of the LNA and the demodulator where

NF_{LNA} is the LNA's noise figure, NF_{demod} is the demodulator's noise figure and G_{LNA} is the LNA's gain [3].

4.2 Adding the IQ Reflected Power Canceller

Adding an RPC to a radar receiver will have an effect on the receiver's power handling capabilities most significantly because these new components make their own noise contributions to the system. The components of the RPC are chosen to maximise the dynamic range of the RPC, thus minimising its detrimental effect on the initial radar receiver.

The feedback of the RPC is added to the system, as shown in Figure 4.2, indicating only the components that will have a significant effect on the dynamic range. The loss in the receiver path due to the coupler is also taken into account by the $(1 - c^2)$. Figure 4.2 contains the symbolic definitions referring to each section of the RPC feedback system's maximum power and Minimum Detectable Signal (MDS). It can be assumed that all the definitions for P are the maximum possible power for that specific section of the canceller, while N refers to the smallest possible signal power (noise floor).

A condition that has to be true for the dynamic range calculations to be valid is:

$$c^2 P_{feedback} <= P_{initial} \tag{4.2.1}$$

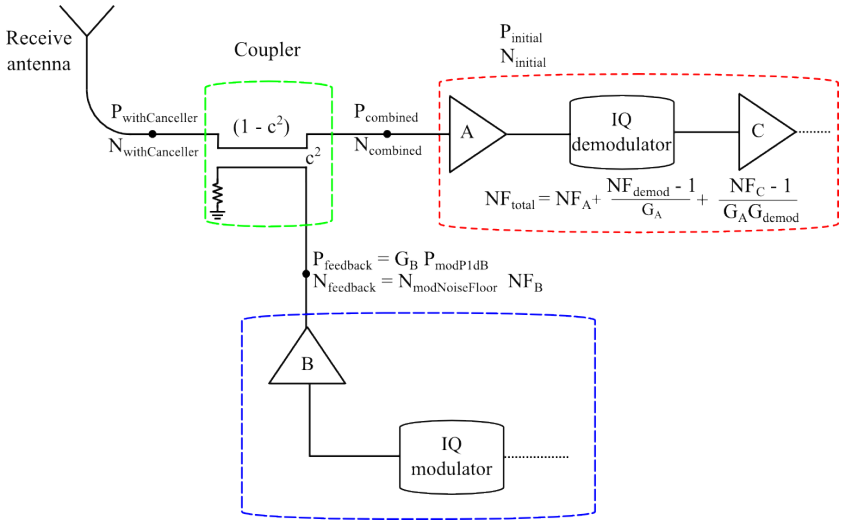

Figure 4.2: Receiver containing an IQ Reflected Power Canceller.

Amplifier B in Figure 4.2 is optional and was added to the calculations in the event that more power was required from the modulator's output.

Since it is known from Table 3.2 that the demodulator's noise figure is 12.3 dB (+3 dB to convert it to its double sideband value), the noise contribution of the cascaded LNA and demodulator is inspected first. The gain of amplifier A has not been chosen but since it will limit the maximum power that can be accommodated,

it can be assumed that the gain will not be very high. Consider the cascaded noise figure equation of Figure 4.1.

$$NF_{total} = NF_{LNA} + \frac{NF_{demod} - 1}{G_{LNA}} \tag{4.2.2}$$

With a demodulator noise figure of 15.3 dB, if the LNA has a low gain the component directly following the demodulator will still have a substantial influence on the total noise figure.

$$NF_T = NF_{LNA} + \frac{NF_{demod} - 1}{G_{LNA}} + \frac{NF_C}{G_{LNA}G_{demod}} \tag{4.2.3}$$

From equation 4.2.3, instead of connecting the demodulator directly to the integrators, a low noise differential operational amplifier is added between the demodulator and the integrator amplifiers as precaution. This ensures that the stages following the low noise differential amplifier will not have a significant influence on the noise figure.

4.3 Developing the equations

The conditions for both the initial system and the RPC system have now been introduced.

This section is aimed at developing the equations for determining an RPC with an optimised dynamic range. The equations are derived by first looking at the MDS of both the initial system and the RPC system. Next, the increase in transmit power due to the addition of an RPC is investigated. Finally, the maximum signal that can be cancelled is taken into account.

4.3.1 Minimum Detectable Signal

From section 4.1, the initial minimum detectable signal is:

$$MDS_{initial} = N_{initial} = N_{noisefloor}NF_{total} \tag{4.3.1}$$

From section 4.2, the MDS with an RPC is determined as

$$\begin{aligned} MDS_{withCanceller} &= N_{withCanceller} \\ &= \frac{N_{combined}}{1 - c^2} \\ &= \frac{N_{initial} + c^2 N_{feedback}}{1 - c^2} \end{aligned} \tag{4.3.2}$$

where $N_{combined}$ is the sum of the uncorrelated noise powers of $N_{initial}$ and $N_{feedback}$ (the modulator's noise floor).

4.3.2 Increase in Tx power

It can be seen from equations 4.3.1 and 4.3.2 that the MDS that can be detected changes for a system with an RPC. The increase in Tx power is a function of the

MDS and determines the price that is paid for adding an RPC to a radar receiver. In other words, it is the amount of extra power that has to be transmitted in order to maintain the same level of MDS as the initial system. Using equations 4.3.1 and 4.3.2 together, the increase in transmit signal power can be calculated as in equation 4.3.3.

$$\begin{aligned} Increase\ in\ Tx\ power &= \frac{MDS_{withCanceller}}{MDS_{initial}} \\ &= \frac{N_{initial} + c^2 N_{feedback}}{(1-c^2)\ N_{initial}} \end{aligned} \tag{4.3.3}$$

This allows for the designer to make an informed choice concerning the addition of an RPC to a system. For example, if the increase in Tx power is 3 dB, it would not be very significant for low power applications. However, if the transmitted power of the radar in question is very high, transmitting 3 dB more power might not be cost effective.

4.3.3 Maximum power that can be cancelled

The next limiting factor brought on by the RPC, is the maximum power that it can cancel. This puts a limitation on the maximum power that can be received, which in turn limits the range of the radar. Equation 4.3.4 gives the maximum amount of power that can be received.

$$\begin{aligned} P_{withCanceller} &= \frac{P_{combined}}{1-c^2} \\ &= \frac{c^2\ P_{feedback}}{1-c^2} \end{aligned} \tag{4.3.4}$$

$P_{combined}$ refers to the maximum signal power that can be cancelled, which from equation 4.3.4 is seen to be influence by the coupling factor c^2. This equation is valid as long as the condition in equation 4.2.1 is true.

4.3.4 Optimising the dynamic range

The equations derived throughout this chapter characterise the MDS and maximum receivable power of the RPC. A Figure of Merit (FOM) is derived from these equations which can be used to optimise the choice of components for the RPC. Since we wish to maximise equation 4.3.4 and we wish to minimise the MDS in equation 4.3.2, equation 4.3.5 can be formed as a figure of merit. To take into account the increase in Tx signal power due to the addition of the RPC, equation 4.3.3 is added as a weighing factor to the FOM in equation 4.3.5.

$$\begin{aligned} FOM &= \frac{P_{withCanceller}}{MDS_{withCanceller}\frac{MDS_{withCanceller}}{MDS_{initial}}} \\ &= \frac{(1-c^2)^2 c^2 P_{feedback}}{N_{initial}(1+c^2\frac{N_{feedback}}{N_{initial}})^2} \end{aligned} \tag{4.3.5}$$

The equations developed in this section can now be implemented in MATLAB. This will allow for a visual aid in optimising the dynamic range of the new system

with the RPC. A Microsoft Excel spreadsheet is created, with a list of practical components that would satisfy the FOM criteria. This helps with the choice of components for the RPC and it allows the user to determine which component will reach saturation first. The coupling factor used for the RPC has a large influence in the FOM from equation 4.3.5.

4.4 Results

This section interprets the equations that were derived in the first part of this chapter and presents their results. The results from the maximisation of equation 4.3.5 is presented by means of two methods. First equation 4.3.5 is imported into MATLAB and results are obtained under certain restrictions. The nature of these restrictions are elaborated on in section 4.4.1. The second method uses an Excel spreadsheet that contains the possible products that can be used for an RPC, comparing the results for different combinations of MDS and maximum receivable signal. Figure 4.3 shows the RPC block diagram as it was used in the FOM calculations. The FOM results generated in MATLAB can be used to make an initial choice of a coupling factor for the RPC. After a choice has been made for the coupling factor a more in depth analysis is necessary for the rest of the components in the RPC.

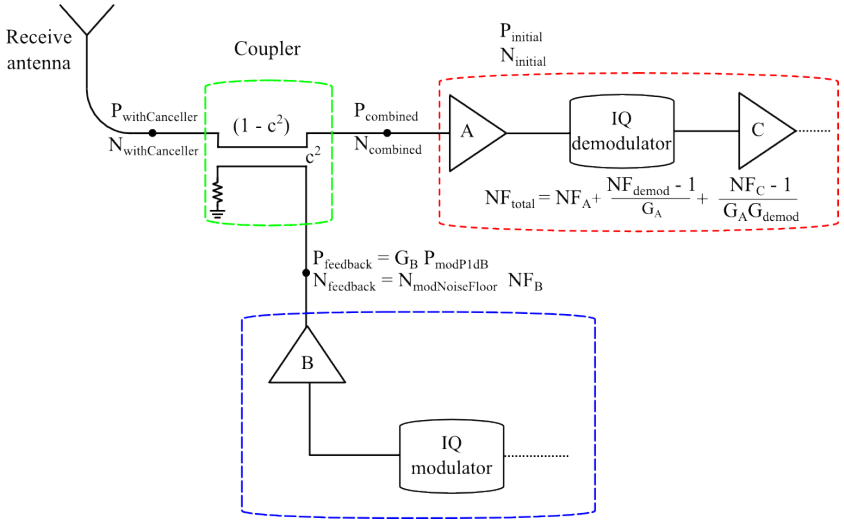

Figure 4.3: This figure shows the IQ RPC in the form it is used to calculated the FOM.

4.4.1 MATLAB results

The results interpreting the FOM are presented in the form of MATLAB figures which are generated using the code shown in Appendix B.1. The FOM equation is repeated in 4.4.1.

$$\begin{aligned} FOM &= \frac{P_{withCanceller}}{MDS_{withCanceller}\frac{MDS_{withCanceller}}{MDS_{initial}}} \\ &= \frac{(1-c^2)^2 c^2 P_{feedback}}{N_{initial}(1+c^2\frac{N_{feedback}}{N_{initial}})^2} \end{aligned} \tag{4.4.1}$$

There are several variables in equation 4.4.1 including the coupling factor (c^2), the LNA A noise figure and the LNA gain (NF_A, G_A). The LNA at the modulator's output is not included in the calculations. In order to calculate an optimised RPC system, the constraints for the variables in the FOM calculation were determined. These constraints refer to the maximum and minimum values when the FOM is no longer in an optimised state. After a wide variable sweep of the MATLAB code in Appendix B.1, the constraints of the FOM were found and are listed in Table 4.1.

Table 4.1: Variable constraints of the IQ RPC when calculating the FOM

	Minimum	Maximum
G_A (dB)	4	25
NF_A (dB)	1.5	1.5
c^2 (dB)	-20	-1

Figure 4.4 shows the FOM vs. Coupling Factor for multiple LNA gain values as listed in Table 4.1. It can be seen that the higher gain values do not make a big difference to the maximum value of the FOM. A lower gain value can be chosen to achieve a higher maximum input power (since one of the constraints on the maximum signal to cancel is given by equation 4.1.1). This is demonstrated in subsection 4.4.2.

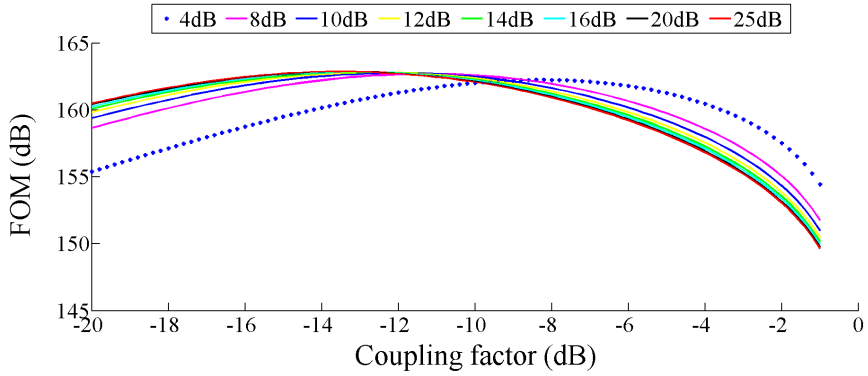

Figure 4.4: The FOM across an increasing coupling factor is shown for multiple values of LNA gain.

Through further investigation of the MATLAB results, it is found that for each separate value of gain, the maximum FOM appears where the increase in Tx power is at 3 dB. To obtain the optimum point of maximum input power vs. MDS there is a loss of 3 dB to the MDS of the original system. Figure 4.5 indicates the 3 dB line where the dynamic range for the various LNA gains is optimised. This figure

also indicated the increase in Tx power and it is found that for minimal loss in the FOM's maximum value, the increase in Tx power can be decreased.

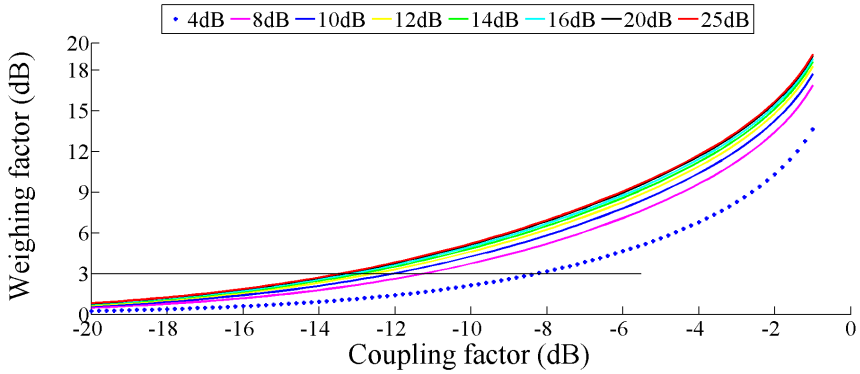

Figure 4.5: The increase in transmission power necessary for a system with an RPC to maintain the same level of MDS as an initial system is shown for an increasing coupling factor across multiple values of LNA gain.

Using both Figures 4.4 and 4.5, an optimum value for the coupling factor can be found as well as the amount of gain required for the LNA A. The best coupling factor for this particular application is found at -14 dB.

4.4.2 Microsoft Excel spreadsheet

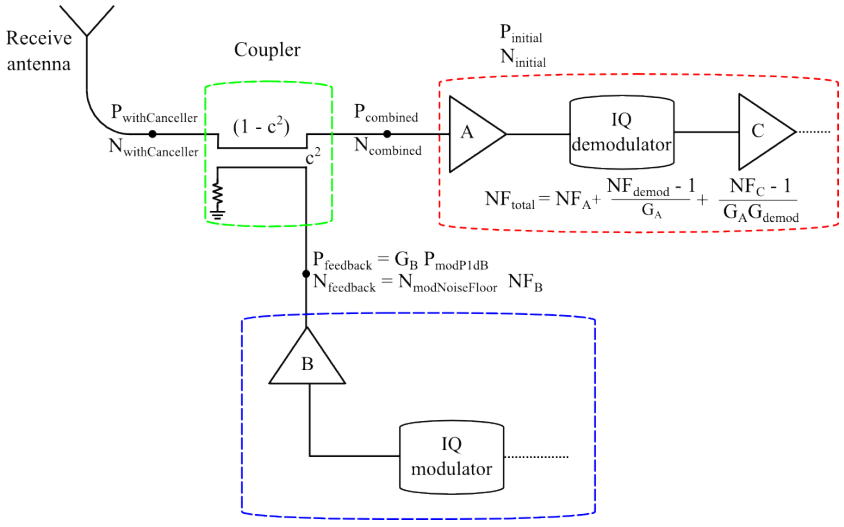

Figure 4.6: System with an IQ canceller.

The results of the FOM equation were used to find an optimum value for both the coupling factor and the gain of the LNA A (indicated in Figure 4.6). However, the values were still theoretical and a method for obtaining practical components was necessary. The available components rarely comply with the exact desired values

from the design, for this reason a spreadsheet is created. The spreadsheet contains a list of possible models for each component given in Figure 4.6. Using the spreadsheet, a component can be chosen from each category and the total dynamic range of the RPC can be calculated for these components. The results are presented in a table of varying coupling factors, just to illustrate how the different components will affect the optimum value that was initially chosen for the coupler. The spreadsheet takes all the power limitations and canceller limitations into account.

Table 4.2: The component options for the LNA A of the RPC given in Figure 4.6.

Part number	Gain (dB)	NF (dB)	$P_{1dB}(dBm)$
MAAL-0120200	10	1.4	17.5
MAAL-010706	17	0.6	17.5
HMC667LP2	18	0.75	16.5
PSA4-5043+	13	1	20
ZX60-272LN+	13	0.9	18
TAMP-272LN+	13	0.9	18

Table 4.3: The component options for the Low noise differential amplifier C of the RPC given in Figure 4.6.

Part number	Input noise $(nV/\sqrt{Hz})$	Total supply (V)	Gain (dB)	NF (dB)
LT1993-4	2.35	5.5	12	14.5
LT6402-12	2.6	5.5	12	15
THS4130	1.3	±15	9	22
LMH6553	1.2	±12	9	23.5
AD8139	2.25	12	14	15
ADA4927	1.4	10	9.5	14.8
ADA4950	3.6	10	9.5	11

Table 4.4: The relevant values of the modulator and demodulator used in the RPC given in Figure 4.6.

Part number	Gain (dB)	Noise contribution	P_{1dB} (dBm)
ADL5380	6.3	NF = 12 dB	input = 12 dBm
ADL5375	-3.2	Noise floor = -160 dBm/Hz	output = 10 dBm

The block diagram containing the system with an RPC is repeated in Figure 4.6. Table 4.2 lists the product options for the LNA A where the main aim of the product search was to keep the noise figure below 1.5 dB, the P_{1dB} below 20 dBm and, from the MATLAB FOM results, the gain kept below 15 dB. Table 4.3 gives a list of the possible low noise differential amplifiers that could be used for the RPC. These differential amplifiers were chosen for their low input noise voltage and large voltage

supply range. The voltage supply range is important, because it gives an indication of what the limit is to the maximum amount of gain that the amplifiers can supply (for a certain maximum V_{pp} output of the demodulator). This concept is elaborated on further in Chapter 6. Table 4.4 repeats the attributes of the chosen modulator and demodulator. Screen shots from the spreadsheet containing all the information mentioned in the tables is given in Appendix C. All the equations used to calculate the results in the spreadsheet were derived in the first part of this chapter.

After a component from Table 4.2 and 4.3 had been chosen, the initial system values were calculated with equations 4.4.2, 4.4.3. These results are given in Table 4.5, where the closed loop parameters are calculated, using equations 4.4.4 and 4.4.5.

$$P_{initial} = \frac{P_{demod1dB}}{G_{LNA}} \tag{4.4.2}$$

$$NF_T = NF_{LNA} + \frac{NF_{demod} - 1}{G_{LNA}} + \frac{NF_C}{G_{LNA}G_{demod}} \tag{4.4.3}$$

$$\begin{aligned} P_{withCanceller} &= \frac{P_{combined}}{1 - c^2} \\ &= \frac{c^2 P_{feedback}}{1 - c^2} \end{aligned} \tag{4.4.4}$$

$$\begin{aligned} MDS_{withCanceller} &= N_{withCanceller} \\ &= \frac{N_{combined}}{1 - c^2} \\ &= \frac{N_{initial} + c^2 N_{feedback}}{1 - c^2} \end{aligned} \tag{4.4.5}$$

The results in Table 4.5 are calculated for a varying coupling factor, which is given in column two of the table. The first column in Table 4.5 shows the power of the maximum signal that can be cancelled. The cells that are highlighted red indicate the values which exceed the maximum input power of the LNA A and IQ demodulator combination. Column three in Table 4.5 shows the Minimum Detectable Signal of the RPC, calculated using equation 4.4.5. The last column in Table 4.5 gives the loss in MDS (increase in Tx power) that the receiver suffers because the RPC was added to the system. Note that there is a cell highlighted red in this column as well, which indicates that the weighing factor has become higher than 3 dB and the loss in MDS has become too high. The following component combination is used in the spreadsheet calculations: LNA A = ZX60-272LN+, low noise differential amplifier C = ADA4927, with no amplifier at LNA B. Using these components, the open loop characteristics are the following: maximum input power = -2 dBm, $MDS_{initial}$ = -169.03 dBm/Hz (the initial noise figure $NF_{initial}$ = 4.97 dB).

From Table 4.5 the trade off between the maximum signal that can be cancelled (or received) and the loss to Minimum Detectable Signal can be seen. This table makes it possible to choose the components for the RPC by making an informed decision.

Table 4.5: This shows the closed loop results of the RPC.

Max cancelled (dBm)	Coupling (dB)	MDS_{RPC} (dBm/Hz)	MDS loss (dB)
2.05	8	-164.33	3.10
0.88	9	-164.89	2.55
-0.24	10	-165.35	2.08
-1.34	11	-165.74	1.70
-2.42	12	-166.06	1.38
-3.48	13	-166.32	1.11
-4.52	14	-166.54	0.90
-5.56	15	-166.71	0.72
-6.59	16	-166.86	0.76

4.5 Conclusion

This chapter contained the derivations used to determine an RPC with an optimised dynamic range. After reviewing the results in both MATLAB and on a spreadsheet, a practical system could be suggested with the components listed in Table 4.6.

Table 4.6: This table contains the suggested components for the RPC when a 14 dB coupler is used.

Component	Part number
Modulator	ADL5375
Demodulator	ADL5380
LNA A	ZX60-272LN+
Low noise diff amp C	ADA4927
LNA B	not used

Chapter 5

Analysis of loop for zero phase error at RF

Chapter 2 contained a derivation of an ideal RPC model. This model was derived without the influence of transmission line delays or the internal phase contribution of the modulator and demodulator. However, it was mentioned that RF phase delays causes cross coupling between the I and Q channel, which can result in instability. This was discussed further as a practical consideration in Chapter 3. The aim of this chapter is to analyse the RPC on a component level and from this analysis derive an equation which can be used to predict the control loop's RF phase. This derivation is similar to that of the ideal model in Chapter 2. If the amount of RF phase error is known, some form of compensation can be applied to reduce the phase error and ensure loop stability.

This chapter consists of three sections. First, a diagram containing the basic components of an RPC is given followed by an investigation into the phase delay for each of these components. Next, these phase delays are combined to form a single equation that can be used to determine the time delay that is necessary for the RPC's feedback loop to remain stable. Finally, the equation derived in section 5.2 is used on a practical system and the results are given.

5.1 Component breakdown

Figure 5.1 shows the ideal RPC model from Chapter 2, with the added transmission line delays. The aim of this section is to show how the phase delay of each component in Figure 5.1 is defined. The phase delay of the transmission lines used in the RF sections of the RPC is also taken into account. In Figure 5.1, the time delay of the transmission lines (t_2 and t_3) that are connected to the modulator and demodulator are already divided into their equivalent I and Q channels. The demodulator is referred to in subscripts as dm and the modulator as m.

5.1.1 Transmission line

Throughout this analysis, it is accepted that all transmission lines are operated under matched conditions. Their transfer functions are represented by equation 5.1.1.

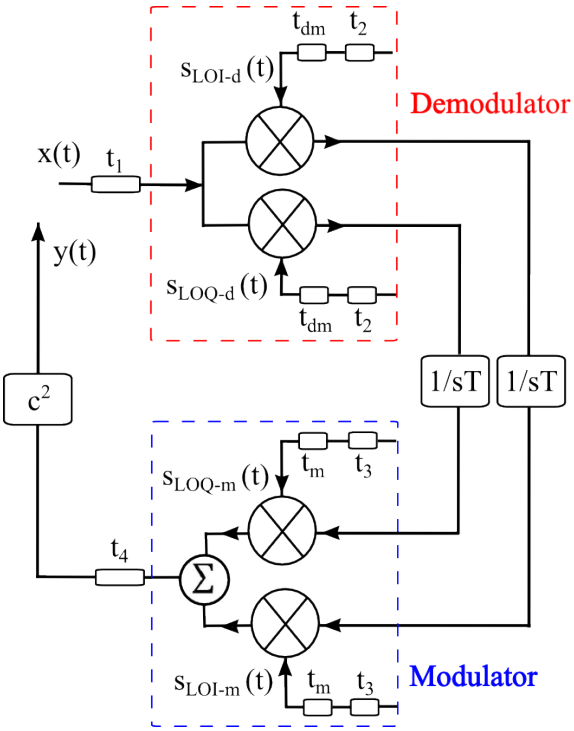

Figure 5.1: The block diagram indicates the RPC as a part of an FMCW Radar's receiver. Each component that is used to make up the RPC is indicated in the block diagram.

$$G_{tl}(j\omega) = e^{-j\omega t_l} \tag{5.1.1}$$

where ωt_l is the phase delay of the transmission line. The time delay t_l is defined as the electrical length l of the line divided by the propagation velocity v, $t_l = \frac{l}{v}$. [3]

5.1.2 Modulator and Demodulator

The practical model for the demodulator is determined first, with the help of Figure 5.2. This process is then repeated for the modulator, with the help of Figure 5.3.

In the derivation of the ideal model, it was assumed that no phase delay was caused by the LO's quadrature splitter. From Chapter 3 it was found that polyphase splitters are used for the LO quadrature generation, which will add its own internal delays to the demodulator. The LO signals are mixed with the RF input signal ($s_{RF}(t)$) to produce the quadrature baseband outputs, $s_I(t)$ and $s_Q(t)$, as shown in Figure 5.2. As in Chapter 2, assume the LO signal input is

$$s_{LO} = e^{-j\omega_0 t}$$

where ω_0 is the centre frequency. This allows the down conversion process to be analysed merely as the multiplication of two signals. The amplitude of the LO signal is taken as unity as it does not feature in the loop transfer function calculations. Assuming an ideal IQ generation process, the LO signal applied to the I and Q mixers are given by 5.1.2.

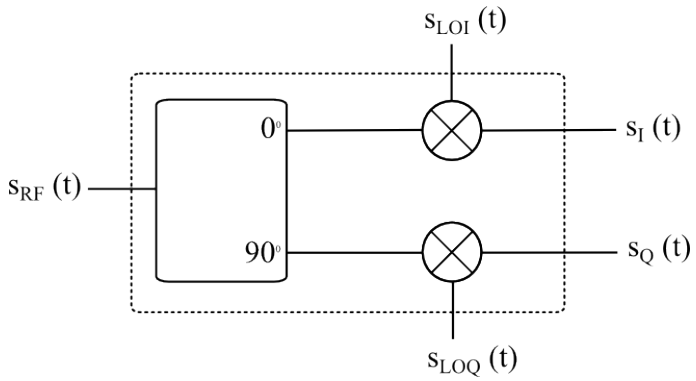

Figure 5.2: The functional diagram of an IQ demodulator that illustrates frequency down conversion.

$$\begin{aligned} s_{LOI-d}(t) &= e^{-(j\omega_0 t - j\omega_0 t_{dm})} \\ s_{LOQ-d}(t) &= e^{-(j\omega_0 t - j\pi/2 - j\omega_0 t_{dm})} \end{aligned} \tag{5.1.2}$$

where t_{dm} is the internal delay in the LO circuits of the demodulator. By convention, the Q signal lags the I signal. The RF input signal is given by

$$s_{RF} = e^{j(\omega_0 t + \omega_r t + \phi)}$$

where ω_r is the baseband frequency and ϕ represents any phase errors in the demodulator. For a demodulator with gain A_d, the I and Q signal outputs are given by equation 5.1.3.

$$\begin{aligned} s_I(t) &= s_{LOI-d}(t)\ s_{RF}(t) \\ &= A_d e^{j(\omega_0 t + \omega_r t + \phi - (\omega_0 t - \omega_0 t_{dm}))} \\ &= A_d e^{j(\omega_r t + \phi + \omega_0 t_{dm})} \\ s_Q(t) &= s_{LOQ-d}(t)\ s_{RF}(t) \\ &= A_d e^{j(\omega_0 t + \omega_r t + \phi - (\omega_0 t - \pi/2 - \omega_0 t_{dm}))} \\ &= A_d e^{j(\omega_r t + \phi + \pi/2 + \omega_0 t_{dm})} \end{aligned} \tag{5.1.3}$$

Next, the transfer function of the modulator is considered. Figure 5.3 shows the baseband I and Q input signals $(s_I(t), s_Q(t))$ mixed with the quadrature LO signals $(s_{LOI}(t), s_{LOQ}(t))$ to produce the RF output at the modulator $(s_M(t))$. The modulator's input and LO signals are labelled the same as they are for the demodulator, since the components are used together in the application of an RPC.

It has already been verified that the generation of the quadrature LO components of the modulator and demodulator are similar, but it is not known if the order of the polyphase splitters used for the modulator are the same as the order of the ones used for the demodulator. Thus the internal delay of the modulator's LO I and Q signals is represented by t_m. The $s_I(t)$ and $s_Q(t)$ inputs in Figure 5.3 are the output from Figure 5.2. In the modulator process the phase of the I and Q LO signals are added to the phase of the baseband I and Q channels together. The signs of the LO input signals are adjusted in order to apply the up conversion as multiplication

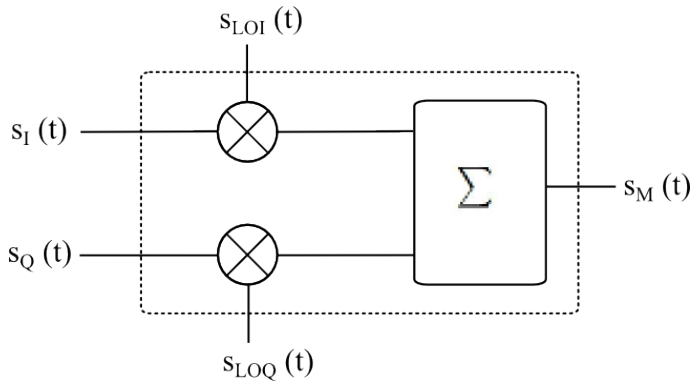

Figure 5.3: The functional diagram of an IQ modulator that illustrates frequency up conversion.

of two signals. The output signals of the mixers are summed to the output of the modulator. Assume the I and Q baseband inputs of the modulator are characterised by equation 5.1.3 and the LO signals are given by equation 5.1.4.

$$\begin{aligned} s_{LOI-m}(t) &= e^{j\omega_0 t - j\omega_0 t_m} \\ s_{LOQ-m}(t) &= e^{j\omega_0 t - j\pi/2 - j\omega_0 t_m} \end{aligned} \tag{5.1.4}$$

Then the output of the modulator is given by equation 5.1.5.

$$\begin{aligned} s_M(t) &= s_{LOI-m}(t)s_I(t) + s_{LOQ-m}(t)s_Q(t) \\ &= A_d A_m[e^{j(\omega_0 t - \omega_0 t_m + \omega_r t + \phi + \omega_0 t_{dm})} \\ &\quad + e^{j(\omega_0 t - \pi/2 - \omega_0 t_m + \omega_r t + \phi + \pi/2 + \omega_0 t_{dm})}] \\ s_M(t) &= A_t(e^{j(\omega_0 t + \omega_r t + \phi + \omega_0 t_{dm} - \omega_0 t_m)}) \end{aligned} \tag{5.1.5}$$

Where A_t refers to the total gain of the demodulation and modulation process. From equation 5.1.4 alone there is already a large amount of added RF phase (if it is compared to the RF input signal).

5.1.3 Coupler

A parallel coupled line directional coupler is used to sum the received and cancelling signals. To demonstrate the influence of this coupler on the phase response of a system, an example is generated. Consider a 20 dB parallel coupler, analysed in AWR Microwave Office. Figure 5.4 shows the results.

The transfer function between the input and the coupled port of the coupler with respect to the reference planes at the ends of the coupled lines is given by equation 5.1.6.

$$C(j\omega) = ce^{-j\omega/4f_{qw} + j\pi/2} \tag{5.1.6}$$

where c is the coupling coefficient and f_{qw} is the frequency where the coupler lines have an electrical length of a quarter wavelength. This is the centre frequency of the coupler response. To this transfer function must be added the cascaded sections of

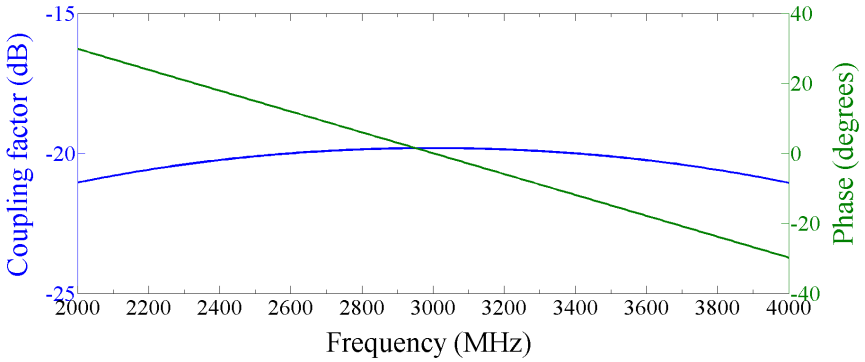

Figure 5.4: Transfer function of coupler between the input and the coupled port.

transmission lines connecting the ports of the coupler to the coupled line sections, with delay τ_c to give a total transfer function as in 5.1.7.

$$C(j\omega) = ce^{-j\omega/4f_{qw} - j\omega\tau_c + j\pi/2} \tag{5.1.7}$$

5.2 Loop calculation

This section combines the information of all the components that was provided in the first part of this chapter and use it to determine a practical model for the RPC which takes all of the RF phase delays in the system into account. Figure 5.5 gives a block diagram of the transfer function loop. All of the delays due to transmission lines and components are indicated on the figure.

The magnitude of the loop gain is the product of the gains of the blocks. The main concern is with the phase of the loop, which is the sum of the phase contributions of each component. This can be written down by inspection of the block diagram with the receive frequency offset at zero and the baseband transfer function $G_b = 1$.

Starting with the phase of the input signal

$$x(t) = e^{j(\omega_0+\omega_r)t} \tag{5.2.1}$$

Consider Figure 5.5, with the help of section 5.1 and with $\omega_r = 0$, the phase of the I and Q paths up to the modulator's output h on the diagram just prior to summing them is found as

$$\begin{aligned}
I : \theta_h &= \omega_0 t - \omega_0 t_1 - (\omega_0 t - \omega_0 t_2) + \pi S_2 + \omega_0 t - \omega_0 t_3 \\
&\quad + \omega_0 t_{dm} - \omega_0 t_m \\
&= -\omega_0 t_1 + \omega_0 t_2 + \pi S_2 - \omega_0 t_3 + \omega_0 t_{dm} - \omega_0 t_m \\
Q : \theta_h &= \omega_0 t - \omega_0 t_1 - (\omega_0 t - \frac{\pi}{2} - \omega_0 t_2) + \pi S_1 + \omega_0 t - \frac{\pi}{2} - \omega_0 t_3 \\
&\quad + \omega_0 t_{dm} - \omega_0 t_m \\
&= -\omega_0 t_1 + \omega_0 t_2 + \pi S_1 - \omega_0 t_3 + \omega_0 t_{dm} - \omega_0 t_m
\end{aligned} \tag{5.2.2}$$

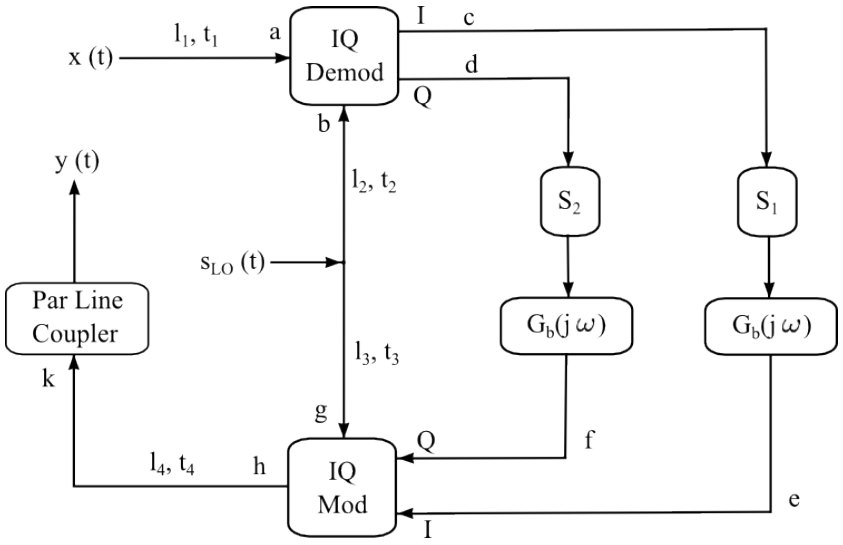

Figure 5.5: Loop phase calculation diagram indicating each component as its equivalent transfer function block.

Equation 5.2.2 verifies the RPC model from chapter 2: once again showing that the I and Q channels are identical if both $S_1 = S_2 = S = 0$. Completing the loop, the phase of the signal $y(t) = e^{j\theta_y}$ with $S = 0$ is found in equation 5.2.3.

$$\begin{aligned}\theta_y &= \theta_h + \theta_{coupler} \\ &= \omega_0 t - \omega_0 t_1 - (\omega_0 t - \omega_0 t_2) + \omega_0 t - \omega_0 t_3 - \omega_0 t_4 - \omega_0 (t_c + \frac{1}{4 f_{qw}}) \\ &\quad + \frac{\pi}{2} + \omega_0 t_{dm} - \omega_0 t_m \\ &= \omega_0 t + \omega_0 (t_2 - t_1 - t_3 - t_4 - t_c - \frac{1}{f_{qw}}) + \frac{\pi}{2} + \omega_0 t_{dm} - \omega_0 t_m\end{aligned} \tag{5.2.3}$$

The phase of the loop gain equals the phase of the output signal minus the phase of the input signal, as shown in equation 5.2.4.

$$\begin{aligned}\theta_{loop} &= \theta_y - \theta_x \\ &= \omega_0 (t_2 - t_1 - t_3 - t_4 - t_c - \frac{1}{f_{qw}}) + \frac{\pi}{2} + \omega_0 t_{dm} - \omega_0 t_m\end{aligned} \tag{5.2.4}$$

The RF phase can be calculated as a certain value by choosing the length of the LO line to the demodulator (t_2). This calculation is valid for a certain centre frequency, and will dictate the range wherein the loop is stable. In Chapter 7 the RF phase error is measured for various centre frequencies. Equation 5.2.4 consists of all of the RF phase added to the RPC's feedback loop. If the control system diagram in Figure 5.6 is considered, the negative feedback provides the required 180 degree phase shift through the loop. The RF phase error calculated in equation 5.2.4 is represented on the vector diagram in Figure 5.7. If the total phase θ_{loop} exceeds the total 90 degree error limit, the cross coupling shown in Figure 5.6 causes instability in the RPC.

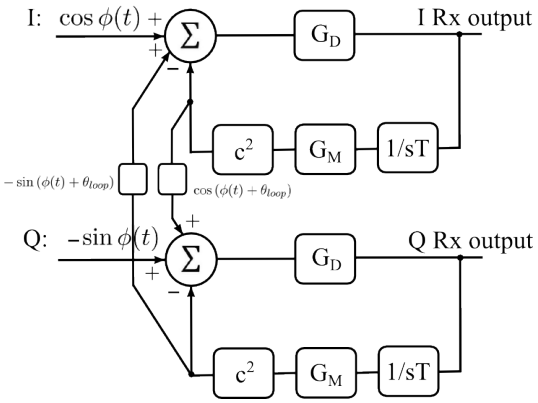

Figure 5.6: Cross coupling between I and Q baseband control systems.

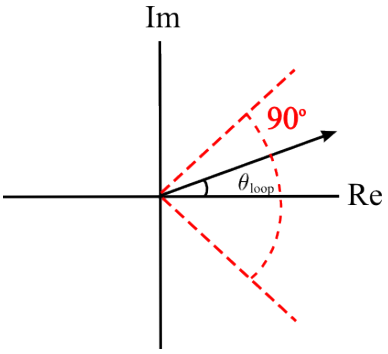

Figure 5.7: Vector diagram of RF phase error. The total 90 degree error constraint is also indicated.

5.3 Results and measurements

The previous section has provided a way of predicting the RF phase through the RPC's control loop. The result, in equation 5.2.4, is represented by its equivalent time delay which makes the calculations for the loop delay much simpler. Time delays t_1, t_2, t_3 and t_4 are the lengths of the transmission lines used in the loop phase calculation. These values are the variables in the equation and can be adjusted by using different length transmission lines. However, several of the values are also constant, this includes the delay through the coupler (t_c) and the internal delays of the modulator and demodulator (t_m and t_{dm}). The internal delays of the modulator and demodulator are difficult to measure directly since there are both an RF and a low frequency component present. This difficulty can be overcome by a measurement on the network analyser which is described in this section. This measurement is also used to show that the phase through the control loop can be accurately predicted.

This section consists of two subsections, the first subsection contains the description of the test setup as well as the assumptions that were made in order to complete the measurement. The second subsection contains the results of the test described in the first subsection together with its conclusions.

5.3.1 Test setup

A network analyser is used to measure the system, which is a simplified model of the system in Figure 5.5. The test setup is shown in Figure 5.8, with l_1 and l_4 used to calibrate the network analyser. The phase calculation is done from $x(t)$ to $y(t)$, as indicated in Figure 5.8.

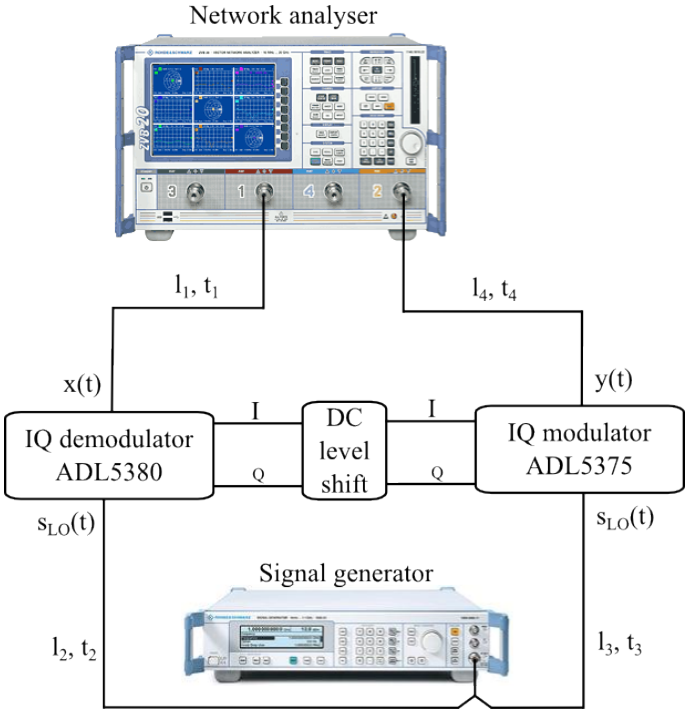

Figure 5.8: The test setup to measure the combined internal delay of the IQ modulator and IQ demodulator.

There is a unity gain amplifier between the modulator and demodulator used to shift the DC offset to the required value of $0.5V$ for the modulator. According to Nash [27], if the DC offset of the modulator input is not at the specified value, a small portion of the unmodulated carrier will appear at the modulator's output. In other words, the LO leakage suppression will be less than the value that was specified in the ADL5375's datasheet. If the RF phase delay equation 5.2.3 is evaluated to be applicable to the test setup in Figure 5.8, the result is:

$$\theta_{loop} = \omega_0(t_2 - t_1 - t_3 - t_4 + t_{dm} - t_m) \tag{5.3.1}$$

If the combined time delay of the demodulator and modulator $(t_{db} - t_m)$ is unknown, the following method can be used to determined the equivalent value.

$$t_{system} = t_2 - t_3 + t_{dm} - t_m \tag{5.3.2}$$

where t_{system} is the total phase delay measured through the demodulator and modulator, and t_1 and t_4 are calibrated out of the equation. The transmission line lengths of l_2 and l_3 are chosen as specific values. If equation 5.3.2 is considered again,

the only variables left is the time delay through the demodulator and modulator $(t_{dm} - t_m)$ which can now be calculated.

This calculation is applied for a specific centre frequency. If the centre frequency changes too much, θ_{loop} will no longer be within the 90 degree error limit, indicated in Figure 5.7, and the system will become unstable.

5.3.2 Results

With the combined delay of the modulator and demodulator known, it is possible to recalculate the values in equation 5.3.2 and obtain the values needed for a zero phase error through the system in Figure 5.8. With $t_{system} = 0$, the transmission line lengths of l_2 and l_3 are adjusted to suit the calculations. Figure 5.9 shows the result on the network analyser over a 1 MHz bandwidth.

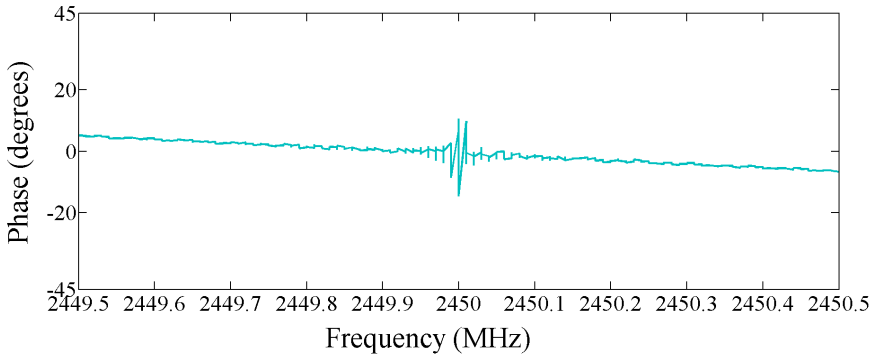

Figure 5.9: The results of the network analyser measurement shown in Figure 5.8 with cables lengths adjusted to produce a zero phase error.

5.4 Conclusion

This chapter explained the derivation of a practical model of the RPC as a combination of its component. This resulted in an equation that can be used to predict the phase through the RPC's control loop. It is now possible to ensure a 180 degree phase shift through the RPC feedback loop, no matter which components are used.

Chapter 6

Final design

The design of an optimised RPC has been covered in some detail in the preceding chapters. In the course of the design several problems facing the design of an RPC were identified and solved. In Chapter 4 a system, consisting of components chosen to obtain an optimum dynamic range, was identified. These chosen components are analysed further in this chapter by means of practical measurements. Form these measurements it is determined whether the practical RPC will meet the dynamic range specifications designed in Chapter 4. The chosen components were tested separately and their results were compared to those of their expected values. The low noise design of the baseband amplifiers is also given and the final PCB layout is described. This chapter incorporates all the information provided throughout the earlier chapters to produce a final design.

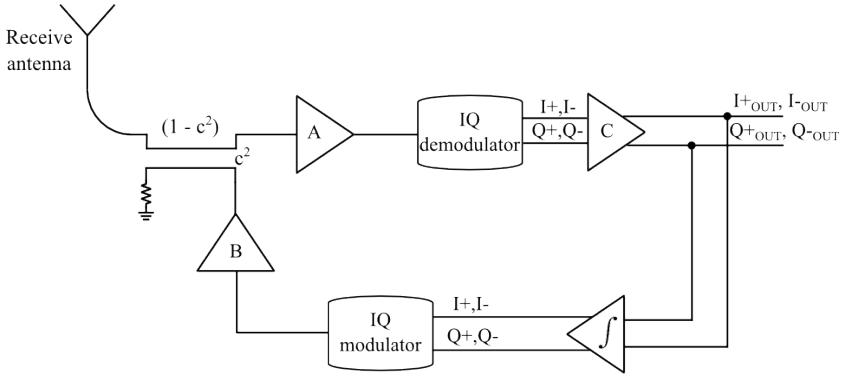

Figure 6.1: The final block diagram showing the IQ Reflected Power Canceller with all of its components.

6.1 Final block diagram

Figure 6.1 gives a block diagram of the final RPC. Each component block in Figure 6.1 represents a corresponding component in Table 6.1. In Chapter 4 these components were chosen specifically to optimise the dynamic range of the canceller. The

aim of this section is to measure the characteristics of these components in order to determine whether they meet with the dynamic range requirements set in Chapter 4. First, the output power of the modulator is compared against the input power of the demodulator in order to verify the conversion gain of the two components. Next the LNA and coupler are measured on a Vector Network Analyser (VNA), followed by a revision of the dynamic range design. Finally the design of the operational amplifiers at baseband is completed, followed by the theoretical calculation of the cancellation bandwidth of the RPC.

Table 6.1: This table contains the suggested components for the RPC when a 14 dB coupler is used.

Component	Part number
IQ Modulator	ADL5375
IQ Demodulator	ADL5380
LNA A	ZX60-272LN+
Low noise diff amp C	ADA4927
Integrator diff amp	LTC6362
Coupler	SYBD-14-272HP+

6.1.1 IQ modulator and IQ demodulator power relations

The equivalent voltage conversion gains of the modulator and demodulator are measured and compared to the values provided in their datasheets. The datasheet values are given in Table 6.2. A balun is used to transform the input to the demodulator into a differential signal. The loss due to the balun was de-embedded from the conversion gain supplied in the ADL5380's datasheet. The maximum undistorted output voltage of the demodulator is measured and used to determine what the restrictions should be on the baseband components that drive the modulator in order to not exceed the modulator's input voltage restrictions. The undistorted output power of the modulator is measured on a spectrum analyser and compared to its equivalent value in the ADL5375's datasheet. The modulator's output power is one of the limiting factors in the maximum signal power that can be cancelled.

Table 6.2: The voltage conversion gains of the modulator and demodulator.

Component	Voltage gain (dB)
ADL5380	5.9
ADL5375	-3.4

Table 6.3 contains the maximum input and output power that is expected from the demodulator and modulator respectively. The test setup used to measure these characteristics is given in Figure 6.2. A signal generator was used to produce the RF_{IN} signal. The input signal power (P_{IN}) was varied across values below the maximum input power of the demodulator, as given in Table 6.3. The LO signals of

both the modulator and demodulator were generated by a second signal generator and its output was split into two equal signals to drive both components. The output of the modulator was observed on a spectrum analyser. A unity gain operational amplifier was connected between the modulator and demodulator which was used to shift the DC offset of the demodulator to 0.5V, which is a requirement of the modulator.

Table 6.3: The maximum power ratings of the IQ modulator and IQ demodulator are repeated here. The test values should not exceed the values given in this table. The test frequency is $f_{RF} = 2.450001GHz$ and $f_{LO} = 2.45GHz$.

Position	P_{1dB} dBm
RF_{IN}	11 dBm
RF_{OUT}	9.6 dBm

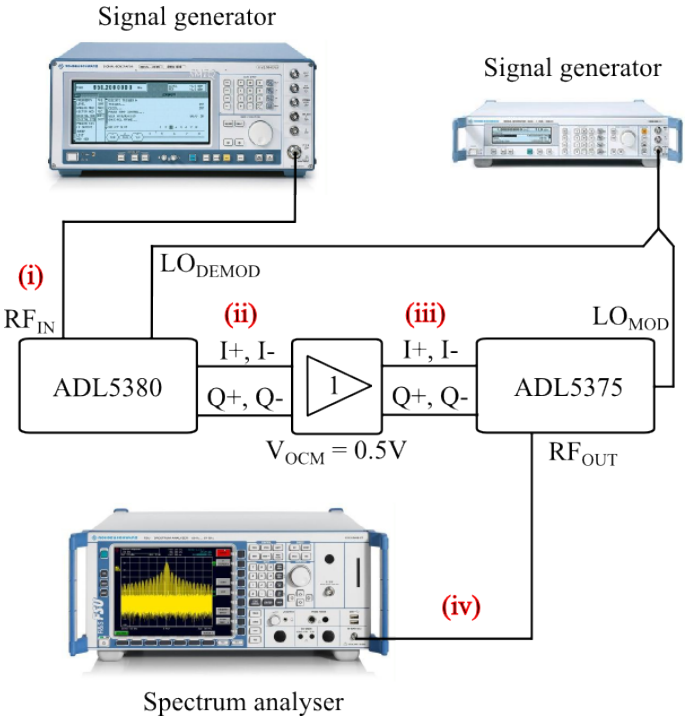

Figure 6.2: Test set up to determine the relationship between the output voltage of the IQ demodulator and the output power of the modulator.

An analysis of the equivalent voltage gain of the demodulator is required. Figure 6.3 shows a circuit diagram of the demodulator's input followed by a fully differential operational amplifier at baseband. The I channel's output is used for this analysis as the process is identical for the Q channel. The block diagram of the demodulator is obtained from its datasheet.

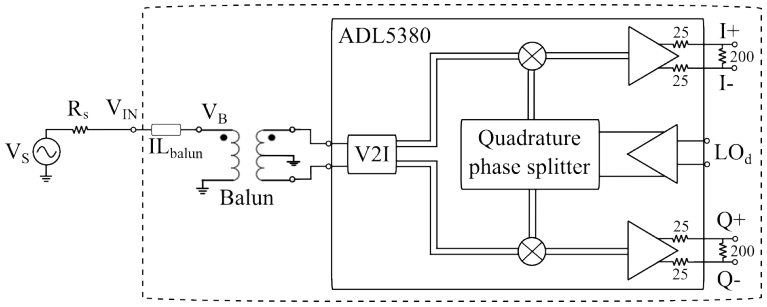

Figure 6.3: Block diagram showing the application of a demodulator.

The demodulator is driven by a single ended RF input (RF_{IN}) with an input power P_{IN} indicated on Figure 6.3. This input is converted into its balanced equivalent by a balun specified in the ADL5380's datasheet as the TC1-1-13 from Mini-Circuits. The same balun is used to convert the single ended LO into its differential input. An insertion loss of $IL_{balun} = -1.62$ dB is specified for the balun, after the theoretical 3 dB loss of the 180 degree split has been subtracted [28]. The loss from the balun is included in the voltage conversion gain measurement for the demodulator, since the single ended conversion gain of the demodulator is calculated. The gain for the calculation is defined from the $I+_{in}$ of the demodulator to its $I+_{out}$. The dB quantity of the balun's insertion loss adds directly to the noise figure of the demodulator [3]. The demodulator's conversion gain is specified into a 200 ohm load at its output as indicated in Figure 6.3.

Table 6.4 contains the measured values of the demodulator's output as a peak to peak per channel ($I+$) value. Using this result, the practical voltage conversion gain of the demodulator can be calculated.

Table 6.4: Comparing the expected conversion gain of the ADL5380 to its measured values.

(i) RF_{in} (dBm)	(ii) Measured I/Q $V_{pk-pk-per-channel}$
-4	0.156
-2	0.192
0	0.242
2	0.304
4	0.362
6	0.46
11	1.4

Consider an input power of $P_{IN} = 0$ dBm that is applied to a 50 Ω load; the equivalent rms input voltage is calculated as:

$$V_{IN} = 0.2236\ V_{rms}$$

The peak to peak differential voltage of the input to the circuit in Figure 6.3, is determined as:

$$\begin{aligned} V_S &= 2\sqrt{2}V_{IN} \\ &= 632\ mV_{pk-pk-diff} \end{aligned} \tag{6.1.1}$$

.

In order to compare the measured results in Table 6.4 to the input voltage in equation 6.1.1, the results from the table have to be converted to their differential values as shown:

$$\begin{aligned} V_d &= 2V_{IQ-measure} \\ &= 484\ mV_{pk-pk} \end{aligned}$$

.

From these measurement results, the voltage conversion gain of the demodulator is calculated as $G_{Vnew} = \frac{V_d}{V_S} = 0.7658\ V/V$, which is much lower than the specified voltage conversion gain.

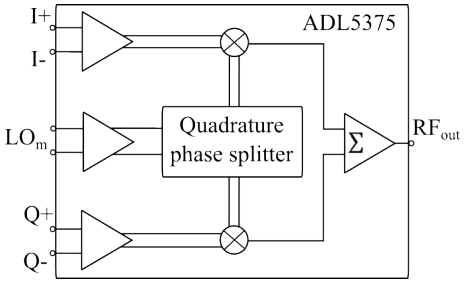

Figure 6.4: Block diagram showing the application of a modulator.

The modulator's block diagram from the ADL5375 datasheet is given in Figure 6.4. Its equivalent gain is defined as the voltage gain measured from the RF_{out} output in a 50 ohm load to the baseband input voltage ($1V_{pp}$ baseband input gives a 0.6 dBm output power). The peak to peak input voltage vs. theoretical and measured output power is given in Table 6.5.

Table 6.5: Determining the maximum output power of the ADL5375

(iii) I/Q input $V_{peak-peak-per-channel}$	(iv) RF_{out} Theoretical (dBm)	(iv) RF_{out} Measured (dBm)
0.468	0.0036	-1.7
0.576	1.8064	0.33
0.726	3.8169	2.4
0.915	5.8259	4.39
1.086	7.3155	5.69
1.380	9.3964	7.27

From the results in Table 6.5, it can be seen that the practical 1 dB output power of the modulator is not 9.6 dBm. It is at a lower level of 7.27 dBm, which reduces the expected dynamic range of the RPC by lowering the maximum signal power

that can be cancelled. A possible solution is to add a low gain amplifier between the modulator's output and the coupler, as shown in Figure 6.1. This has the advantage of increasing the maximum power that can be cancelled; however, it also adds more noise to the system. Another observation that can be made from the measurements in Table 6.5 is that the output voltage of the demodulator is $1.4V_{pp}$ (per channel) for its maximum input power; this information is required in subsection 6.1.5.

6.1.2 Low noise amplifier (LNA) A

The LNA chosen for this design is given in Table 6.1 as the ZX60-272LN+ from Mini-Circuits. The characteristics of this LNA are summarised in table 6.6.

Table 6.6: A summarised version of the characteristics of the ZX60-272LN+.

Bandwidth (MHz)	Noise figure (dB)	Gain (dB)	$P1dB$ (dBm)
2300 - 2700	0.8 (typically)	13 (typically)	18.5 (typically)

From Table 6.6 it is seen that the 1 dB output power of the LNA is higher than the 1 dB input power of the demodulator. The LNA's output power is high enough so as not to cause any unwanted harmonics in the feedback loop. In order to verify the gain of the LNA provided in Table 6.6, it is measured on a VNA using a two port set up as shown in Figure 6.5.

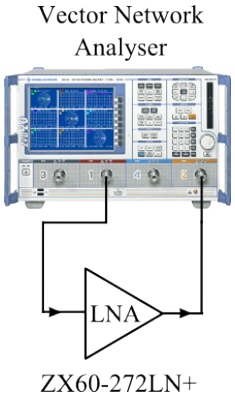

Figure 6.5: Two port open loop measurement of the RPC's gain response.

The measured gain is given in Figure 6.6, where it is found that the gain across a 100 MHz bandwidth (2.4 - 2.5 GHz) is 15 dB, instead of the advertised 13 dB. This higher gain value will have an influence on the dynamic range calculations that were presented in Chapter 4. After the coupler has been measured, the optimised dynamic range results will be revised in subsection 6.1.4.

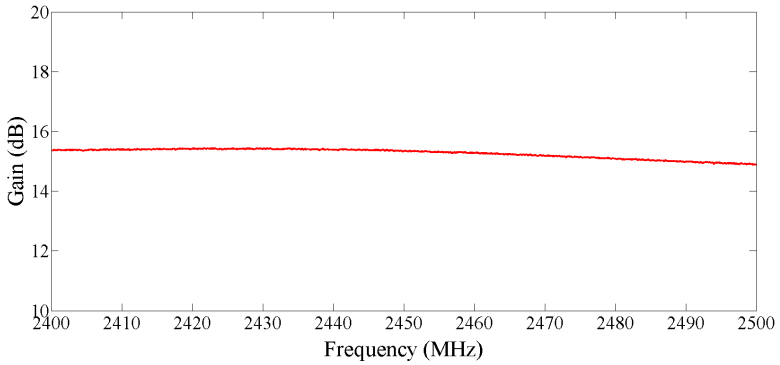

Figure 6.6: Measured gain of the ZX60-272LN+ across the FMCW radar bandwidth as defined in chapter 2.

6.1.3 Coupler

Table 6.1 gives details of the bi-directional coupler used for the RPC. The SYBD-14-272HP+ is supplied by Mini-Circuits and a summary of its characteristics is given in Table 6.7.

Table 6.7: A summarised version of the characteristics of the SYBD-14-272HP+.

Bandwidth (MHz)	Coupling (dB)	Insertion loss (dB)
2300 - 2700	13.5	0.4

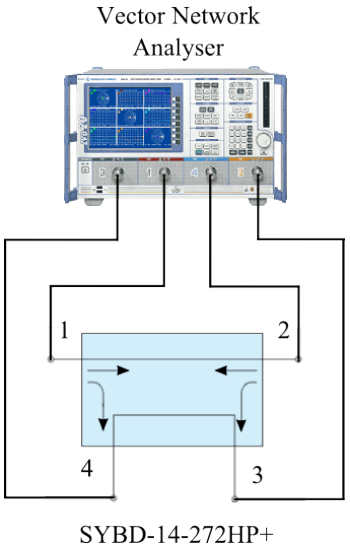

Figure 6.7: Four port measurement set up of coupler.

In order to verify the coupling factor of the SYBD-14-272HP+ it is measured on a VNA with a four port test set up, as shown in Figure 6.7. The result of the

measurement is given in Figure 6.8, where it is seen that the coupling factor (S_{31}) is at 11 dB. This is 3 dB lower than the expected coupling factor and will affect the results of the dynamic range calculations. According to the coupler's datasheet, the coupling factor value can vary up to 1.5 dB from the specified value. The 11 dB measured coupling factor is 1 dB lower than the absolute minimum value that was specified by the datasheet.

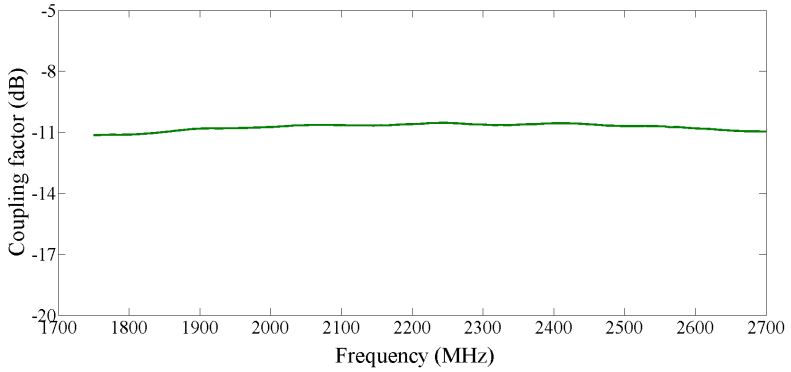

Figure 6.8: Measured coupling factor of the SYBD-14-272HP+.

6.1.4 Revised dynamic range results

From the measurements of the LNA A and the coupler it was clear that the dynamic range calculations in Chapter 4 are no longer valid. The calculations are repeated for the values obtained in the measurements given in the preceding two subsections. From subsection 6.1.1, the practical maximum output power of the modulator is found to be 7.27 dBm, from subsection 6.1.2 the gain of the LNA is found to be 15 dB and finally, from subsection 6.1.3, the coupling factor is found to be 11 dB. The open loop characteristics are the following: the maximum input power = -4 dBm, $MDS_{initial}$ = -168.6847 dBm/Hz (the initial noise Figure $NF_{initial}$ = 5.315 dB).

Table 6.8 shows the results of the revised calculations. From this table it can be seen that the maximum input power to the RPC is now -4.64 dBm.

6.1.5 Operational amplifier design

From Chapter 4, it is seen that a voltage gain of 9.5 dB is used as the voltage gain of the low noise differential operational amplifier. The process leading up to the choice for the resistor values and the amount of gain used is discussed in this subsection. The components are chosen to maintain a low noise contribution to the rest of the system. The ADA4927 is chosen as the low noise differential amplifier for this application and is studied by using an analysis tool from Analog Devices (Diff-Amp Calculator), which calculates the operational amplifier's output referred voltage noise [29]. In section 3.2.3 an equation was given that can be used to calculate the noise figure of an operational amplifier, given the values of its resistors and output referred noise voltage. This equation is repeated in 6.1.2.

Table 6.8: This shows the closed loop results of the RPC with the following component combination: LNA A = ZX60-272LN+, low noise differential amplifier C = ADA4927 with no amplifier at LNA B.

Max cancelled (dBm)	Coupling (dB)	MDS_{RPC} (dBm/Hz)	MDS loss (dB)
-0.03	7	-164.15	4.54
-1.25	8	-164.90	3.79
-2.42	9	-165.54	3.15
-3.54	10	-166.08	2.60
-4.64	11	-166.54	2.14
-5.72	12	-166.93	1.75
-6.78	13	-167.26	1.43
-7.82	14	-167.52	1.16
-8.86	15	-167.75	0.94

$$NF_{diffamp} = \frac{v_{NO}^2}{4kTR_S G_{FB}^2 (\frac{R_T}{R_S+R_T})^2} \tag{6.1.2}$$

where $R_S = 50\Omega$, $R_T = 200\Omega$, $G_{FB} = 2.5$ and $v_{NO} = 10\ nV/\sqrt{Hz}$ for this calculation.

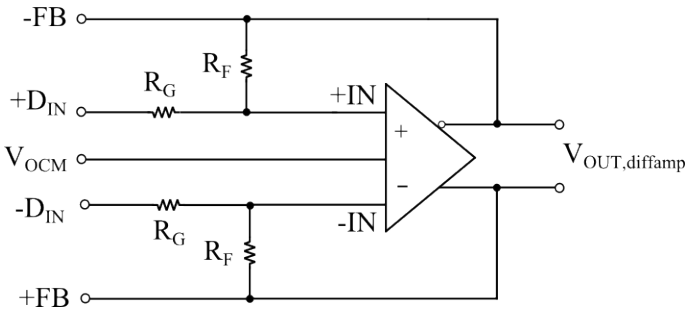

Figure 6.9: Low noise differential amplifier model.

The model of the low noise differential amplifier is given in Figure 6.9. To design the gain, the constraints that will limit this amplifier needs to be defined first.

- The low noise differential amplifier should always work in its linear region; it should not add any harmonics to the feedback system.
- The opamp should be able to linearly amplify the maximum output from the demodulator.
- The maximum output voltage of the low noise differential amplifier should not exceed the maximum input of the integrator amplifier, which is limited by its supply voltages.

If all these constraints are taken into account, the maximum amount of gain that the low noise differential amplifier can have is 3 (or 9.5 dB). Using the Diff-Amp Calculator, the values for R_F and R_G are chosen in order to add as little extra noise as possible. The Diff-Amp Calculator's output is shown in Appendix A.

Table 6.9 is a summary of the values chosen for this RPC's baseband components.

Table 6.9: This table contains the values that are to be used for the final RPC's baseband section.

Component	$\boldsymbol{R_G}$	$\boldsymbol{R_F}$
Value	100Ω	300Ω

6.1.6 Cancellation bandwidth

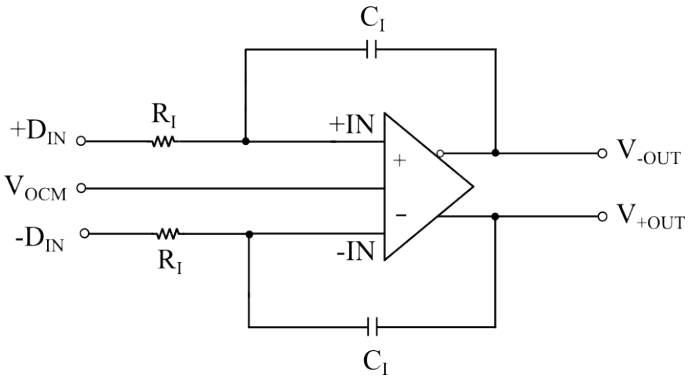

Figure 6.10: Integrator differential amplifier model.

The next practical consideration is the RPC's cancellation bandwidth which is controlled by the combination of the capacitor (C_I) and resistor (R_I) used in Figure 6.10 as well as the total gain from the rest of the components in the canceller (G_{RPC}). The cancellation bandwidth was introduced as a function of the RPC's control system in Chapter 2. The open loop unity gain cut off of the integrator can be calculated as shown in equation 6.1.3.

$$f_{cutoff} = \frac{G_{RPC}}{2\pi R_I C_I} \tag{6.1.3}$$

Depending on the amount of gain that is added by the rest of the RPC (G_{RPC}), the closed loop bandwidth is determined by equation 6.1.4.

$$|T(s)| = |\frac{s\ 2\pi R_I C_I}{s\ 2\pi R_I C_I + G_{RPC}}| \tag{6.1.4}$$

G_{RPC} is calculated as in equation 6.1.5:

$$G_{RPC} = G_{v-new}\ G_{diffamp}\ G_m\ c^2 \tag{6.1.5}$$

where G_{v-new} is the conversion gain of the demodulator and balun, $G_{diffamp}$ is the gain of the fully differential opamp C, G_m is the modulator's conversion gain and c^2 is the coupling factor.

The expected cancellation bandwidth of the practical RPC can now be simulated. This is done with the help of MATLAB's sisotool, the closed loop response is given in Figure 6.11.

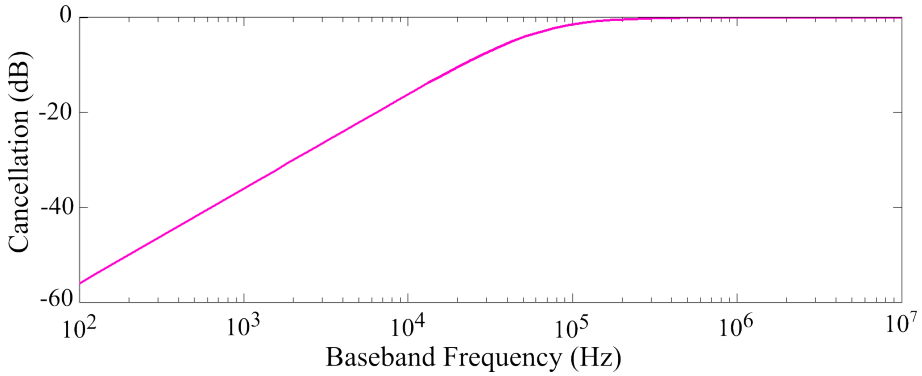

Figure 6.11: Prediction of the practical cancellation bandwidth for the IQ Reflected Power Canceller.

Table 6.10: The component values of the integrator for the baseband section of the final RPC.

Component	R_I	C_I
Value	1 kΩ	10 nF

The resistor and capacitor values that are used to represent the integrator amplifier in the RPC is given in Table 6.10.

6.2 Board layout and PCB

Throughout this chapter a practical solution for the RPC has been developed. The component values were determined in order to maintain a low noise system and the integrator values were chosen for a specific cancellation bandwidth. A modular form of the RPC has already been assembled and used throughout the preliminary tests. However, a PCB is produced for measuring the final system in Chapter 7. This section gives a brief overview of the process followed to design the PCB for the RPC. In order to maintain a level of modularity, only the demodulator, low noise differential amplifier, integrator amplifier and modulator are designed on the PCB. This makes it possible to change the coupler and LNAs of the system shown in Figure 6.1. In order to ensure a functional PCB design, the design for each component is based on the information provided in their respective application notes (ADL5380, ADL5375 and ADA4927).

The PCB layout used a four layer configuration, where the two inner layers were ground planes. Only the modulator output and demodulator input, as well

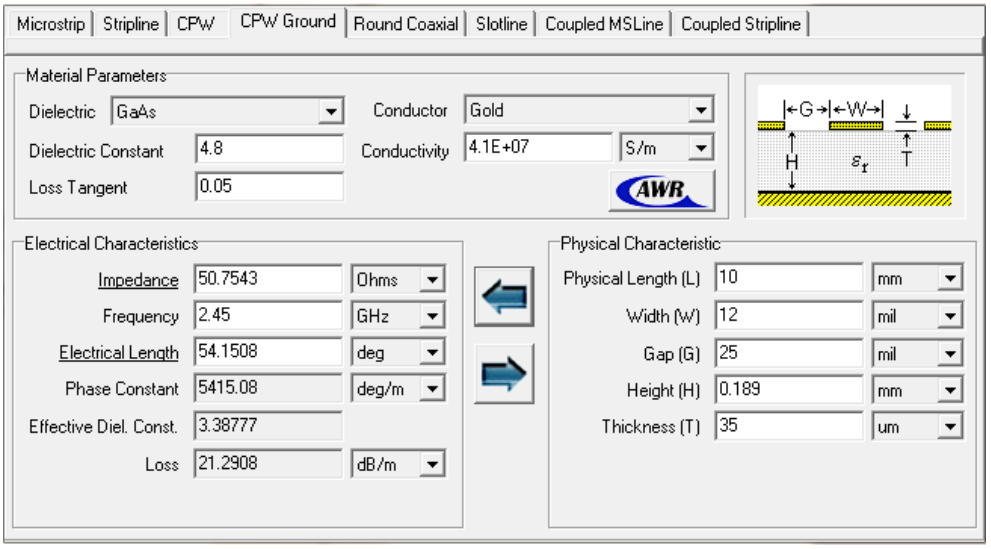

Figure 6.12: The AWR Microwave Office tool TXLINE used to calculate the track width of the RPC PCB.

as both LO inputs, were at RF frequencies (2.4 GHz - 2.5 GHz). The board was designed to have 50Ω line impedances in the high frequency sections of the RPC. This was ensured with the help of the AWR tool TXLINE. The calculation is shown in Figure 6.12.

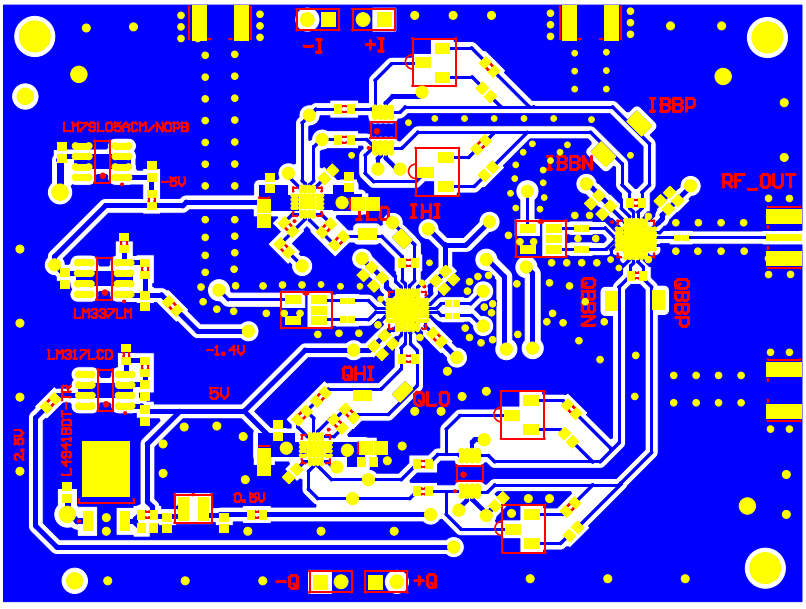

Figure 6.13: Top layer of the IQ Reflected Power Canceller PCB.

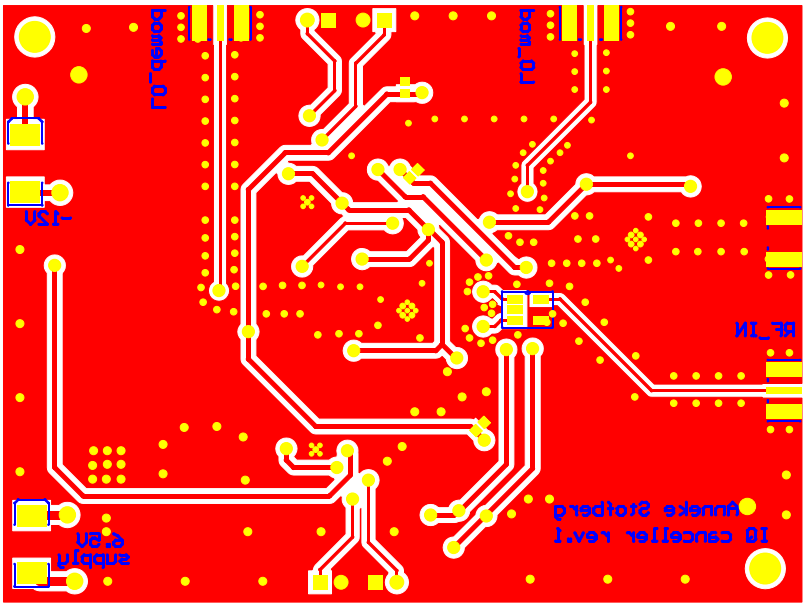

Figure 6.14: Bottom layer of the IQ Reflected Power Canceller PCB.

Via stitching was used along the 50Ω lines to ensure a good ground around the RF lines. Also, the I and Q lines at baseband were kept symmetrical in order to minimise LO amplitude and phase error in the modulator [12]. Figure 6.13 and Figure 6.14 shows the top and bottom layer of the PCB (with their respective silk screen and overlay). The left side of the PCB is used for the voltage regulators. A full circuit diagram depicting the RPC with all of its component values, is given in Appendix D. This is followed by a photo of the final RPC setup that was used in the measurements.

6.3 Conclusion

This chapter contained the final details of the design for a practical RPC. The components that were chosen in earlier chapters were measured and compared with their expected values. From these results the dynamic range calculations could be repeated to finally produce the optimum system from the available components. The PCB in Figures 6.13 and 6.14 can now be used in the final tests of the RPC.

Chapter 7

Measurements and results

The aim of this chapter is to describe and carry out the tests to verify the characteristics of the RPC. The theoretical and practical systems are compared, where the total cancellation of the RPC is displayed on a magnitude cancellation vs. frequency graph. The dynamic range of the RPC is measured and compared to the theoretically predicted values from Chapter 4. The compensation for the RF phase error that was designed in Chapter 5, is implemented in the RPC and the RF phase range wherein the system will remain stable is measured. Table 7.1 contains the components used for the final RPC, along with their relevant noise and power attributes.

Table 7.1: This table contains the suggested components for the RPC when an 11 dB coupler is used.

Component	Part number	Gain	Noise figure
IQ Modulator	ADL5375	-3.3 dB	NA
IQ Demodulator + Balun	ADL5380 +TC1-1-13	-2.3 dB [1]	16.92 dB
LNA A + Coupler	ZX60-272LN+ + SYBD-14-272HP+	13.94 dB	2.1 dB
Low noise diff amp C	ADA4927	9.5 dB	14.8 dB

7.1 Cancellation

The focus of the research throughout this report was the evaluation of an RPC. The most important attribute of the RPC, is the amount of cancellation that it will supply. The test setup that was used to measure the RPC's cancellation is described in subsection 7.1.1. This is followed by the measurement results in section 7.1.2. In the results, the cancellation of the practical RPC is compared to that of the theoretically predicted cancellation that was simulated in Chapter 6.

[1] The voltage conversion gain of the demodulator used in this chapter is the equivalent open circuit gain and is thus 6 dB higher than the value provided in this table.

7.1.1 Test setup

The aim of the RPC is to be used in an FMCW radar receiver, however the tests described in this section use only single frequency inputs as used in the derivations in Chapters 2 and 5. Figure 7.1 shows the test setup that is used. Two signal generators are used to produce the LO and RF signals. An external reference is used to synchronise the two signal generators. The LO signal generator's output is divided by a 3 dB splitter in order to supply both the modulator and demodulator with the same LO signal.

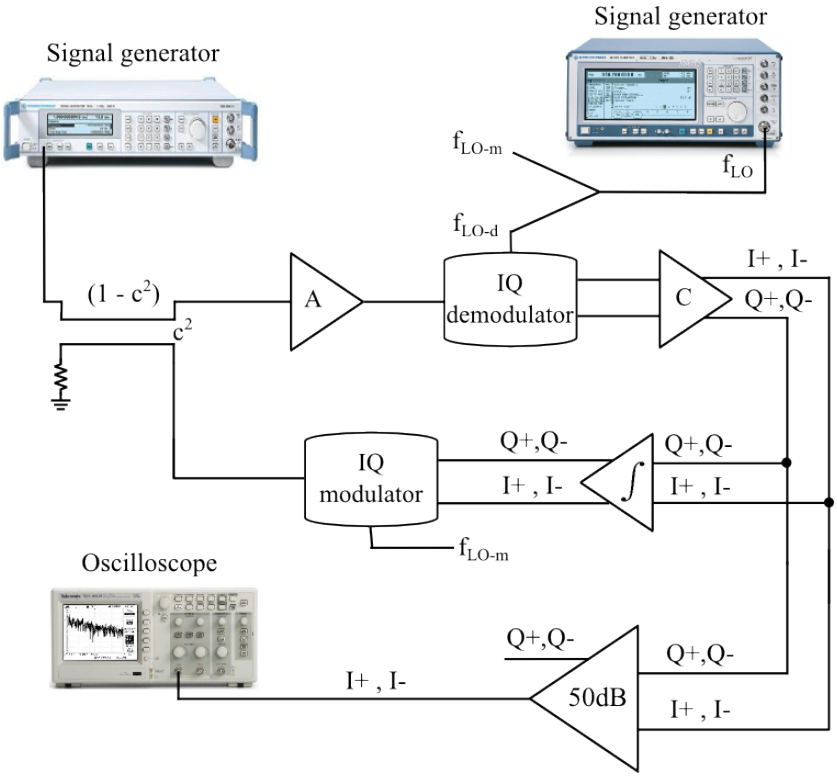

Figure 7.1: Test setup for measuring the IQ Reflected Power Canceller's cancellation across its baseband frequency.

The RF signal is supplied at the coupler's input port (port one), the output of the coupler is at the through port (port two) which is then amplified by LNA A and taken as the input to the demodulator. The output of the demodulator is the I and Q IF signals in differential form. This is used as the input to the low noise differential amplifiers C. This is also taken as the output of the RPC which is measured on an oscilloscope. During a measurement, the input power remains constant while the IF frequency is varied across the baseband bandwidth by adjusting the RF input frequency. The next stage includes the integrators, whose outputs are taken as the inputs to the modulator. The modulator's output is fed into the coupled port (port three) of the coupler. The fourth port of the coupler is terminated on a 50 Ω load.

The cancellation results that are presented in this section was measured on the I channel's output. The results are similar for the output of the Q channel.

7.1.2 Results

The test setup, as given in subsection 7.1.1, is used with the test values as given in Table 7.2. The results presented in Figure 7.2 are normalised to 0 dB in order to compare the results of the separate input powers. The theoretically predicted cancellation is also shown on the figure.

Table 7.2: The test values used to measure the linear working region of the RPC

LO (GHz)	IF (Hz)	RF power (dBm)
2.45	100:1 000 000	-20,-10,-4.6

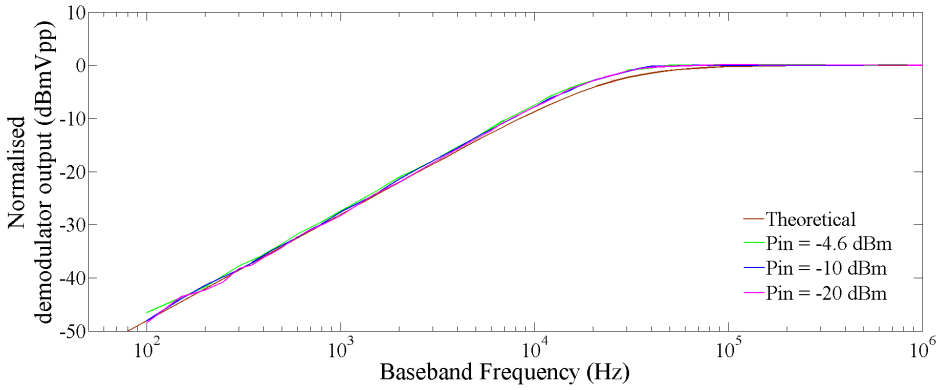

Figure 7.2: Measurement of the RPC's cancellation results for various RF input power compared with a theoretical prediction.

From the results in Figure 7.2 it is seen that a cancellation of more than 40 dB is achieved for an IF signal frequency of 100 Hz. For the smallest measured input power ($-20\ dBm$) result presented in Figure 7.2, it was expected that the measured cancellation would follow the predicted cancellation closely. However this is not the case. The amplitude of the measured voltage was very small, and this resulted in measurement inaccuracies when the measurement was taken on the oscilloscope. For the highest input power ($P_{in} = -4.6dBm$), the output of the demodulator started to saturate below 100 Hz and no longer followed the straight line of the theoretical prediction. This non linear region places a limit on the closest reflection that the RPC can cancel without causing unwanted harmonics in the output of the system.

7.2 Dynamic range

In Chapter 3 the concept of dynamic range was introduced by describing two components that can be used to characterise it. The 1 dB compression point characterised the top limit while the noise floor could be used to describe the lower limit of the dynamic range. It was also established that adding an RPC to a radar receiver would impact the dynamic range of the receiver, and so a method was derived in

Chapter 4 that could be used to produce an RPC with an optimised dynamic range. This would allow the RPC to have a minimal effect on the radar receiver's detection performance.

The dynamic range of the RPC designed throughout this report, is determined by two measurements. The first measurement consists of determining the maximum signal power that the RPC can cancel while remaining linear (not producing any harmonics that are less than 30 dB below the measured target signal power). This measured value is compared to the value that was predicted using the FOM calculations from Chapter 4. The second measurement that is used to characterise the dynamic range of the RPC, is the noise figure measurement. If the noise figure of the system is known, the equivalent noise floor can be calculated and thus the minimum detectable signal of the receiver can be determined. There are several methods that can be used to measure the noise figure of a network. Since the expected noise figure is relatively high (> 5 dB), the Y factor method has sufficient accuracy [21].

7.2.1 Maximum signal power

The maximum signal power that can be cancelled was defined in Chapter 4 as

$$P_{maxCancel} = \frac{c^2 \ P_{mod}}{1 - c^2} \tag{7.2.1}$$

where $P_{maxCancel}$ is the maximum signal power that can be cancelled by the RPC, P_{mod} is the maximum output power of the modulator and c^2 is the coupling factor of the coupler. This value has already been seen in the measurement result of Figure 7.2, as the non linear region below 100 Hz. This region is where the modulator has reached its maximum output power. Even though the integrators in the feedback loop should have an increase in gain as the frequency decreases, the modulator has already reached its maximum output power at 100 Hz. From equation 7.2.1, the maximum signal power that can be cancelled is calculated using the maximum output power of the modulator that was measured in Chapter 6.

7.2.2 Minimum detectable signal

In Chapter 4, it was assumed that the noise floor characterised the minimum detectable signal of the receiver. In order to measure the minimum detectable signal, the method that was followed to determine the noise figure of the RPC has to be described first, since

$$MDS_{withCanceller} = \frac{N_{noiseFloor} NF_{OL} + c^2 N_{mod}}{1 - c^2} \tag{7.2.2}$$

where NF_{OL} is the open loop noise figure of the RPC, N_{mod} is the noise floor of the modulator and c^2 is the coupling factor. The MDS is related to the noise figure of the closed loop system by

$$MDS_{withCanceller} = N_{noiseFloor} NF_{CL} \tag{7.2.3}$$

Both the open loop (NF_{OL}) and the closed loop (NF_{CL}) noise figure of the RPC are measured in order to compare the designed values from Chapter 6 to their

corresponding measured values in this chapter. The dynamic range of the RPC was designed to be at an optimal value, and the increase in noise figure from the open loop system to the closed loop system is equal to the increase in Tx power(from Chapter 4).

Noise is usually measured at very low power levels, which means that the system will work within its linear region. During a measurement, if the input signal is set to zero but the source impedance remains, the power input to the Device Under Test (DUT) is the thermal noise from the source impedance (50 ohm in this case). If the device is linear, the output power characteristic vs. source temperature will have a straight line relationship, as shown in Figure 7.3.

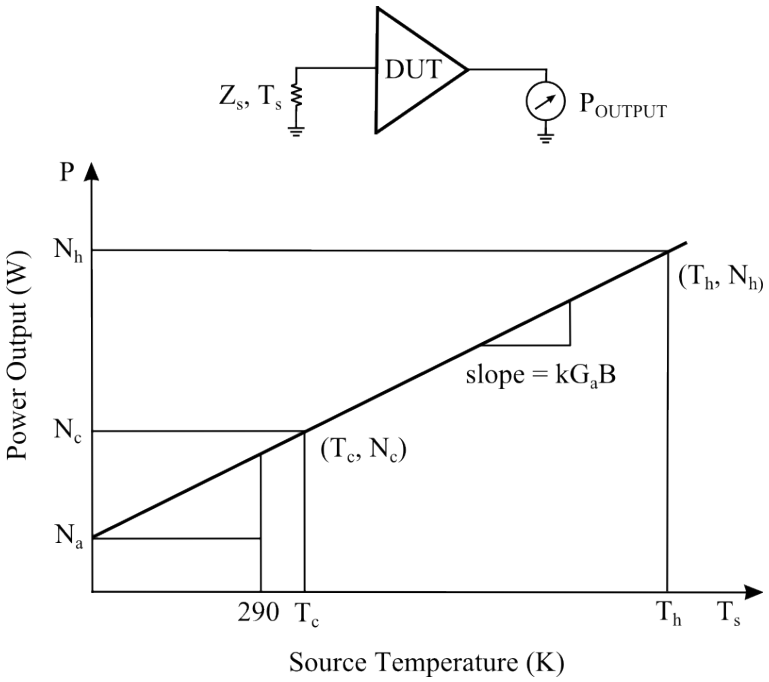

Figure 7.3: Output power vs. source temperature.

At the origin of the X-axis in Figure 7.3, with the temperature at $0K$, the only noise measured at the output is the noise generated in, or added by, the DUT and is represented by the symbol N_a. For any other source temperature T_s, the electron vibrations in the source act like a signal to the DUT with available input noise power density, kT_s W/Hz (-174 dBm/Hz at room temperature). The input noise power is amplified by the gain of the DUT to form additional output noise power, bringing the total output to $N_a + kT_sG_aB$ [21].

Noise figure and effective input noise temperature are usually determined by measuring two points along the straight-line noise characteristic in Figure 7.3. On this figure, two temperatures are indicated, the first is T_c (cold) with a corresponding noise power N_c and the second temperature is T_h (hot), which corresponds to a noise power of N_h. The ratio N_h/N_c is called the Y factor [21].

7.2.3 Y Factor method

The Y factor method is explained with the help of an application note from Hewlett Packard [21]. In order to calculate the noise figure using this method, the temperature (T_h and T_c) of the noise source is required. Noise source manufacturers usually specify T_h in terms of the Excess Noise Ratio (ENR), which is shown in equation 7.2.4 [21].

$$ENR = 10log\frac{T_h - T_0}{T_0} \tag{7.2.4}$$

Figure 7.4 gives a block diagram test setup that shows how to measure the noise figure of a DUT using the Y factor method [3]. The noise figure can be determined as in equation 7.2.5 [21].

$$NF = \frac{(\frac{T_h}{290} - 1) - Y(\frac{T_c}{290} - 1)}{Y - 1} \tag{7.2.5}$$

where $Y = \frac{N_h}{N_c}$.

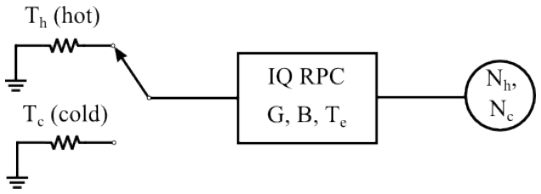

Figure 7.4: The test setup illustrating how to measure noise figure using the Y factor method.

By using the ENR supplied by the noise source, the value for T_h can be calculated while T_c is taken at room temperature, simplifying equation 7.2.5 to 7.2.6. The Agilent 346B is used as the noise source for the noise figure measurement. An extract of the relevant ENR values which are supplied with the noise source is given in Table 7.3.

$$NF = \frac{ENR}{Y - 1} \tag{7.2.6}$$

Table 7.3: An extract from the ENR values of the Agilent 346B noise source.

Frequency (MHz)	ENR (dB)
10	14.94
1000	14.95
2000	14.85
3000	14.75
4000	14.69
5000	14.68

Usually, the noise source is used with a noise figure meter. Figure 7.5 shows a standard test setup using a noise figure meter to measure the noise figure of a DUT. The noise figure meter is calibrated for the specific frequency at which the noise figure measurement is taken. This also allows the noise figure meter to use the correct value of ENR for the measurement [30].

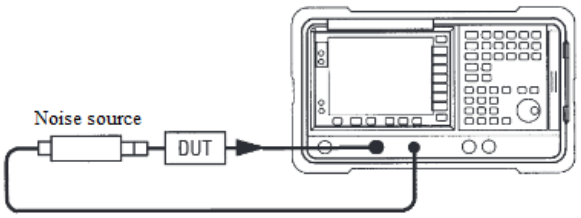

Figure 7.5: Measuring noise figure using a noise figure meter.

From Figure 7.5 it can be seen that the input and output frequencies of the DUT are the same, thus this type of setup is sufficient. Since the input to the RPC is at a different frequency than that of its output (down conversion takes place), and the maximum baseband frequency of the RPC is 1 MHz, the setup in Figure 7.5 is not sufficient. For noise figure measurements where the down converted baseband frequency is above 10 MHz, the noise figure meter setup in Figure 7.5 can still be used because it falls within the noise meter's bandwidth [30]. The noise figure meter can not be used in the Y factor measurement of the RPC, so a different approach is required to measure the RPC's noise figure.

7.2.4 Test setup for open loop Y factor measurement

Figure 7.8 shows the test setup that is used to measure the Y factor of the open loop RPC system. The noise source is applied as the input, which can be switched between a hot and a cold temperature. No cancellation is applied to this measurement.

The output of the low noise differential operational amplifier C is applied to a 50 dB amplifier in order to ensure the noise value to be measured, is higher than the noise floor of the oscilloscope. The output of this amplifier is passed through an anti aliasing filter and measured on an oscilloscope. The oscilloscope's output is read into MATLAB where the power average across 100 measurements is taken for each baseband frequency point. The method for obtaining the oscilloscope data in MATLAB is described in Appendix B.2 and the MATLAB code used to calculate the power average of the oscilloscope measurement is given in Appendix B.1. The design of the 50 dB amplifier and the anti aliasing filter is discussed before the rest of the test setup for the open loop Y factor measurement is described.

The 50 dB amplifier is implemented by connecting two 25 dB amplifier stages in cascade. A single stage using two operational amplifiers connected in a differential configuration is shown in Figure 7.6. It was assumed that the gain added by the components leading up to the 50 dB amplifier was sufficient to make the noise contribution of this high gain stage inconsequential.

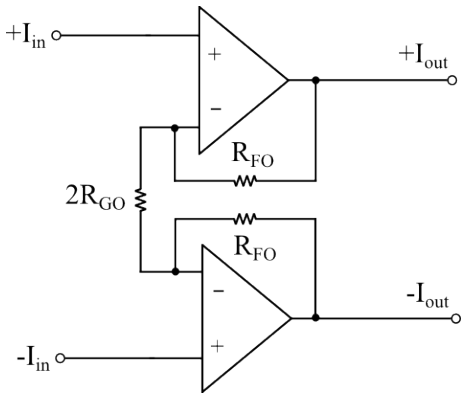

Figure 7.6: The circuit diagram of the 50 dB amplifier used in the y factor noise measurements.

The design of the anti aliasing filter is prescribed by certain specifications set by the oscilloscope. The oscilloscope is an N-bit ADC with an M-word buffer where $N = 8$ and $M = 2500$. Aliasing occurs if the time domain measurement on the oscilloscope has frequency components that are higher than the Nyquist frequency. The Nyquist frequency is defined as half the sampling frequency $f_s/2$. The frequency resolution of the FFT spectrum on the oscilloscope is determined by dividing the sampling frequency by the M-word buffer (f_s/M). In order to measure sufficiently low frequencies, the sampling frequency is set as $f_s = 5\ MHz$. This results in a Nyquist frequency of 2.5 MHz and ensures a frequency resolution of 2 kHz [31]. The anti aliasing filter is designed to have a 1 MHz cut off frequency and is implemented as a second order LC circuit as shown in Figure 7.7.

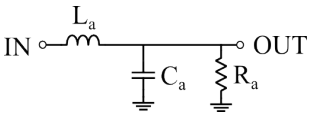

Figure 7.7: A circuit diagram of the anti aliasing filter used in the Y factor noise measurements of the RPC.

The test setup, as described in Figure 7.8, only shows the measurement setup of the noise figure of the I channel. The Q channel noise figure measurement follows the same method.

7.2.5 Open loop noise figure calculation

Throughout the noise calculations in Chapters 4 and 6, it was assumed that the RPC worked under matched conditions. This assumption allowed the available power equivalent models to be used to calculate the system's cascaded noise figure. However, this assumption is not valid for the differential operational amplifier C, or the 50 dB amplifier described in the previous subsection. The difference between the voltage gain and the available power gain of a system with unmatched conditions, can be described with the diagram in Figure 7.9.

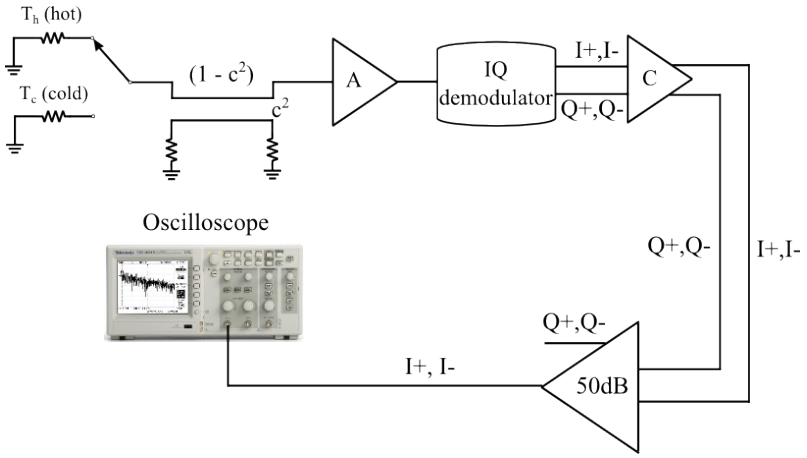

Figure 7.8: The test setup for measuring the open loop noise figure using the Y factor method.

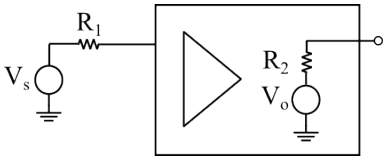

Figure 7.9: Describing the available gain of a system.

Figure 7.9 shows an amplifier with an output impedance R_2, driven by a source with an impedance R_1. The available power gain of this system can be calculated as

$$\begin{aligned} G_A &= \frac{V_o^2}{4R_2}\frac{4R_1}{V_s^2} \\ &= \frac{R_1}{R_2}\frac{V_o^2}{V_s^2} \end{aligned} \tag{7.2.7}$$

Next, consider the open circuit voltage gain of the system in Figure 7.9, given in equation 7.2.8.

$$G_v = \frac{V_o}{V_s} \tag{7.2.8}$$

If the power gain and voltage gain are compared in their equivalent dB values, the power gain becomes

$$G_A = 10\log\frac{R_1}{R_2}\frac{V_o^2}{V_s^2}$$

and the voltage gain becomes

$$G_v = 20\log\frac{V_o}{V_s}$$

For a matched input and output impedance $R_1 = R_2$, the two gains are equal $G_A = G_v$, but for $R_1 \neq R_2$ the voltage gain does not equal the available power gain.

In order to calculate the noise figure of the differential opamp C correctly, the noise figure of the cascaded sections up to the demodulator's output are calculated first using the available power model under matched conditions. Figure 7.10 shows the input cascaded sections of the open loop RPC. The coupler's insertion loss ($10 \log IL_{coupler}$) adds directly to the noise figure of the LNA, and the gain of the coupler ($G_{coupler}$) also directly adds with the dB gain of the LNA [3]. The transmission line used to connect the coupler to the signal generator in the open loop measurement, has an insertion loss of 0.7 dB, which is included in the calculations. The total noise figure of the system in Figure 7.10 can be calculated as in equation 7.2.9, using the values supplied in Table 7.1.

$$\begin{aligned} NF_{Ga} &= NF_1 + \frac{NF_2 - 1}{G_1} \\ &= 1.622 + 1.946 \\ &= 3.568 \\ &= 5.52dB \end{aligned} \tag{7.2.9}$$

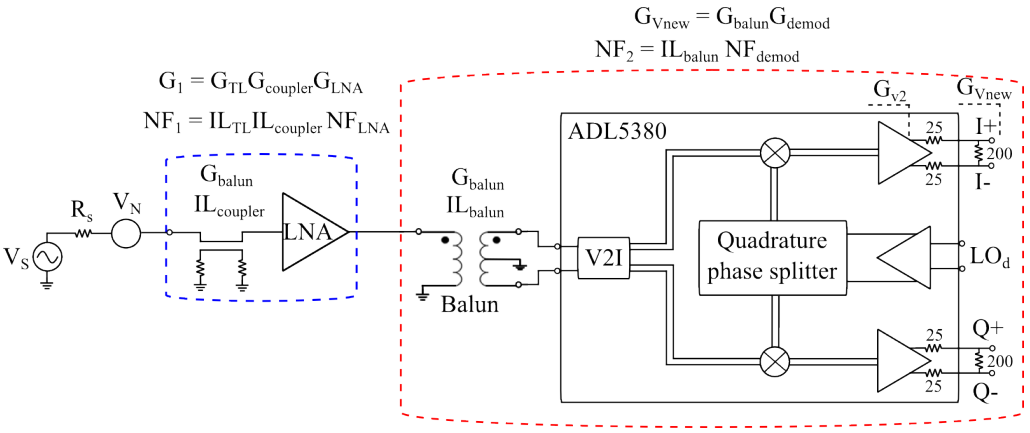

Figure 7.10: Calculating the noise figure of the cascaded system before the differential operational amplifier C.

In order to add the noise of the differential operational amplifier C to the noise figure calculation, the open circuit voltage equivalent noise model is used. First, the equivalent open circuit voltage gain of the system in Figure 7.10 has to be calculated. The available gain G_1 indicated on Figure 7.10 exists under matched conditions and thus $G_1 = G_{v1}$, where G_{v1} is the equivalent voltage gain of the LNA and coupler. The open circuit voltage of the demodulator and balun combination can be calculated using equation 7.2.10.

$$G_{v2} = G_2 \frac{200 + 50}{200} \tag{7.2.10}$$

where G_{v2} is the open circuit voltage gain of the demodulator and balun combination and G_2 is the measured gain of the demodulator and balun across a 200 Ω load. Both of these quantities are indicated on Figure 7.10. The total open circuit voltage gain of the system in Figure 7.10 is calculated as in equation 7.2.11.

$$\begin{aligned} A_v &= G_{v1}G_{v2} \\ &= 10^{13.94/20}10^{-8.3/20}(1.25) \\ &= 2.39V/V \end{aligned} \tag{7.2.11}$$

Using the open circuit voltage equivalent noise model, as well as the definition of noise figure from Chapter 3, the equivalent noise voltage at the output of the demodulator in Figure 7.10 can be calculated.

First, consider the signal to noise ratio at the input of the system in Figure 6.3

$$SNR_{IN} = \frac{v_S^2}{v_N^2} \tag{7.2.12}$$

where v_S is the input signal voltage and v_N is the noise voltage due to the source resistor ($R_S = 50\ \Omega$). The output signal to noise ratio is calculated as

$$SNR_{OUT} = \frac{v_S'^2}{e_d^2 + v_N'^2} \tag{7.2.13}$$

where v_S' is the signal voltage at the output of the system due to the input signal voltage multiplied by the system voltage gain, e_d is the noise voltage contribution of the cascaded system and v_N' is the noise voltage of the source amplified by the system voltage gain in Figure 7.10.

The noise figure of the open loop system is calculated using equations 7.2.12 and 7.2.13

$$\begin{aligned} NF_{Ga} &= \frac{SNR_{IN}}{SNR_{OUT}} \\ &= \frac{e_d^2 + v_N'^2}{A_v^2 v_N^2} \\ &= 1 + \frac{e_d^2}{v_N'^2} \end{aligned} \tag{7.2.14}$$

Next, the input referred voltage noise of the differential opamp C is determined. The noise model is shown in Figure 7.11, where R_{50} is the differential output impedance and R_{200} is the load impedance at the demodulator's output (indicated on Figure 7.10). v_{Nd} is the noise voltage of the opamp and I_{NM} and I_{NP} are the noise currents of the opamp. The values for $R_G = 100\Omega$ and $R_F = 300\Omega$ were determined in Chapter 6.

The noise voltages due to the resistors in the system, are calculated as in equation 7.2.15.

$$\begin{aligned} v_{THt} &= \sqrt{2[4kt\frac{R_{50}||R_{200}}{2}]} \\ v_{RGt} &= \sqrt{2[4kTR_G]} \\ v_{RFt} &= \sqrt{2[4kTR_F]} \end{aligned} \tag{7.2.15}$$

The equivalent noise voltage due to the opamp's current noise I_{NP} and I_{NM} is calculated as in equation 7.2.16.

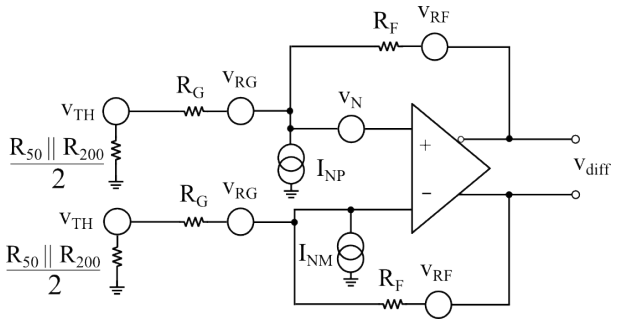

Figure 7.11: Calculating the input referred noise voltage of the differential opamp C.

$$\begin{aligned} v_{INM} &= I_{NM}[(R_G + \frac{R_{50}||R_{200}}{2})||R_F] \\ v_{INP} &= I_{NP}[(R_G + \frac{R_{50}||R_{200}}{2})||R_F] \end{aligned} \tag{7.2.16}$$

Figure 7.12 shows the noiseless model of the differential opamp, the equivalent output signal and noise sources from the input cascaded system (Figure 7.10) are also added to the figure.

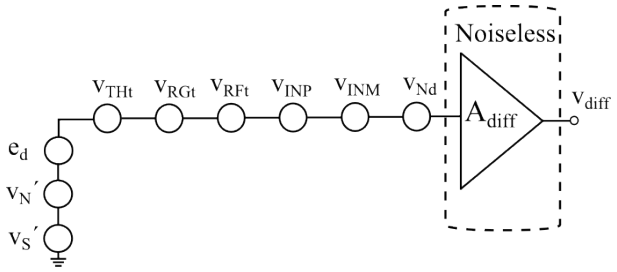

Figure 7.12: Calculating the input referred noise voltage of the differential opamp C.

The noise voltages in Figure 7.12 can now be added as in equation 7.2.18. Both the signal and noise voltages at the output of the differential amplifier are multiplied by the noiseless open circuit voltage gain of the differential amplifier A_{diff} (equation 7.2.17).

$$\begin{aligned} A_{diff} &= \frac{R_F}{R_G}\frac{R_{200}}{R_{200}+R_{50}} \\ &= 2.4V/V \end{aligned} \tag{7.2.17}$$

$$SNR'_{OUT} = \frac{A^2_{diff}v'^2_S}{A^2_{diff}(v'^2_N + e^2_d + v^2_{THt} + v^2_{RGt} + v^2_{RFt} + v^2_{INM} + v^2_{INP} + v^2_{Nd})} \tag{7.2.18}$$

If the noise figure calculation from equation 7.2.14 is repeated for the new SNR'_{OUT} in equation 7.2.19, and the open loop noise figure is calculated as:

$$
\begin{aligned}
NF_{OL} &= \frac{SNR_{IN}}{SNR'_{OUT}} \\
&= \frac{v_S^2}{v_N^2}\frac{v_N'^2 + e_d^2 + v_{THt}^2 + v_{RGt}^2 + v_{RFt}^2 + v_{INM}^2 + v_{INP}^2 + v_{Nd}^2}{v_S'^2} \\
&= 1 + \frac{e_d^2}{v_N'^2} + \frac{v_{THt}^2 + v_{RGt}^2 + v_{RFt}^2 + v_{INM}^2 + v_{INP}^2 + v_{Nd}^2}{v_N'^2} \\
&= 3.568 + 3.978 \\
&= 7.54 \\
&= 8.78\ dB
\end{aligned} \tag{7.2.19}
$$

The values of the noise voltages used in equation 7.2.19 are provided in Table 7.4.

Table 7.4: The noise voltage values of the circuit in Figure 7.12

Symbol	Value
v'_N	2.17 $nV/\sqrt{Hz}$
v_{THt}	0.81 $nV/\sqrt{Hz}$
v_{RGt}	1.82 $nV/\sqrt{Hz}$
v_{RFt}	3.15 $nV/\sqrt{Hz}$
v_{INM}	1.20 $nV/\sqrt{Hz}$
v_{INP}	1.20 $nV/\sqrt{Hz}$
v_{Nd}	1.4 $nV/\sqrt{Hz}$

The noise figure calculation in this subsection assumes that the noise figure contribution of the components following the differential operational amplifier are insignificant.

7.2.6 Measurement: Open loop noise figure

Figure 7.13 and 7.14 shows measurement of N_c and N_h for I^+ relative to ground and I^- relative to ground respectively. The Y factor is determined for each measurement from the ratio $Y = N_h/N_c$ and the noise figure is calculated using equation 7.2.6.

The noise figure for each measurement is calculated as

$$NF_{OL} = \frac{ENR}{Y_{OL} - 1}$$

The results are presented in Table 7.5 for different frequency points.

From Table 7.5 it is seen that the noise figure remains relatively constant across the baseband frequency range. However, the measured and theoretical values do not correspond, this is investigated further in section 7.2.9. From Figures 7.13 and 7.14, flicker noise of the operational amplifiers can be observed for frequencies below 20 kHz. Flicker noise, or 1/f noise, increases as the frequency decreases as seen in Figure 7.13. This type of noise is associated with the dc current in electronic devices and it is inherent in all active and some passive devices [32]. Another

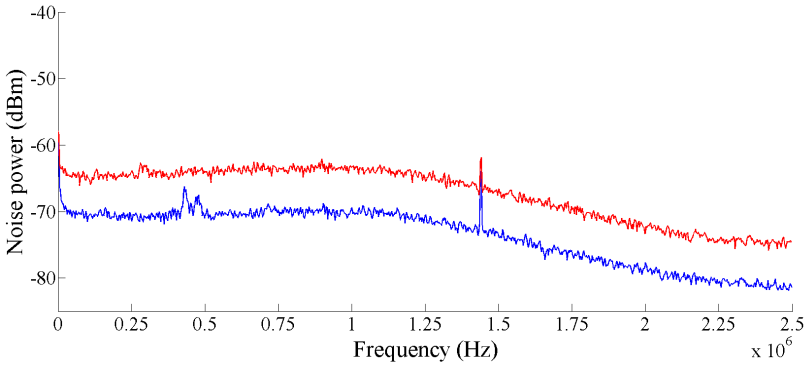

Figure 7.13: Open loop averaged noise power measurement for positive differential output.

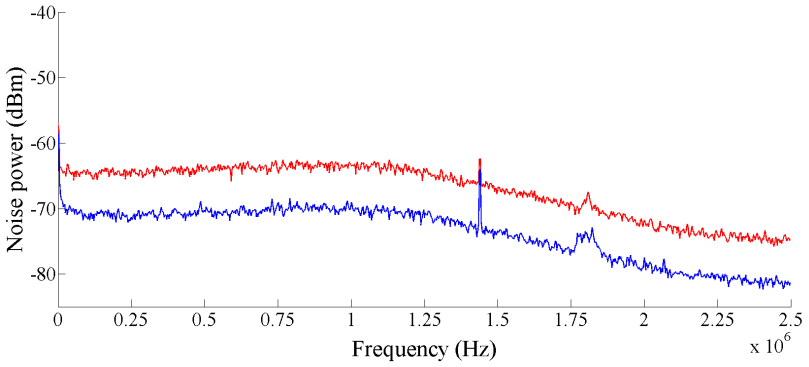

Figure 7.14: Open loop averaged noise power measurement for negative differential output.

Table 7.5: Noise figure results for the open loop RPC measurement.

Frequency (kHz)	NF_{OL-I+} (dB)	NF_{OL-I-} (dB)
Theoretical	8.78	8.78
10	12.97	13.2
100	10.4	9.11
1000	9.6	9.2

observation of the results in Figures 7.13 and 7.14 shows several spikes in the measurements which can be ascribed to environmental noise.

7.2.7 Test setup for closed loop Y factor measurement

The setup for the closed loop noise measurement is similar to that of the open loop system, the only difference is the added feedback supplied by the integrators and the modulator. The test setup is shown in Figure 7.15. From the design of the optimised dynamic range in Chapter 6.1.4, it is known that the system with an RPC will have a higher noise figure. The increase in noise figure is calculated using the increase in Tx power equation from Chapter 4 shown in 7.2.20.

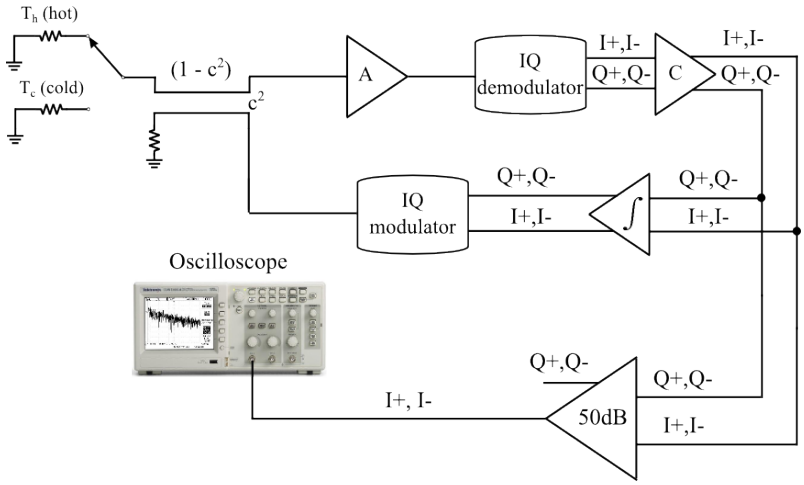

Figure 7.15: The test setup for measuring the closed loop noise figure using the Y factor method.

$$NF_{CL} = NF_{OL}\frac{N_{initial} + c^2 N_{mod}}{(1-c^2)\ N_{initial}} \tag{7.2.20}$$

where N_{mod} is the noise floor of the modulator and $N_{initial}$ is the noise floor of the receiver before an RPC was added to the system.

7.2.8 Measurement: Closed loop noise figure

Figure 7.16 and 7.17 shows the hot and cold noise power measurements for the differential demodulator outputs. The Y factor for each measurement is calculated using $Y = N_h/N_c$.

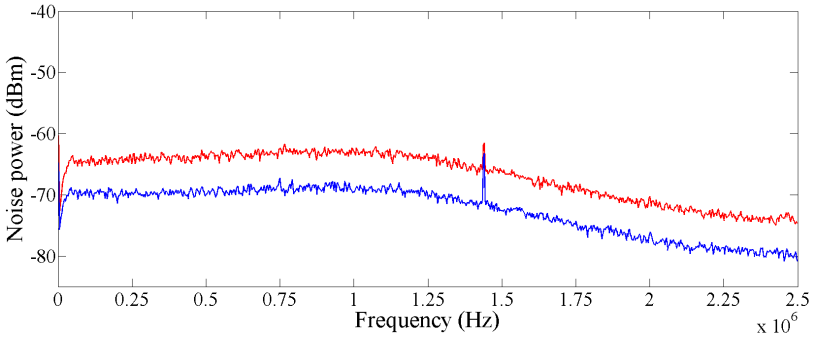

Figure 7.16: Closed loop averaged noise power measurement for positive differential output.

The noise figure for each single ended measurement is calculated as

$$NF_{CL} = \frac{ENR}{Y_{CL} - 1}$$

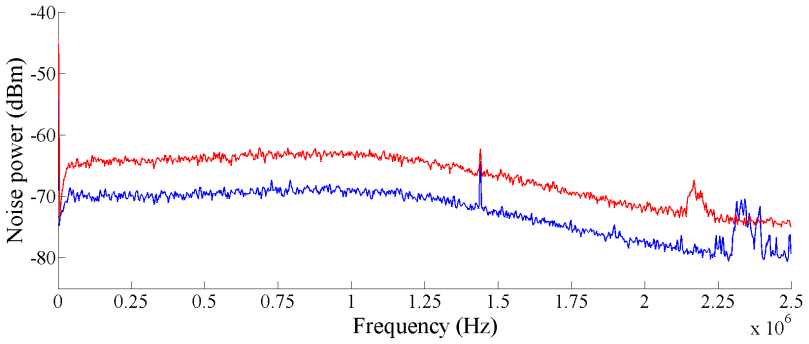

Figure 7.17: Closed loop averaged noise power measurement for negative differential output.

The results for different frequency points are presented in Table 7.6.

Table 7.6: Noise figure results for the closed loop RPC measurement.

Frequency (kHz)	NF_{d-I+} (dB)	NF_{d-I-}
Theoretical	9.80	9.80
10	15.2	18.5
100	11.5	11.7
1000	9.6	10.23

From Figures 7.16 and 7.17, the spikes in the measurements due to environmental noise can be seen again, as in the open loop measurement. From these measurements, however, the cancellation of the signal can be observed for frequencies below 50 kHz. It can also be seen from the results in Table 7.6 that a reduced noise figure is measured where the cancellation is taking place. This is due to the noise added by the components at low frequencies (i.e. flicker noise).

7.2.9 Discussion

From the results in Tables 7.5 and 7.6, it is seen that the measured noise figure is higher than the theoretically expected values. Using the open circuit noise voltage model derived in subsection 7.2.5, the noise contribution of the 50 dB amplifier can be calculated and added to the equation. The 50 dB amplifier consists of two 25 dB cascaded sections. Consider only the first 25 dB section shown in Figure 7.18

In order to compare the influence of this amplifier on the noise of the cascaded sections from Figure 7.12, the noise sources of this amplifier are referred to their equivalent input values. The resistor values in Figure 7.18 are given in Table 7.7.

The following simplifications are made to the noise model in Figure 7.18. The noise voltage of the two opamps (e_0) in Figure 7.18, are uncorrelated and can be added as root sum squares

$$e_{0t} = \sqrt{e_0^2 + e_0^2} \tag{7.2.21}$$

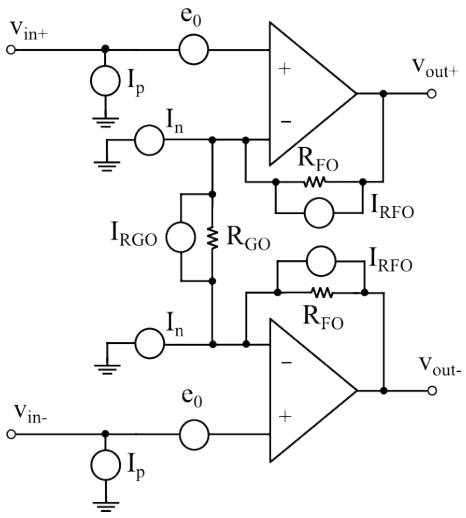

Figure 7.18: Noise model of a 25 dB section of the operational amplifiers used in the Y factor measurements.

Table 7.7: The resistor values as well as the voltage and the current noise values of the opamp.

Symbol	Value
R_{FO}	10kΩ
R_{GO}	1kΩ
e_0	$2.4nV/\sqrt{Hz}$
I_N	$1.9pA/\sqrt{Hz}$
I_{RFO}	$1.29pA/\sqrt{Hz}$
I_{RGO}	$4.07pA/\sqrt{Hz}$

To calculate the noise voltages due to the resistor feedback network, consider Figure 7.19. This figure includes the current noise sources due to the resistors, where $I_{RFO} = \sqrt{4kT\frac{1}{R_{FO}}}$ is the current noise due to R_{FO} and $I_{RGO} = \sqrt{4kT\frac{1}{R_{GO}}}$ is the current noise due to the resistor R_{GO}. The current noise at the negative terminals of the opamps (I_N) are also included in the figure.

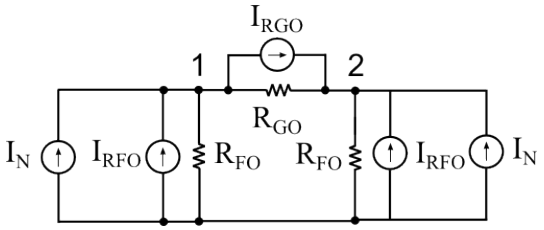

Figure 7.19: The feedback resistors noise model.

Consider the resistor network in Figure 7.19 as a two port network, where the y-parameters are given by

$$y = \begin{bmatrix} G_{FO} + G_{GO} & -G_{GO} \\ -G_{GO} & G_{FO} + G_{GO} \end{bmatrix} \tag{7.2.22}$$

where $G_{FO} = \frac{1}{R_{FO}}$ and $G_{GO} = \frac{1}{R_{GO}}$. If the y-parameters in equation 7.2.22 are converted to their equivalent z-parameters, the result is given in equation 7.2.23.

$$z = \begin{bmatrix} \frac{G_{FO}+G_{GO}}{(G_{FO}+G_{GO})(G_{FO}+G_{GO})-G_{GO}^2} & \frac{G_{GO}}{(G_{FO}+G_{GO})(G_{FO}+G_{GO})-G_{GO}^2} \\ \frac{G_{GO}}{(G_{FO}+G_{GO})(G_{FO}+G_{GO})-G_{GO}^2} & \frac{G_{FO}+G_{GO}}{(G_{FO}+G_{GO})(G_{FO}+G_{GO})-G_{GO}^2} \end{bmatrix} \tag{7.2.23}$$

Next, the admittance values in equation 7.2.23 are replaced with their equivalent impedance values to give

$$z = \begin{bmatrix} \frac{R_{FO}R_{GO}+R_{FO}R_{FO}}{R_{FO}+R_{GO}+R_{FO}} & \frac{R_{FO}R_{FO}}{R_{FO}+R_{GO}+R_{FO}} \\ \frac{R_{FO}R_{FO}}{R_{FO}+R_{GO}+R_{FO}} & \frac{R_{FO}R_{GO}+R_{FO}R_{FO}}{R_{FO}+R_{GO}+R_{FO}} \end{bmatrix} \tag{7.2.24}$$

Using z-parameters, the two port network in Figure 7.19 can be described as in equation 7.2.25.

$$\begin{bmatrix} v_1 \\ v_2 \end{bmatrix} = \begin{bmatrix} z_{11} & z_{12} \\ z_{21} & z_{22} \end{bmatrix} \begin{bmatrix} i_1 \\ i_2 \end{bmatrix} \tag{7.2.25}$$

where $i_1 = -I_{RGO} + I_{RFO} + I_N$ and $i_2 = I_{RGO} + I_{RFO} + I_N$. If equation 7.2.24 is applied to equation 7.2.25, the voltage matrix is represented by equation 7.2.26.

$$\begin{bmatrix} v_1 \\ v_2 \end{bmatrix} = \begin{bmatrix} \frac{(I_{RGO}+I_{RFO}+I_N)R_{FO}R_{FO}}{R_{FO}+R_{GO}+R_{FO}} + \frac{(-I_{RFO}+I_{RFO}+I_N)(R_{FO}R_{FO}+R_{FO}R_{GO})}{R_{FO}+R_{GO}+R_{FO}} \\ \frac{(-I_{RFO}+I_{RFO}+I_N)R_{FO}R_{FO}}{R_{FO}+R_{GO}+R_{FO}} + \frac{(I_{RFO}+I_{RGO}+I_N)(R_{GO}R_{FO}+R_{FO}R_{FO})}{R_{FO}+R_{GO}+R_{FO}} \end{bmatrix} \tag{7.2.26}$$

With the two node voltages v_1 and v_2 known, the differential voltage across R_{GO} can be calculated as $v_x = v_2 - v_1$ and the result is given in equation 7.2.27.

$$\begin{aligned} v_x =& \frac{I_{RGO}R_{FO}R_{GO}}{2R_{FO}+R_{GO}} + \frac{I_{RFO}R_{FO}R_{GO}}{2R_{FO}+R_{GO}} + \frac{I_N R_{FO}R_{GO}}{2R_{FO}+R_{GO}} + \\ & \frac{I_{RGO}R_{FO}R_{GO}}{2R_{FO}+R_{GO}} - \frac{I_{RFO}R_{FO}R_{GO}}{2R_{FO}+R_{GO}} - \frac{I_N R_{FO}R_{GO}}{2R_{FO}+R_{GO}} \end{aligned} \tag{7.2.27}$$

The equivalent noise voltage due to the resistive feedback network can be calculated by taking the sum of the squares of each component as in equation 7.2.28.

$$\begin{aligned} v_x^2 =& (\frac{2I_{RGO}R_{FO}R_{GO}}{2R_{FO}+R_{GO}})^2 + (\frac{I_{RFO}R_{FO}R_{GO}}{2R_{FO}+R_{GO}})^2 + (\frac{I_N R_{FO}R_{GO}}{2R_{FO}+R_{GO}})^2 + \\ & (-\frac{I_{RFO}R_{FO}R_{GO}}{2R_{FO}+R_{GO}})^2 + (-\frac{I_N R_{FO}R_{GO}}{2R_{FO}+R_{GO}})^2 \end{aligned} \tag{7.2.28}$$

Using the resistor and current noise values supplied in Table 7.7, the value for v_x^2 can be calculated. The new output SNR is calculated as shown in equation 7.2.29.

$$SNR''_{OUT} = \frac{v'_S A^2_{diff} A^2_{25dB}}{A^2_{25dB}[v^2_{diff} + e^2_{0t} + v^2_x]} \tag{7.2.29}$$

where $v^2_{diff} = A^2_{diff}(v'^2_N + e^2_d + v^2_{THt} + v^2_{RGt} + v^2_{RFt} + v^2_{INM} + v^2_{INP} + v^2_{Nd})$. The new open loop noise figure is calculated as in equation 7.2.30.

$$\begin{aligned} NF_{OL-new} &= \frac{SNR_{IN}}{SNR''_{OUT}} \\ &= \frac{A^2_{25dB}[v^2_{diff} + e^2_{0t} + v^2_x]}{A^2_{diff} A^2_{25dB} v'^2_N} \\ &= NF_{OL} + \frac{e^2_{0t} + v^2_x}{A^2_{diff} v'^2_N} \\ &= 7.54 + 0.86 \\ &= 8.40 \\ &= 9.24 \ dB \end{aligned} \tag{7.2.30}$$

Table 7.8: The equivalent noise voltage used in equation 7.2.30.

Symbol	Value
e_0	2.4 $nV/\sqrt{Hz}$
v_x	4.19 $nV/\sqrt{Hz}$
$A_{diff} v'_N$	5.208 $nV/\sqrt{Hz}$

Table 7.9: Noise figure results for the open loop RPC measurement.

Frequency (kHz)	NF_{OL-I+} (dB)	NF_{OL-I-} (dB)
Theoretical	9.24	9.24
10	12.97	13.2
100	10.4	9.11
1000	9.6	9.2

The theoretical closed loop noise figure can be calculated as

$$NF_{CL-new} = \frac{N_{initial} + c^2 N_{mod}}{(1 - c^2)\ N_{thermal}} \tag{7.2.31}$$

The results are presented in Table 7.10.

Table 7.10: Noise figure results for the closed loop RPC measurement.

Frequency (kHz)	NF_{d-I+} (dB)	NF_{d-I-}
Theoretical	10.17	10.17
10	15.2	18.5
100	11.5	11.7
1000	9.6	10.23

7.3 RF phase error

The RF phase error was introduced as a practical consideration in Chapter 3. This practical consideration was elaborated on in Chapter 5 by means of a derivation. This derivation took the non ideal behaviour of the modulator and demodulator into account, as well as RF phase delays due to transmission lines in the RPC, and an equation consisting of the transmission line delays was obtained which could be used to compensate for the RF phase error in the RPC. The transmission line lengths were calculated for a specific centre frequency and this test will verify whether the canceller loop will remain stable for a 90 degree phase error as predicted by Stove [10].

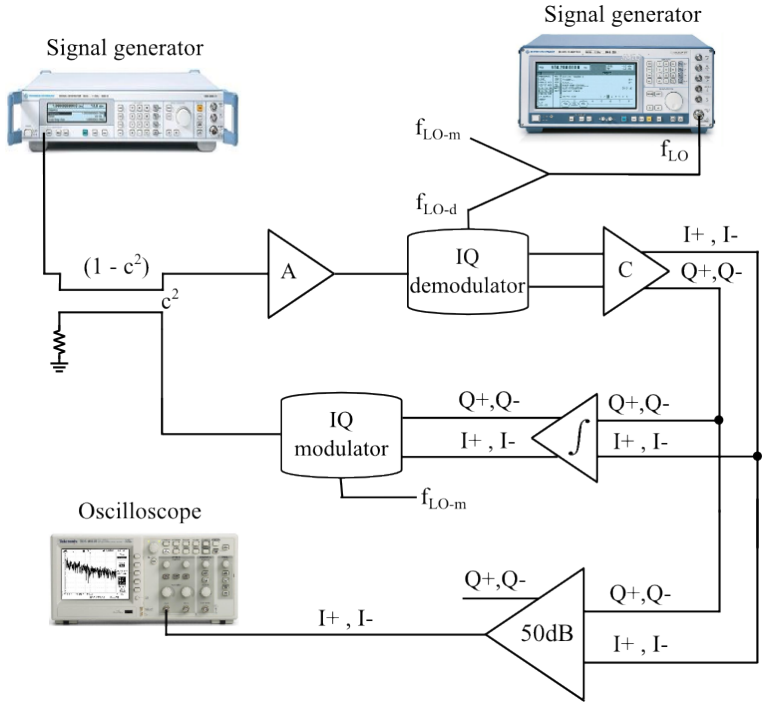

Figure 7.20: Test setup for measuring the IQ Reflected Power Canceller's cancellation across its baseband frequency.

7.3.1 Result

The measurement is approached by first predicting the transmission line lengths of the RPC at 2.45 GHz as described in Chapter 5. By varying the centre frequency across a test frequency band, the point at which the system becomes unstable can be measured. The test setup given in Figure 7.20 is used for the measurement with a sufficiently low input power to ensure that the RPC remains linear. The output of the demodulator is monitored on an oscilloscope and the frequency at which the RPC becomes unstable is noted.

Table 7.11 shows the results of the measurement with the corresponding phase shift from the calculated 180 degrees. First the table gives the minimum frequency that can be used as the centre frequency before instability, followed by its corresponding phase shift from 180 degrees. This is followed by the maximum frequency that can be used, followed by its corresponding phase shift.

Table 7.11: The result of the RF phase error measurement.

Min (GHz)	Phase (deg)	Max (GHz)	Phase (deg)
2.048	-28.9	3.053	45.3

7.4 Conclusion

In conclusion, the results that were obtained for the practical RPC correspond with what was theoretically predicted. The Y factor method produced successful noise figure results. The linear working region of the RPC produced a cancellation of more than 40 dB for IF signals below 100 Hz. From the non linear tests it could be verified that the maximum signal that the RPC can cancel is equal to the value which was predicted in the dynamic range calculations. It was also verified that the RPC remains stable for an RF phase error of 74.2 degrees.

Chapter 8

Conclusions and Recommendations

This study consisted of the design, build and evaluation of an IQ Reflected Power Canceller for FMCW radar. The RPC is a valuable solution to solve low isolation and close range reflection problems in FMCW radar.

8.1 Research

The aim of this study was to evaluate an RPC, which included first analysing the ideal RPC and then expanding the model to include the non ideal aspects of the system. A mathematical model of the ideal RPC was derived in Chapter 2. This model was used to describe the control system of the RPC and the model was simulated in both MATLAB and LTSpice. Next, some practical issues that had arisen during the research into the RPC were introduced and described. One of the practical considerations included the effect of an RF phase error on the stability of the feedback system. Another practical consideration that was introduced, was the dynamic range of the RPC. A method of designing an RPC with an optimised dynamic range was derived. The practical considerations that were identified were evaluated further with practically applicable results. By using this optimising method it was possible to find values for the components that were used for the RPC. This was followed by a technique that was derived for calculating the transmission line lengths required in the RPC to obtain a 180 degree phase shift through the control loop. Finally, the practical RPC was assembled and tested, comparing the theoretically predicted results with the practically measured results.

8.2 Findings and Recommendations

From the results in Chapter 7 it was found that the RPC's measurements correspond very well with the theoretically predicted values. However it was found during these measurements that not all of the components performed as was stated in their respective datasheets, which resulted in a recalculation of the dynamic range in Chapter 6. Apart from the discrepancy between the expected and measured values of the components, the RPC performed very well.

From the dynamic range calculations in Chapter 4, the modulator was identified as the critical component in the RPC. It was found that the RPC's output contained large harmonic components when the modulator's output started to compress. Thus even though the modulator had a high 1 dB output power specification, it could only be used in its linear output power region. From the research into different modulators that are available, in Chapter 3, it was found that the maximum output power of the available components is not very high. In order to improve the dynamic range of the RPC even further, an IQ/vector modulator with a higher dynamic range is required. The results of the derivation of an optimised dynamic range for an RPC showed that, even though an optimum system could be found, there was still a price to pay for this optimisation. There was a 3 dB increase in transmit power for the maximised FOM value. For high power applications, this is not a practical solution since a 3 dB increase in power could mean a very significant increase in cost for the components that are required.

The dynamic range derivations from Chapter 4 aimed to produce an RPC with a maximised dynamic range, which would significantly improve upon the dynamic range of the system without an RPC. However, it was found that due to the output power limitations of the modulator, the maximum signal power that could be handled at the input of the RPC was not very different from that of the system without an RPC. In systems where the RPC is intended to decrease the possibility of the receiver front-end saturating, it might not be a beneficial solution.

Even though the RPC cancels the unwanted reflections in the system, a bigger problem pertaining to the transmitted signal's phase noise at high offset frequencies remains unsolved. If the performance at maximum range is limited by the phase noise associated with large reflections from nearby objects, the addition of an RPC will not improve the long range detection performance of the radar.

8.3 Conclusion

From the measurement results in Chapter 7, the RPC produced favourable results. The amount of cancellation achieved in the measurement, corresponded to the theoretically calculated values. A cancellation of more than 45 dB was measured for low baseband frequencies. The measured dynamic range of the RPC correlated with its equivalent calculations. It was found that the RPC remained stable over a wide range of RF centre frequencies (1 GHz) and thus the RPC will not limit the modulation bandwidth of the FMCW radar.

References

[1] Beasley, P., Stove, A., Reits, B. and As, B.: Solving the problems of a single antenna frequency modulated cw radar. In: *IEEE International Radar Conference*, pp. 391–395. 1990.

[2] Skolnik, M.: *Introduction to radar systems*. McGraw-Hill Book Company, 1962.

[3] Pozar, D.: *Microwave engineering*. 3rd edn. John Wiley and Sons, 2005.

[4] Jiming, Q., Xinjian, Q. and Zhijiu, R.: Development of a 3cm band reflected power canceller. In: *CIE International Conference on Radar Proceedings*, pp. 1098–1102. October 2001.

[5] Kim, J., Ko, S., Jeon, S., Park, J. and Hong, S.: Balanced topology to cancel tx leakage in cw radar. *Microwave and Wireless Components letters*, vol. 14, pp. 443–445, September 2004.

[6] Lin, K. and Wang, Y.: Real-time dsp for reflected power cancellation in fmcw radars. In: *Vehicular Technology Conferene*, vol. 6, pp. 3905–3907. September 2004.

[7] Grazzini, G., Pieraccini, M., Parrini, F. and Atzeni, C.: A clutter canceller for continuous wave gpr. In: *4th International Workshop on Advanced Ground Penetrating Radar*, pp. 212–216. June 2007.

[8] Venkatamuni, T., Sarma, L. and Kalghatgi, A.: Adaptive reflected power canceller for single antenna fmcw radar. In: *Microwave Conference*, pp. 1841–1844. December 2009.

[9] Pursula, P., Kiviranta, M. and Seppa, H.: Uhf rfid readar with reflected power canceller. *Microwave and Wireless Components Letters*, vol. 19, pp. 48–50, December 2008.

[10] Stove, A.: Linear fmcw radadr techniques. In: *IEEE Proceedings-F*, vol. 139, pp. 343–350. October 1992.

[11] Gopal, M.: *Control Systems, Principles and Design*, chap. 4. 2nd edn. Tata McGraw-Hill Education, 2002.

[12] Zhang, Y.: *Wireless Transmitter IQ Balance and Sideband Suppression*. Analog Devices, One Technology way, P.O. Box 9106,Norwood MA, 0th edn, 2010.

[13] Kaukovuori, J., Stadius, K., Ryynanen, J. and Halonen, K.: Analysis and design of passive polyphase filters. *IEEE Transactions on Circuits and Systems - I: Regular Papers*, vol. 55, no. 10, pp. 3023–3038, November 2008.

[14] Behbahani, F., Kishigami, Y., Leete, J. and A.A., A.: Cmos mixers and polyphase filters for large image rejection. *IEEE Journal of Solid-State Circuits*, vol. 36, no. 6, pp. 873–888, June 2001.

[15] Arnold, M., Class, R., Dantoni, F., Jaganathan, S. and Sperlich, R.: Lo harmonic effects on i/q balance and sideband suppression in complex i/q modulators. Application report, Texas Instruments, May 2010.

[16] Newman, E. and Soni, R.: Assess quadrature-demodulator noise figure using vector signal analysis. Tech. Rep., Analog Devices, November 2008.

[17] Wolff, C.: Requirements for radar receivers. Http://www.radartutorial.eu/09.receivers/rx04.en.html.

[18] Watson, R.: Receiver dynamic range: Part 1. Tech. Rep. 14, Watkins-Johnson Company, address, January/February 1987. Tech-notes.

[19] Vendelin, G., Pavio, A. and Rohde, U.: *Microwave Circuit Design Using Linear and Nonlinear Techniques*. John Wiley and Sons, 1990.

[20] Friss, H.: Noise figure of radio receivers. In: *Proc. of the IRE*, pp. 419–422. July 1944.

[21] *Fundamentals of RF and Microwave Noise Figure Measurements*. Hewlett Packard. Application Noe 57-1.

[22] Egan, W.: *Practical RF system design*, chap. 3, pp. 47–49. 1st edn. John Wiley and Sons, 2003.

[23] Unknown: Op amp noise figure: Don't be mislead. Tutorial MT-052, Analog Devices, October 2008.

[24] *AN-1719 Noise Figure Analysis Fully Differential Amplifier*. Texas Instruments, Post Office Box 655303, Dallas, Texas 75265, 2nd edn, May 2013.

[25] Lee, P.: Low noise amplifier selection guide for optimal noise performance. Tech. Rep. AN-940, Analog Devices, P.O. Box 9106, Norwood, MA.

[26] Venkatamuni, T., L.S.S., S. and A.T., K.: Adaptive reflected power canceller for single antenna fmcw radar. pp. 1841–1844. Central research laboratory, IEEE, 2009.

[27] Nash, E.: Correcting imperfections in iq modulators to improve rf signal fidelity. Application report, Analog Devices, One Technology Way, PO Box 9106, Norwood, MA, 2009.

[28] Circuits, M.: Application note on transformers. Tech. Rep. AN-20-002, Mini Circuits, 2010.

[29] Devices, A.: Diffampcalc: Adi's differential amplifier calculator. http://www.analog.com/en/amplifier-linear-tools/adi-diff-amp-calc/topic.html.

[30] *Noise Figure Measurement Accuracy - The Y-Factor Method*. Agilent Technologies, April 2013. Application Note 57-2.

[31] *TDS1000/2000-Series Digital Oscilloscope User Manual*. Tektronix, 1st edn.

[32] Mancini, R.: *Op Amps for Everyone*, chap. 10. Texas Instruments, August 2002.

Appendices

Appendix A

Diff-Amp Calculator

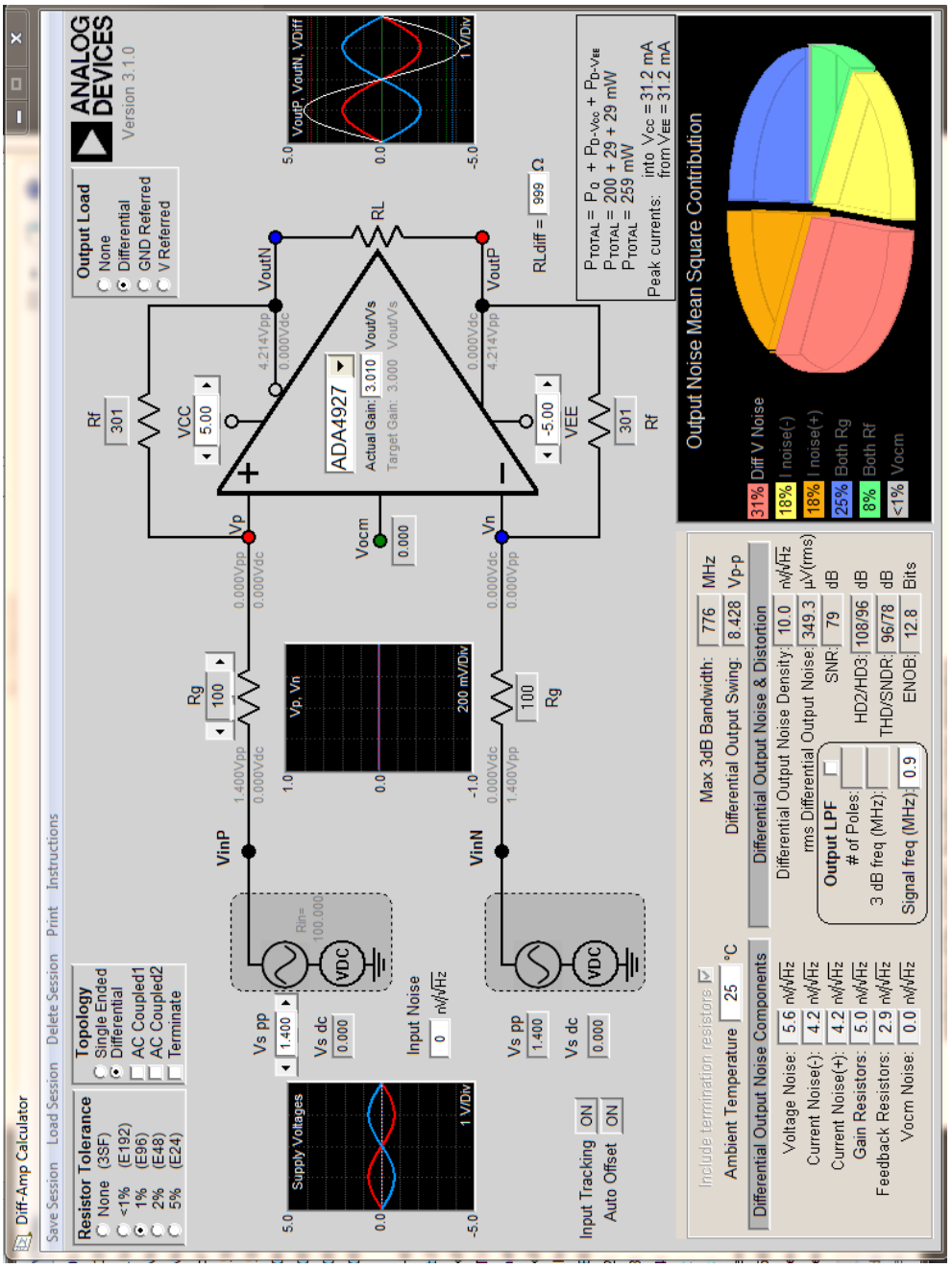

Figure A.1: Screen shot of the Diff-Amp Calculator from Analog Devices used to calculate the output referred noise voltage density.

Appendix B

MATLAB code

B.1 FOM Calculation

```
clear all
pfeedback = 10^(9.6/10);                                % The maximum signal power that is fed back from the modulator
nfeedback = 10^(-159.5/10);                             % The noise floor of the modulator
g = [4 8 10 12 14 16 20 25];                            % LNA A gain values. The FOM is evaluated for varying LNA gains.
gcolor = ['*' 'm' 'b' 'y' 'g' 'c' 'k' 'r'];
nf = 10^(1.5/10) + (10^(12.3/10) - 1)./10.^(g./10);     % The cascaded noise figure of the open loop system is calculated for each LNA gain
c = 1:0.2:20;                                           % c is the coupling factor. The FOM is evaluated across a range of coupling factors
c = 10.^(-c./20);
pwithcanceller=[];


for i = 1:length(g)                                     % The first for loop runs through the gain from variable g
    ninitial(i) = 10^((-174+nf(i))/10);                 % The initial noise floor is calculated for a specific gain value

    for j = 1:length(c)                                 % The second for loop runs through the coupling factors for a specific gain
        fom(j,i) = (1 - c(j)^2) * c(j)^2 * pfeedback/(ninitial(i) *(1 + c(j)^2*nfeedback/ninitial(i))^2); % The Figure Of Merit is calculated
```

```
17          pwithcanceller(j) = c(j)^2 * pfeedback/(1 - c(j)^2);
                                                                %
               The maximum signal power that can be received is
               calculated
18          mds_withcanceller(j) = (ninitial(i) + c(j)^2*
               nfeedback) / ((1 - c(j)^2)*ninitial(i));
                           % The increase in Tx power is
               calculated
19      end
20
21      figure(1)                                               % Plot
           the Figure of Merit
22      hold on
23      plot(10*log10(c.^2), 10*log10(fom(:,i)),gcolor(i))
24      hold off
25
26      figure(2)                                               % Plot
           the Increase in Tx power
27      hold on
28      plot(10*log10(c.^2), 10*log10(mds_withcanceller),gcolor(
           i))
29      hold off
30  end
31
32  figure(1)
33  title('Figure of Merit for various LNA gains')
34  xlabel('Coupling factor (dB)')
35  ylabel('FOM (dB)')
36  legend('4 dB', '8 dB', '10 dB', '12 dB', '14 dB', '16 dB', '
       20 dB', '25 dB')
37
38  figure(2)
39  title('Increase in Tx power for various LNA gains')
40  xlabel('Coupling factor (dB)')
41  ylabel('Increase in Tx power (dB)')
42  legend('4 dB', '8 dB', '10 dB', '12 dB', '14 dB', '16 dB', '
       20 dB', '25 dB')
```

B.2 Noise figure measurement: Oscilloscope setup

```
1  % Create a VISA-USB object.
2  interfaceObj = instrfind('Type', 'visa-usb', 'RsrcName', '
       USB0::0x0699::0x0363::C061395::0::INSTR', 'Tag', '');
3
4  % Create the VISA-USB object if it does not exist
5  % otherwise use the object that was found.
6  if isempty(interfaceObj)
```

```
    interfaceObj = visa('NI', 'USB0::0x0699::0x0363::C061395
        ::0::INSTR');
else
    fclose(interfaceObj);
    interfaceObj = interfaceObj(1);
end

% Create a device object.
deviceObj = icdevice('tektronix_tds2000B.mdd', interfaceObj)
    ;

% Connect device object to hardware.
connect(deviceObj);


% Execute device object function(s).
groupObj = get(deviceObj, 'Waveform');
groupObj = groupObj(1);
[X,Y,XUNIT,YUNIT] = invoke(groupObj, 'readwaveform', 'math')
    ;
```

B.3 MATLAB: Processing measurements

```
% In order to obtain 100 consecutive measurements, the data
    aquisition is placed in a for loop

for i=1:100
    [X,Y,XUNIT,YUNIT] = invoke(groupObj, 'readwaveform', '
        math');
    cold_ol_In(i,:) = X;
    f(i,:)= Y;
end

% This for loop is repeated for each measurement of I+, I-
    open loop and I+ and I- closed loop

% The averaging of the 100 measurements for each frequency
    point is given here

for k=1:length(cold_ol_In(1,:))
    ftest=10.^(cold_ol_In(1,k))./10;
for j=2:length(cold_ol_In(:,k))
    ftest = ftest+10.^(cold_ol_In(j,k)./10);
end
c_ol_In(k)=ftest/length(cold_ol_In(:,k));
end
```

Appendix C

Dynamic range: Excel results

Components

LNA (Demodulator)

Part number	Gain (dB)	NF (dB)	P1dB (dBm)
MAAL-0120200	10	1.4	17.5
MAAL-010706	17	0.6	17.5
HMC667LP2	18	0.75	16.5
PSA4-5043+	13	1	20
ZX60-272LN+	13	0.9	18
TAMP-272LN+	13	0.9	18

Demodulator

Part number	Gain (dB)	NF (dB)	max input power (dBm)
ADL5380	6	12	12

Low noise differential amplifier

Part number	BW (MHz)	Input noise (nV/sqrt(Hz)	Max output swing (Vpp_diff)	Total supply (V)	Gain(dB)	NF (dB)
LT1993-4	900	2.35	7	5.5	12	14.5
LT6402-12	300	2.6	7	5.5	12	15
THS4130	150	1.3		-15	9	22
LMH6553	900	1.2		-12	9	23.5
AD8139	53	2.25		12	14	15
ADA4927	774	1.4	8.4	7	9.5	10.7
ADA4950	239	3.6	8.4	10	9.5	11

Modulator

Part number	Output P1dB (dBm)	Noise floor (dBm/Hz)
ADL5375	5.5	-160

LNA (Modulator)

Part number	Gain (dB)	NF (dB)	P1dB (dBm)
MAAL-010706	17	0.6	17.5
HMC667LP2	18	0.75	16.5
PSA4-5043+	13	1	20
ZX60-272LN+	13	0.9	18

Figure C.1: List of components for the IQ RPC in an Excel spreadsheet.

Calculation values	
	Test Values
Gain (dB)	13
NF (dB)	0.9
Max input (dBm)	2
P1dB (dBm)	18
Gain (dB)	7.4
NF (dB)	12.3
Max output (Vpp_pch)	1.4
Max input (dBm)	11
Gain (dB)	9.5
NF (dB)	10.7
Max input (Vpp_pch)	
Max output (Vpp_pch)	3.5
	Test Values
Output_max (dBm)	9.3
Noise floor (dBm/Hz)	-160
P1dB	0
Gain (dB)	0
NF (dB)	0
Resultant NF (dB)	0
Attenuator NF (dB)	0

Figure C.2: Components chosen from the list in figure C.1 for the IQ RPC in an Excel spreadsheet.

Results			
Initial (without canceller)			
Max input power (dBm)	**MDS_initial (dBm/Hz)**		**NF_s (dB)**
-2	-167.4351817		6.56481829
Final (with canceller)			
Max signal to be cancelled (dBm)	**Coupling factor (dB)**	**MDS_rpc (dBm/Hz)**	**MDS_loss due to canceller (dB)**
9.320624399	**3**	-159.2618558	8.173325902
7.504808305	**4**	-160.7472543	6.687927441
5.950885386	**5**	-161.9180442	5.517137555
4.556275775	**6**	-162.8739091	4.561272628
3.266528953	**7**	-163.6677189	3.767462803
2.049403674	**8**	-164.3316085	3.103573239
0.884351739	**9**	-164.8875047	2.547676981
-0.242425094	**10**	-165.3519307	2.083251001
-1.340554858	**11**	-165.7383249	1.696856854
-2.416952162	**12**	-166.0581663	1.377015438
-3.476693273	**13**	-166.321503	1.113678745
-4.523568543	**14**	-166.5371894	0.897992331
-5.560445661	**15**	-166.7129968	0.722184902
-6.589516667	**16**	-166.8556814	0.579500292
-7.612470706	**17**	-166.9710491	0.464132653
-8.630617681	**18**	-167.0640304	0.371151308
-9.644978493	**19**	-167.1387671	0.296414613

Figure C.3: Results of the dynamic range calculations using the components listed in figure C.1.

Appendix D

Final RPC

Table D.1: The values of the components indicated on Figure D.1.

Symbol	Value
V+	5 V
V-	-5 V
V_p	2.5 V
V_n	-1.4 V
V_{ocm1}	0 V
V_{ocm2}	0.5 V
R_G	100 Ω
R_F	300 Ω
R_{GO}	1 kΩ
R_{FO}	10 kΩ
C_{in}	10 uF
R_{in}	10 kΩ
R_1	1 kΩ
C_1	10 nF

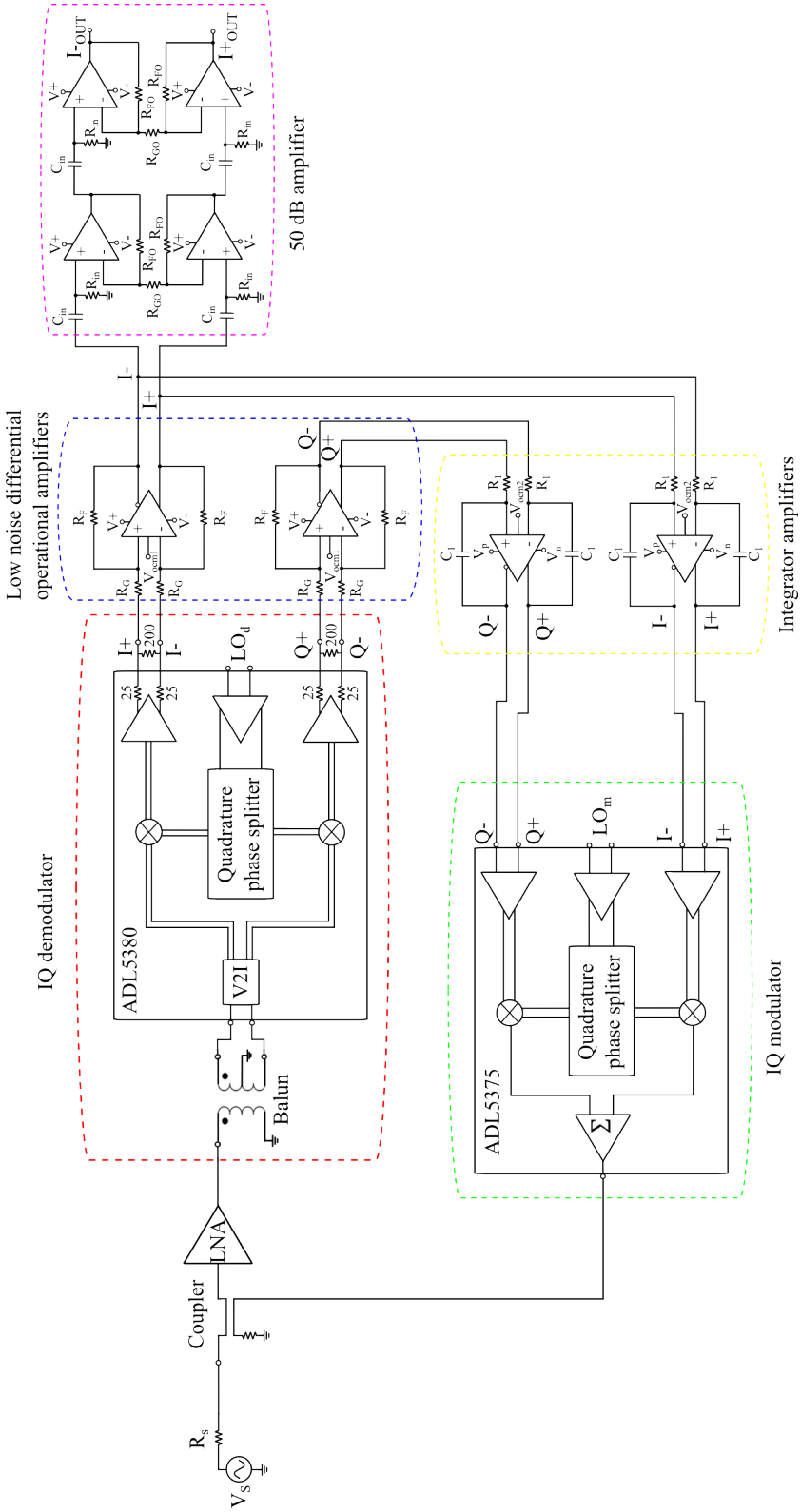

Figure D.1: The final circuit diagram of the RPC.

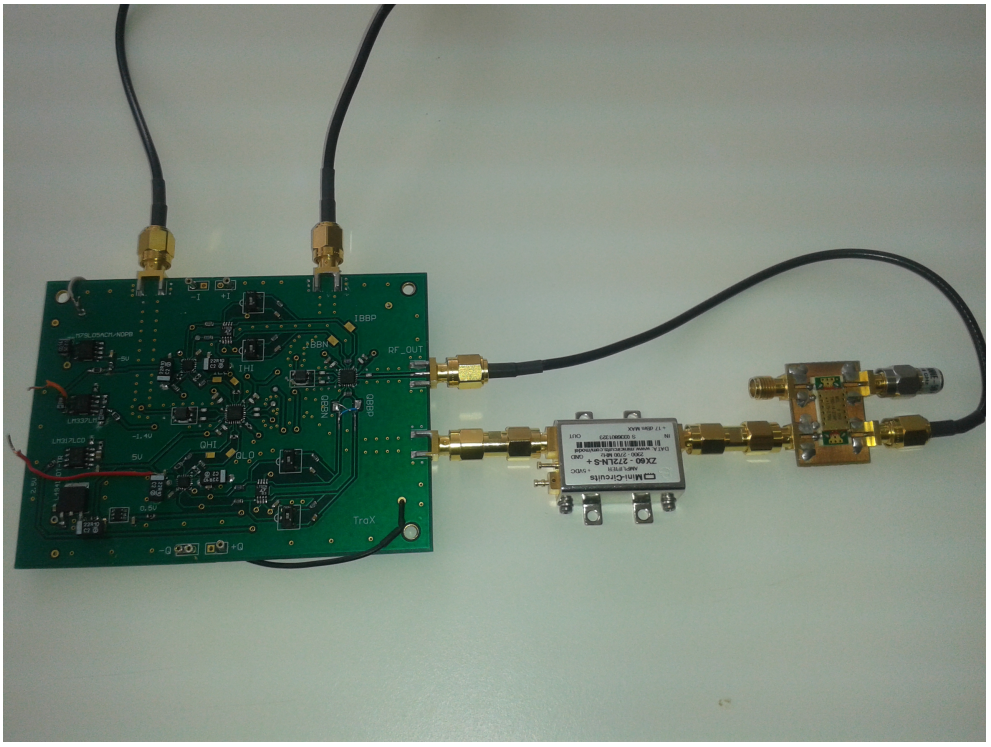

Figure D.2: The IQ Reflected Power Canceller.